Poly(acrylonitrile/methyl acrylate) copolymers and clay nanocomposites: Structural and property relationships

Thesis submitted in partial fulfillment of the requirements for the degree

of Master of Science (Polymer Science)

by

Eddson Zengeni

at

University of Stellenbosch

Supervisor: Dr. P.C Hartmann
Co-supervisor: Prof. R.D Sanderson

December 2009

Declaration

I, the undersigned, hereby declare that the work contained in this thesis is my own work and that I have not previously in its entirety or in part submitted it at any university for a degree.

Eddson Zengeni 17.11.2009

Date

Abstract

The preparation of poly(acrylonitrile/methyl acrylate) [poly(AN-co-MA)] copolymers and poly(AN-co-MA)/clay nanocomposites, via emulsion polymerization, their characterisation, and the relationships between their molecular structures and physical properties are described. The copolymer composition was varied, and the properties of the products were analysed and correlated to copolymer composition.

The free volume properties of the copolymer were dependent on the glass transition temperature (T_g), which is dependant on the copolymer composition. The copolymer crystallinity decreased with increasing MA content. The decrease in crystallinity and increase in both o-Ps lifetime and o-Ps intensity with decreasing T_g was caused by the enhanced chain mobility brought about by the incorporation of methyl acrylate.

The poly(acrylonitrile-co-methyl acrylate)/clay nanocomposites with 60% AN:40% MA (mol:mol) ratio were prepared using montmorillonite clay modified via adsorption, using 2-acrylamido-2-methyl-1-propanesulphonic acid (AMPS), via in-situ intercalation polymerization. The poly(AN-co-MA)/clay nanocomposites with different clay loadings showed no difference in morphology. They exhibited improved thermomechanical properties and higher thermal stability than the neat copolymers.

The melt rheology results of these nanocomposites showed an improved storage modulus as well as increased shear thinning behaviour with increasing clay content. However, the nanocomposites exhibited long-time relaxation behaviour and their chemical structures evolved during analysis. This was attributed to cyclisation reactions taking place at the temperature used during the oscillatory tests.

The sorption isotherms of water vapour in these nanocomposites followed a dual-mode sorption behaviour (BET type II mode). Hysteresis was observed in sorption/desorption isotherms of these nanocomposites. The equilibrium water uptake was higher in the

nanocomposites compared to the neat copolymers, and it increased with increasing clay content, especially at high water activities (0.8).

Although diffusion and permeability decreased with increasing clay content the solubility increased due to the hydrophilic nature of the clay. Despite the decrease in diffusion and permeability parameters the free volume hole radius of the nanocomposites remained constant, but a slight decrease in free volume hole number was observed.

Opsomming

Die bereiding van poli(akrilonitriel/metielakrilaat) [poli(AN-ko-MA)] kopolimere en poli(AN-ko-MA)/klei nanosamestellings deur middel van emulsiepolimerisasie, hul karakterisering asook die ooreenkoms tussen hul molekulêre strukture en fisiese eienskappe is beskryf. Die kopolimeersamestelling is gevarieer, en eienskappe is geanaliseer en dan gekorreleer met die kopolimeersamestelling.

Die vrye-volume eienskappe van die kopolimeer was afhanklik van die glasoorgangstemperatuur (T_g) wat weer afhanklik is van die kopolimeersamestealling. Die kristalliniteit van die kopolimeer het verminder met die hoeveelheid MA teenwoordig. Die afname in kristalliniteit en toename in beide die o-Ps leeftyd en o-Ps intensiteit met afname in T_g is veroorsaak deur die beter kettingbeweegbaarheid wat veroorsaak is deur die byvoeging van metielakrilaat.

Die poli(akrilonitriel-ko-metielakrilaat)/klei nanosamestellings met 60% AN:40% MA (mol:mol) verhouding is berei deur die gebruik van montmorillonietklei, gemodifiseer deur die adsorpsie van 2-akrielamido-2-metiel-1-propaansulfoonsuur (AMPS) deur middel van 'n *in-situ* interkaleringspolimerisasie. Die poli(AN-ko-MA)/klei nanosamestellings het, ten spyte van die verskillende hoeveelhede klei wat gebruik is, geen verandering in morfologie getoon nie. Hulle het wel beter termodinamiese eienskappe en hoër termiese stabiliteit as die oorspronklike kopolimere getoon.

Die smeltreologie resultate van hierdie nanosamestellings het ‘n beter stoormodulus getoon, sowel as toenemende skuifverdunningsgedrag met 'n verhoogde klei inhoud. Tog het die nanosamestellings lang tyd-ontspanningsgedrag getoon en die chemiese struktuur het verander tydens analise. Dit word toegeskryf aan die sikliese reaksies wat plaasvind by die temperatuur wat gebruik is tydens die ossillatoriese toetse.

Die sorpsie isoterme van waterdamp in hierdie nanosamestellings het ‘n dubbel-styl sorpsiegedrag gevolg (BET tipe II styl). Histerese is waargeneem in sorpsie/desorpsie

isoterme van hierdie nanosamestellings. Die ewewig in wateropname van die nanosamestellings was hoër as vir dié van die oorspronklike kopolimere en dit het toegeneem met 'n toenemende klei inhoud, veral by hoë humiditeit (0.8).

Al het die diffusie en deurlaatbaarheid afgeneem met 'n toename in die klei inhoud, het die oplosbaarheid toegeneem as gevolg van die hidrofiliese karakter van die klei. Ten spyte van die afname in diffusie en deurlaatbaarheidsparameters, het die radius van die vrye-volume openinge van die nanosamestellings konstant gebly, maar ‘n klein afname in die aantal vrye-volume openinge is gevind.

Acknowledgements

Blessed be God the Father, the Lord Jesus Christ and the Holy Ghost who made the heavens and the earth.

I would like to extent my special gratitude to my study leaders, Prof R. D. Sanderson and Dr. P. C. Hartmann, for all the guidance, financial and academic support.

In the same spirit I thank Dr P. E. Mallon for his contributions to PALS work

I would also want to thank all the Department of Polymer Science, Dr Margie Hurndall, Mrs Erinda Cooper, Mrs Aneli Fourie, Mr Deon Koen, Mr Jim Motshweni and Mr Calvin Maart.

Also to the Mondi paper coatings group, Adine, Austin, Ineke, Lee-sa, Nagi, Niel, Pauline, Vernon, Yolande as well as Prof Pasch and his group, Helen, Dr Weber, Nhlanhla, Christoper, Rafael, Nadine.

Thanks to all those who helped with the analyses, Elsa Malherbe for NMR analysis, Illana Bergh for PAS-FTIR, Dr Jan Gertenbach for TGA, Mahommed Jaffer for TEM, Itemba labs for WAXD, Phillipe Dieudonne for SAXS, Richard Murden for IGA, Mahommed Sweed for PALS, PSS for SEC.

Not forgetting the people who supported the long road, my mum and my family, Mr/Mrs Zengeni (Byo), Mr/Mrs Kapofu (Byo), Mrs Zengeni (Mtre), Mr/Mrs Maraire

Mondi paper coatings and NRF for funding

Lastly to Grace, my beautiful wife whose love surpasses all lab stresses.

May the Lord Jesus Christ, author and perfector of our faith supply all your needs according to his reaches in glory.

Table of contents

List of figures

List of abbreviations

AN	acrylonitrile
AMPS	2-acrylamido-2-methyl-1-propanesulphonic acid
BET	Brunauer, Emmett and Teller
CEC	cationic exchange capacity
D	diffusion coefficient
DLS	dynamic light scattering
DMA	dynamic mechanical analysis
$DMSO_{d6}$	deutrated dimethyl sulphoxide
f_{AN}	acrylonitrile feed composition
F_{AN}	acrylonitrile copolymer composition
FTIR	Fourier transform infrared
GAB	Guggenheim-Anderson-de Boer
G'	storage modulus
G"	loss modulus
IGA	intelligent gravimetric analyzer
KPS	potassium persulphate
LVE	linear viscoelastic range
MA	methyl acrylate
MMT	montmorillonite
Mn	number average molecular weight
NMP	N-methyl-2-pyrrolidinone
o-Ps	ortho positronium
P	permeablility coefficient
PALS	positron annihilation lifetime spectroscopy
PCN	polymer-clay nanocomposite

PAN	polyacrylonitrile
PMA	polymethyl acrylate
PMMA	poly(methyl methacrylate)
Poly(AN-co-MA)	poly(acrylonitrile-co-methyl acrylate)
RAFT	Reversible addition-fragmentation chain transfer
S	solubility coefficient
SAXS	small angle X-ray scattering
SEC	size exclusion chromatography
SDS	sodium dodecyl sulphate
TEM	transmission electron microscope
Tg	glass transition temperature
TGA	thermogravimetric analysis
TMS	tetramethylsilane
THF	tetrahydrofuran
WAXD	wide angle X-ray diffraction

List of symbols

a	penetrant activity
A	area of membrane
A'	measure of penetrant/microvoid interaction
a_w	water vapour activity
b	hole affinity constant
C_D	concentration of penetrant molecules dissolved in the polymer matrix
C_H	concentration of penetrant molecules trapped in specific sites
C'_H	hole saturation constant
C_p	weighted mean value of polymer sorption capacity to penetrant
d	interlayer distance
F_{vR}	relative fractional free volume
I_3	o-Ps intensity
k	time exponential constant
k'	measure of penetrant/polymer interaction
k_D	solubility coefficient of gas in polymer independent of concentration at a given temperature
l	membrane thickness
L	mass of latex
M	molar mass of penetrant
M_0	initial mass of sample
M(t)	mass of sample after exposure to penetrant for time(t)
M_∞	mass of sample at equilibrium penetrant uptake
n	order of interference
p	pressure
P_D	mass of dry polymer

p_1	high pressure side
Q	the amount of penetrant that cross a membrane at time (t)
R	free volume hole radius
ΔR	thickness of the homogeneous electron layer in which positron annihilates
t	time
T_{50}	temperature at 50% weight loss
V_f	free volume size
Vp	polymer volume
Z	time lag
λ	wavelength of the X-ray
θ	diffraction angle
τ_3	o-Ps lifetime

CHAPTER 1

Introduction and objectives

1.1 Introduction

Polyacrylonitrile (PAN) exhibits desirable properties such as very low permeability to gases (e.g. oxygen and carbon dioxide) and resistance to most chemicals but it is rarely used as a homopolymer due to its poor processability.[1] Different techniques to improve its processability, and simultaneously utilising these desirable properties, have been developed, e.g. blending and copolymerisation. Copolymerisation has been widely used, and copolymers of PAN have wide applications, e.g. as fibre precursors and in packaging materials.[2-4]

The physical properties of most polymer materials are related to their free volume. The Positron annihilation lifetime spectroscopy (PALS) technique is commonly used to probe free volume in polymers due to its high sensitivity to the nanoscale holes.[5,6] It has however mainly been used on polymer blends[7,8] and commercial polymers;[9,10] only a few reports describe its use on copolymers.[11,12] In this study the changes in free volume properties in acrylonitrile/methyl acrylate copolymers, with varying comonomer compositions, was studied as a function of the glass transition temperature (T_g) of the copolymers.

The physical properties of polymers can be improved by the addition of fillers. Research on filled polymers led to the discovery of polymer clay nanocomposites (PCNs) in the early 1990s and they have become an area of both academic and industrial interest to date[13-25]. PCNs are produced by finely dispersing clay in a polymer matrix and have been found to exhibit improved properties when compared to their parent neat polymers due to the strong interaction between the polymer matrix and clay platelets. The clay, being hydrophilic in nature cannot be easily dispersed in most polymers, which are usually hydrophobic in nature, and hence the need to modify the clay to enhance compatibility between the clay and the polymer. Methods such as ion exchange[26,27], adsorption[28,29] and sonication[30] have been used

to achieve this goal. Depending on the extent to which the clay platelets are separated from their natural tactoids, PCNs are classified into two morphological structures: intercalated and exfoliated nanocomposites. These morphological structures of PCNs play a determining role in their physical properties.

Despite the numerous studies done on PCNs there are no reports on clay nanocomposites of poly(AN-co-MA). In this study poly(AN-co-MA)/clay nanocomposites were prepared and their morphological, rheological and water vapour sorption properties were investigated and correlate the physical properties to molecular and morphological stuctrures.

1.2 Objectives

The main objectives of this study were to:

a) Synthesise acrylonitrile-methyl acrylate copolymers of different compositions and then:
    - Determine the effect of copolymer composition on T_g, crystallinity and free volume properties
    - Establish correlations between T_g, crystallinity and free volume properties

b) Synthesise poly(AN-co-MA)/clay nanocomposites using free-radical polymerisation in emulsion and evaluate how the clay nanofiller content and dispersion impacts the following:
    - Comonomer composition, monomer to polymer conversion and morphological features
    - Thermomechanical properties and thermal stability
    - Rheological properties in the rubbery state
    - Water vapour transport properties and free volume properties

1.3 Thesis layout

A short introduction and the objectives of the study are described in Chapter 1.

The theoretical background to this work is presented in Chapter 2. It includes a brief definition of polymer/clay nanocomposites, their preparation and characterisation; it introduces the concepts of penetrant transport in polymers and nanocomposites; and also gives a brief overview on polyacrylonitrile and its copolymers.

In Chapter 3 the synthesis of poly(AN/MA) copolymers, with different comonomer compositions, by emulsion polymerisation is described and discussed. The copolymers were characterised using nuclear magnetic resonance spectroscopy (NMR) and size exclusion chromatography (SEC). The investigations on the effects of varying the comonomer composition on T_g, crystallinity and free volume properties are described.

Chapter 4 describes the synthesis and characterisation of poly(AN-co-MA)/clay nanocomposites with different clay content, up to 7% clay. Syntheses were carried out using emulsion polymerization. The morphological characteristics of these nanocomposites were confirmed by small angle X-ray scattering (SAXS) and transmission electron microscope (TEM). Dynamic mechanical analysis (DMA) was used to investigate the thermomechanical properties and thermogravimetric analysis (TGA) was used for thermal stability investigations. Copolymer composition, particle size and conversion were also investigated.

The rheological properties of the nanocomposites prepared as described in Chapter 4 are described in Chapter 5. This chapter describes the viscoelastic properties of these nanocomposites as determined by melt rheology. Results of the dynamic time sweeps, carried out in order to investigate the melt stability of the nanocomposites, are also reported.

Chapter 6 describes the water vapour transport properties [i.e. the water vapour sorption mechanisms, diffusion coefficient, and permeability coefficient] of neat poly(AN-co-MA) and two nanocomposites: poly(AN-co-MA)/1%clay and poly(AN-co-MA)/5% clay. The free volume properties of these three samples are also described in relation to the water vapour transport properties and the morphological features of poly(AN-co-MA)/clay nanocomposites.

Finally, Chapter 7 summarises the main conclusions of this study, and suggestions for future research are given.

References

1. Wu, M. M., *Encyclopedia of Polymer Science and Technology*. John Wiley and Sons: New Jersey, 2003.
2. Bortner, M. J.; Bhanu, V.; McGrath, J. E.; Baird, D. G. *Journal of Applied Polymer Science* **2004**, 93, (6), 2856–2865.
3. Soulis, S.; Simitzis, J. *Polymer International* **2005**, 54, (11), 1474–1483.
4. Bortner, M. J.; Bhanu, V. A.; McGrath, J. E.; Baird, D. G. *Polymer* **2004**, 45, (10), 3413–3422.
5. Pethrick, R. A. *Progress in Polymer Science* **1997**, 22, 1–47.
6. Bamford, D.; Dlubek, G.; Lupke, T.; Kilburn, D.; Stejny, J.; Menke, T. J.; Alam, M. A. *Macromolecular Chemistry and Physics* **2006**, 207, 492–502.
7. Ranganathaiah, C.; Kumaraswamy, G. N. *Journal of Applied Polymer Science* **2009**, 111, 577–588.
8. Wastlund, C.; Schmidt, M.; Schantz, S.; Maurer, F. H. J. *Polymer Engineering and Science* **1998**, 38, (8), 1286–1294.
9. Jiang, Z. Y.; Jiang, X. Q.; Yang, Y. X.; Huang, Y. J.; Huang, H. B.; Hsia, Y. F. *Nuclear Instruments & Methods in Physics Research: Section B: Beam Interactions with Materials and Atoms* **2005**, 229, (2), 309–315.
10. Fang, Z. P.; Xu, Y. Z.; Tong, L. F. *Journal of Applied Polymer Science* **2006**, 102, (3), 2463–2469.
11. Wastlund, C.; Maurer, F. H. J. *Polymer* **1998**, 39, (13), 2897–2902.
12. Wastlund, C.; Maurer, F. H. J. *Positron Annihilation* **1997**, 255–257, 363–365.
13. Messersmith, P. B.; Giannelis, E. P. *Chemistry of Materials* **1994**, 6, (10), 1719–1725.
14. Usuki, A.; Koiwai, A.; Kojima, Y.; Kawasumi, M.; Okada, A.; Kurauchi, T.; Kamigaito, O. *Journal of Applied Polymer Science* **1995**, 55, (1), 119–123.

15. Krishnamoorti, R.; Vaia, R. A.; Giannelis, E. P. *Chemistry of Materials* **1996**, 8, (8), 1728–1734.

16. Kawasumi, M.; Hasegawa, N.; Kato, M.; Usuki, A.; Okada, A. *Macromolecules* **1997**, 30, (20), 6333–6338.

17. Chen, G.; Yao, K.; Zhao, J. *Journal of Applied Polymer Science* **1999**, 73, 425–430.

18. Burnside, S. D.; Giannelis, E. P. *Journal of Polymer Science: Part B: Polymer Physics* **2000**, 38, 1595–1604.

19. Beyer, G. *Special Chemistry* **2002**, 1–11.

20. Gorrasi, G.; Tortora, M.; Vittoria, V.; Pollet, E.; Lepoittevin, B.; Alexandre, M.; Dubois, P. *Polymer* **2003**, 44, (8), 2271–2279.

21. Fornes, T. D.; Hunter, D. L.; Paul, D. R. *Macromolecules* **2004**, 37, (5), 1793–1798.

22. Gain, O.; Espuche, E.; Pollet, E.; Alexandre, M.; Dubois, P. *Journal of Polymer Science: Part B: Polymer Physics* **2005**, 43, (2), 205–214.

23. Meneghetti, P.; Qutubuddin, S. *Thermochimica Acta* **2006**, 442, (1–2), 74–77.

24. Jung, H. M.; Lee, E. M.; Ji, B. C.; Deng, Y. L.; Yun, J. D.; Yeum, J. H. *Colloid and Polymer Science* **2007**, 285, (6), 705–710.

25. Samakande, A.; Juodaityte, J. J.; Sanderson, R. D.; Hartmann, P. C. *Macromolecular Materials and Engineering* **2008**, 293, (5), 428–437.

26. Meincke, O.; Hoffmann, B.; Dietrich, C.; Friedrich, C. *Macromolecular Chemistry and Physics* **2003**, 204, (5-6), 823–830.

27. Solomon, M. J.; Almusallam, A. S.; Seefeldt, K. F.; Somwangthanaroj, A.; Varadan, P. *Macromolecules* **2001**, 34, (6), 1864–1872.

28. Greesh, N.; Hartmann, P. C.; Cloete, V.; Sanderson, R. D. *Journal of Colloid and Interface Science* **2008**, 319, (1), 2–11.

29. Xu, M. Z.; Choi, Y. S.; Wang, K. H.; Kim, J. H.; Chung, I. J. *Macromolecular Research* **2003**, 11, (6), 410–417.

30. Bongiovanni, R.; Mazza, D.; Ronchetti, S.; Turcato, E. A. *Journal of Colloid and Interface Science* **2006**, 296, (2), 515–519.

CHAPTER 2

Theoretical background

2.1 Polymer/clay nanocomposites

2.1.1 Introduction

Polymer/clay nanocomposites (PCNs) comprise of a polymer matrix filled with nanoscale clay platelets. The reinforcement by clay takes place on a nano level, contrary to the micron scale reinforcement offered by conventional fillers. This means that clay nanofillers add value to the properties of the material they are incorporated in without necessarily compromising the processibility and mechanical properties of the material. PCNs have been reported to exhibit improved properties compared to their respective neat polymers[1-6] due to the strong interaction between the clay platelets and the polymer chains.[7-10]

2.1.2 Clay structure

Clay has become one of the most common reinforcement materials in polymers due to its abundance and low cost. Clays consist of alumino-silicate building blocks made up of silica (tetrahedral) and aluminium (octahedral). Clays are classified into two groups, namely 1:1 phylosilicates and 2:1 phylosilicates.

In 1:1 phylosilicates, also known as non-swelling clays, each platelet consists of a single sheet unit of tetrahedral silicate, which is sandwiched between alumina octahedral sheets, e.g. kaolinite, nacrite and dickite.

On the other hand, the 2:1 phylosilicates, also known as swelling clays, consist of an octahedral sheet between two tetrahedral sheets. Examples of these are smectites,

montmorillonite, rectorite, saponite and laponite. Fig. 2.1 shows the 2.1 phyllosilicate clay structure.[11]

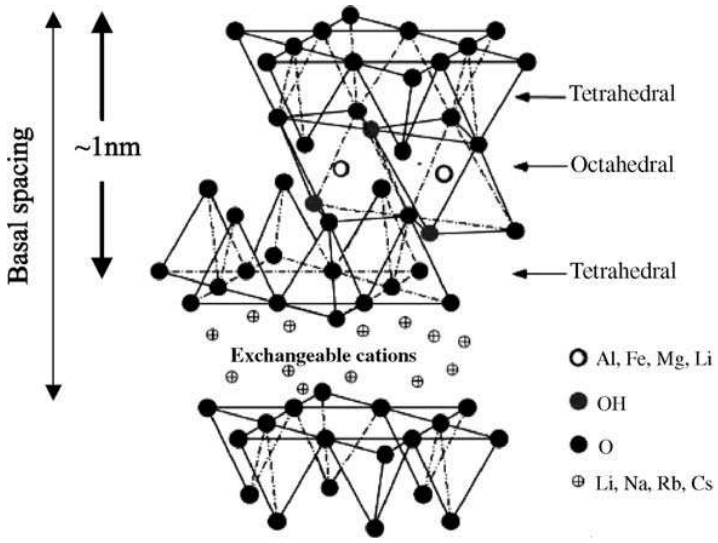

Fig. 2.1: The 2.1 phyllosilicate clay structure.

The most commonly used clays in PCNs are the 2:1 phylosilicates (swelling clay).

2.1.3 Modification of clay

In order to ensure efficient blending between the polymer matrix and the clay, the tactoids must be modified to facilitate wetting and intercalation of monomer or polymer. The three commonly used methods to modify clay are ion-exchange, adsorption and edge-wise modification.

2.1.3.1 Ion-exchange

The ion-exchange method involves the replacement of the exchangeable inorganic cations in clay galleries by positively charged species especially organic cations like quaternary alkyl ammonium cations. The number of replaceable small inorganic cations is called the cation exchange capacity (CEC). The organic cations facilitate wetting and intercalation of monomer

or polymer by reducing the surface energy and expanding the interlayer distance. Ion exchange is the most commonly used method in clay modification.[12-15]

2.1.3.2 Adsorption

Modification by adsorption utilises species that are capable of interacting with the hydrated cations in the clay galleries through dipole-dipole interactions, ion-dipole interactions, or hydrogen bonding.[16-19] The amount of material that gets adsorbs in between the galleries by this method is difficult to predict, however this method facilitates expansion of the interlayer distance.[18-20] Choi *et al.*[7,16,17,21,22] and Xu *et al.*[19,20] utilised this method and prepared a variety of exfoliated nanocomposites; at one time reporting exfoliation morphology in nanocomposites with clay content of up to 20% using 2-acrylamido-2-methyl-1-propanesulphonic acid (AMPS) to modify the clay. The use of AMPS to facilitate exfoliation was initially understood to be through ion exchange, until later studies on its interaction with clay revealed an adsorption mechanism.[18] In this study AMPS was used to modify clay by the adsorption method.

2.1.3.3 Edge modification

The hydroxyl groups on the aluminium or silica on the platelet edges react with organic species, e.g. titanates or silanes,[23,24] to yield ether linkages. In this method the interlayer distances do not change because the modification is restricted to the edges of the clay platelets.

2.1.4 Preparation of PCNs

The methods used to prepare nanocomposites include the following: in situ intercalation, melt intercalation, template synthesis, and intercalation of prepolymer from solution.

2.1.4.1 In situ intercalation polymerisation

The silicate layers are mixed with the monomer so that the monomer diffuses into the clay platelets' interspace, called galleries. This allows polymerisation to takes place in the clay

galleries so that the clay platelets are pushed apart from each other as the polymer chains grow in between the silicate layers.[8,25] In situ intercalation has received considerable attention in the academic field because it is the only method that can be used for dispersed polymerisation methods like emulsion, solution, bulk and suspension. This method also allows the synthesis of polymers that are tethered to the clay platelets. The PCNs described in this study were prepared using the in-situ intercalation method, whereby the monomers were intercalated between the clay galleries before polymerisation was initiated.

2.1.4.2 Melt intercalation

Here the polymer is heated to a temperature above its softening or melting point. The molten soft polymer is then mixed with the layered silicate to promote its diffusion into the clay galleries. For instance, Fornes *et al*. reported the preparation by blending of nanocomposites of nylon 6 nanocomposites using a twin screw extruder.[26] The melt blending method was also used to prepare amorphous PS/clay nanocomposites using a Brabender batch mixer[27]. Melt intercalation has been reported to be applicable to all polymers, and it can be implemented in industrial processes like injection molding. To date, it is the most popular procedure for preparing nanocomposites for industrial applications.[15]

2.1.4.3 Intercalation from prepolymer

Here the layered silicate layers are swollen in a solvent. The polymer is then dissolved in the solvent/clay mixture allowing the polymer to diffuse into the silicate galleries and displace the solvent. The nanocomposite is formed when the solvent molecules in the galleries are replaced by the polymer molecules[28]. Here a negative Gibbs free energy difference between the solvent intercalated platelets and the polymer matrix is required.

2.1.4.4 Intercalation by sonication

Bongiovanni has reported on the use of sonication in intercalating epoxy monomer in unmodified clay.[29] In this method the sonicator provides ultrasound energy with sufficient

energy to overcome the forces holding the platelets, thus aiding intercalation. However, this method is not commonly used.

2.1.5 PCN morphology

The dispersion of clay platelets in a polymer matrix can afford three types of morphologies: conventional polymer/clay microcomposite, intercalated polymer/clay nanocomposite, and the exfoliated polymer/clay nanocomposite depending on the extent of dispersion of clay platelets in the polymer matrix.

2.1.5.1 Microcomposite structure

In the microcomposites, clay particles are incorporated in the polymer matrix in their original form (i.e. tactoids) and limited interactions between polymer matrix and the clay platelets take place. (see Fig. 2.2(a))

2.1.5.2 Intercalated structure

When the polymer chains diffuse between the silicate layers without distorting the layered structure, but widen the interlayer distance (basal spacing), with the retention of the crystal order an intercalated structure is formed.(see Fig. 2.2(b))

2.1.5.3 Exfoliated structure

Complete distortion of the clay crystal morphology gives the exfoliated structure. The clay platelets are evenly dispersed in the polymer matrix so that strong polymer-clay interactions take place. (see Fig. 2.2(c))

The intercalated and the exfoliated morphologies have received the most focus because they impart enhanced properties to the polymer matrix properties, which are better than those imparted by the microcomposites.[30]

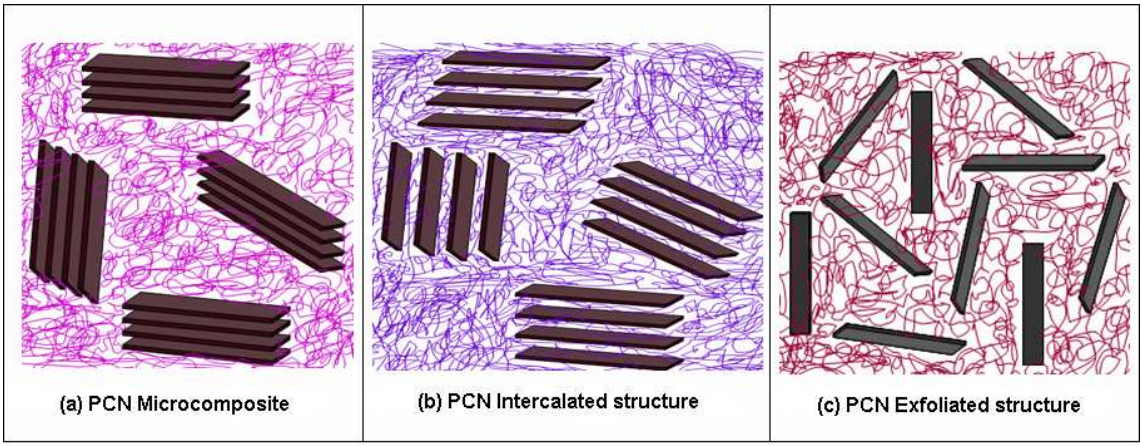

Fig. 2.2: Polymer-clay microcomposite and nanocomposite structures.

2.1.6 Analysis of PCN structure and properties

Different techniques are used to analyse PCNs in order to evaluate both their morphological structures and physical properties.[16,31-34]

2.1.6.1 X-ray diffraction

X-ray diffraction (XRD) is commonly used to study the morphological structure of PCNs. Using Bragg's law (Equation 2.1), the basal spacing of the clay platelets can be determined.

$$n\lambda = 2d\sin\theta \qquad \textbf{(2.1)}$$

where n is the order of interference, λ corresponds to the wavelength of the X-ray, θ is the measured diffraction angle and d is the interlayer distance.

Microcomposites show a significant Bragg peak. The Bragg peak of pristine clay may or may not shift to lower diffraction angles in the microcomposite. However, little or no increase in basal spacing of the microcomposites compared to that of pristine clay is observed. This is because very little or no polymer would have penetrated the galleries to increase the basal spacing.

The intercalated PCN shows an increase in the clay's basal spacing and a shift of the Bragg peak to lower angles compared to pristine clay. The changes in Bragg peak and basal spacing is used to prove the penetration of polymer molecules into the clay galleries.[5,27]

The absence of Bragg peak in PCNs has been attributed to the exfoliated structure because the platelets order has been totally disturbed by the presence of the polymer molecules.[5,27] Typical XRD results of different morphological features are shown in Fig. 2.3.[35]

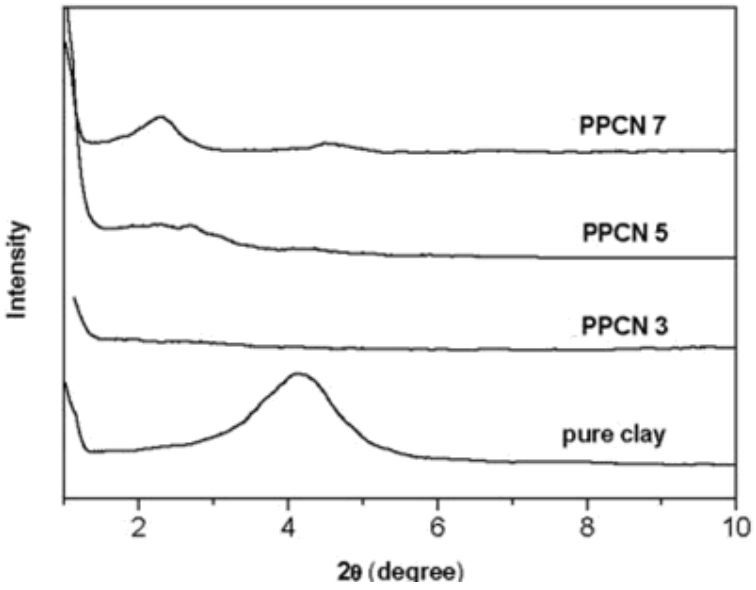

Fig. 2.3: Typical XRD results of clay and polypropylene/clay nanocomposites: PPCN 3 (exfoliated), PPCN 5 (intercalated), PPCN 7 (micromposite).

2.1.6.2 Transmission electron microscopy

Transmission electron microscopy (TEM) is a qualitative technique used to analyse PCNs structure. It is generally used in conjunction with XRD. TEM gives a pictorial description of the dispersion of the clay platelets in the polymer matrix. In a microcomposite the clay is seen in layers, which appear as dark layers; in an intercalated structure the platelets are seen in a layered structure showing small spaces between; them and in the exfoliated structure the single platelets are seen evenly dispersed in the polymer matrix, indicating that polymer has effectively broken the platelets' tactoids.[8,36] Fig 2.4 shows typical TEM results of the different morphological structures.[5]

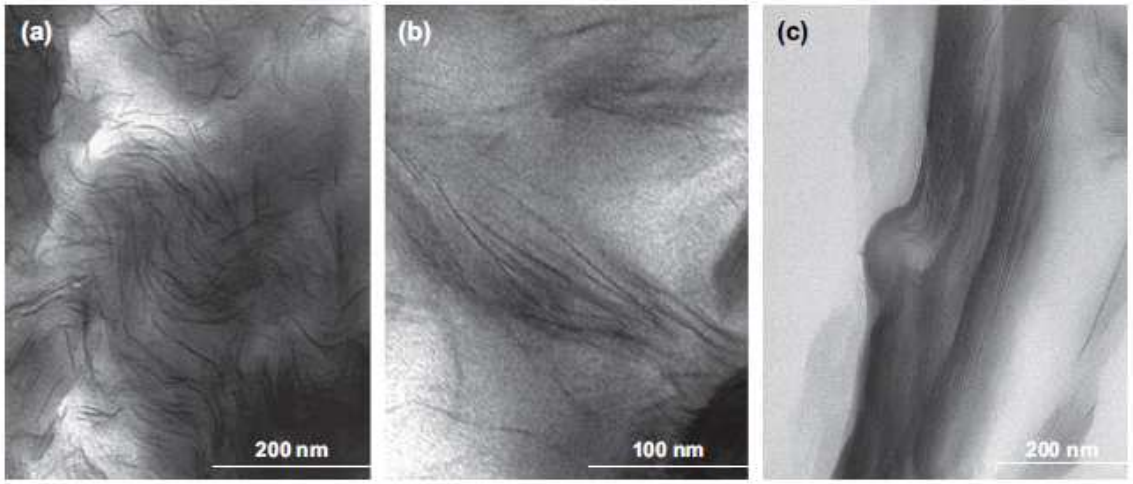

Fig. 2.4: Typical TEM images of (a) exfoliated nanocomposite (b) intercalated nanocomposite and (c) microcomposite.

In the exfoliated nanocomposite, Fig. 2.4(a), the clay platelets can be seen as finely dispersed randomly oriented and bent dark strips, while in the intercalated structure, Fig 2.4(b), the clay is seen as stacked strips oriented in the same direction and in the microcomposite, Fig. 2.4(c), the clay is not seen as dark strips but dark areas meaning the platelets still exist in their original tactoids.

2.1.6.3 Thermogravimetric analysis

Thermogravimetric analysis (TGA) is used to evaluate the thermal stability of PCNs. It measures weight loss as a function of temperature. An example is shown in Fig. 2.5. This weight loss may result from evaporation of residual moisture or solvent and even polymer degradation, especially at higher temperature. The temperature at the onset of degradation or temperature at a particular weight loss (e.g. temperature at 50% weight loss) can be deduced from a TGA thermogram. This temperature is used as an indication of thermal stability. PCNs have been reported to exhibit improved thermal stability compared to the respective polymers.[8,34,37]

From Fig. 2.5 the 80% weight loss temperature which increased with increasing clay loading can be used as an indication of improved thermal stability with increasing clay content.[6]

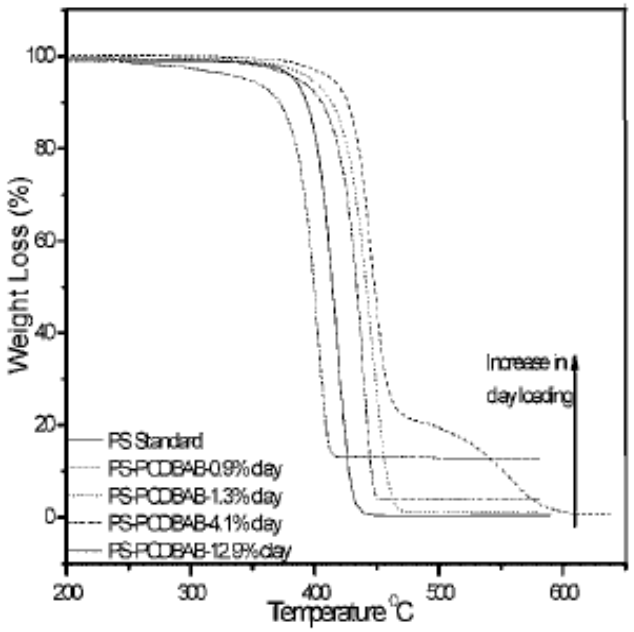

Fig. 2.5: Typical thermogravimetric thermograms of polystyrene and its nanocomposites.

2.1.6.4 Dynamic mechanical analysis

Dynamic mechanical analysis is used to measure the viscoelastic properties of PCNs. It measures the material responses to cyclic deformation as a function of temperature. It gives important information on the relaxation and molecular motions taking place in the PCN hence information such as glass transition temperature (T_g), storage and loss modulus can be obtained from this analysis.

The T_g,[5] storage modulus[20] and the temperature corresponding to the maximum of tan(δ) peak[16] have been reported to increase upon incorporation of clay into the matrix because the clay restricts the mobility of the chains[15,34].

2.1.6.5 Oscillatory tests

Oscillatory tests, e.g. frequency sweeps, are done at variable strain frequency but constant strain amplitude values. The time dependence shear behaviour of PCNs are examined, with

the short term behaviour simulated by the rapid movements at high angular frequency while the long term behaviour is given by the slow movements at low frequencies.

The rheological properties of PCNs in the molten state can be correlated to the microstructure, i.e. the structural evolution and the dispersion quality of the clay in the PCNs. PCNs have been reported to exhibit early shear thinning onsets[38,39], increased shear thinning with increasing shear rates[14,40] and high elastic moduli[40] when compared to their respective neat polymers. Fig. 2.6 is a typical result of oscillatory tests, showing the variation in complex viscosity of PCNs as a function of angular frequency, with varying clay content.[33]

The storage modulus increases with increasing clay content in the low angular frequency region yet there is no major change in the high angular frequency region due to clay's ability to align in the direction of stress at high angular frequencies.[12,14,38]

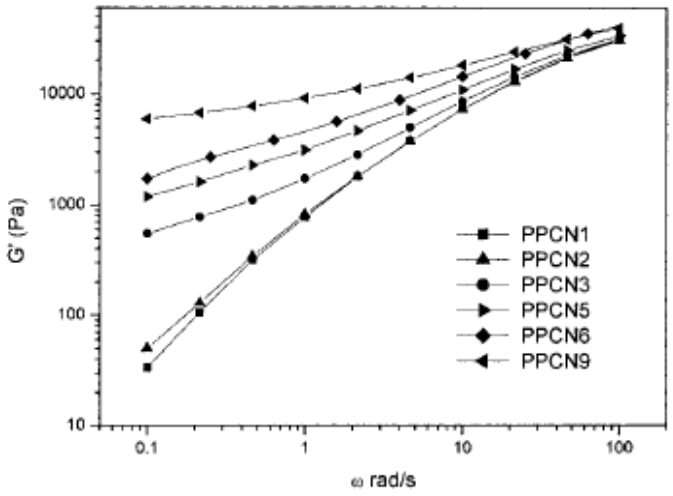

Fig. 2.6: Storage modulus of polypropylene nanocomposites as a function angular frequency.

2.2 Gas and vapour transport in and through PCN membranes

PCNs have been reported to show enhanced barrier properties compared to their respective neat polymers.[30,41-44] In this study the author studied the permeability properties of poly(AN-co-MA)/clay nanocomposities to water vapour. Transport of small molecules (penetrant)

across polymer films is generally described using three correlated parameters: the permeability coefficient (P), diffusion coefficient (D) and solubility coefficient (S).

2.2.1 Permeability

Permeability is the steady state transport of a specific penetrant across a membrane.[45,46] In this study the membrane that was used is a polymer film. The permeability coefficient (P) is dependent on the diffusion and solubility parameters of the penetrant within the polymer membrane and is given by the equation:

$$P = DS \qquad \textbf{(2.2)}$$

where D is the diffusion coefficient and S is the solubility coefficient.

The diffusion coefficient (D) is related to the mobility of the penetrant in the membrane[45-49] while the solubility coefficient (S) gives an indication of the polymer–penetrant interaction and penetrant condensability within the polymer matrix.[47,48] The P value gives an idea of the ease with which the penetrant moves through polymer membrane matrix under a pressure gradient and it is dependent on the nature of the polymer, the penetrant and the pressure gradient of the penetrant across the membrane.

The solution-diffusion model is a well accepted model to describe the general movement of penetrants (vapours and gases) across a polymer membrane, from a high pressure region to a low pressure region. In this model the movement of penetrants across a membrane is proposed to follow three steps: (1) adsorption of penetrant on the matrix surface exposed to the high pressure region, (2) diffusion of penetrant through the matrix under a concentration gradient in liquid form, and finally (3) desorption of the penetrant from the matrix surface exposed to the low pressure region.

Initially, the diffusive flux and the gas concentration at every point in the membrane vary with time. This flux at every point in the membrane is proportional to the gradient of the gas concentration. After a while a steady state condition is reached, where the penetrant

concentration in the membrane varies linearly from the high pressure region to the low pressure region and the diffusive flux is the same at every section in the membrane.

2.2.2 Diffusion behaviour in polymers

Diffusion is a kinetic term, and different diffusion models have been used to describe the movement of penetrants across polymer membrane. The diffusion models used today are based on Fick's laws of diffusion.[50] Diffusion models in polymers are classified as Fickian, non-Fickian and anomalous. The sorption data can be fitted to the following equation:

$$\frac{M_t}{M_\infty} = kt^n \qquad \textbf{(2.3)}$$

where M_t is the mass of sample after exposure to penetrant for time (t), M_∞ is the mass of sample at equilibrium penetrant uptake, k is a constant and the n value indicates the type of diffusion.

2.2.2.1 Case I diffusion (Fickian)

In case I sorption curves are dependent on the square root of time. Initially the penetrant absorption linearly increases with time until it reaches a plateau, i.e. equilibrium absorption,[51] as shown in Fig. 2.7(a). This is because the polymeric relaxations are greater than the rate of diffusion, so that the sorption equilibrium is reached faster.[47] The amount of diffused penetrant is proportional to the square root of time. The n value in Equation 2.3 is equal to 0.5 for Fickian diffusion.

2.2.2.2 Case II diffusion (Non-Fickian)

Case II diffusion is a deviation from the Fickian diffusion behaviour[52] hence its called non-Fickian. The diffusion rate here is faster than the relaxation processes and the sorption strongly depends on the swelling kinetics so that the n value in Equation 2.3 is equal to 1. The amount of diffused penetrant linearly increases with time, as shown in Fig. 2.7(b).

2.2.2.3 Anomalous diffusion

Anomolous diffusion is an intermediate between the two mechanisms mentioned above. There is a small difference between the diffusion rate and the polymeric relaxations.[53,54] Sorption is affected by the presence of pre-existing microvoids in the polymer matrix and penetrant motion is influenced by the geometric structure of the polymer. The amount of diffused penetrant is proportional to time by a power of between 0.5 and 1, ($0.5 \leq n \leq 1$).

Some of the non-Fickian behaviour cases include continual absorption, two stage sorption behaviour, sigmoid behaviour, a rapid increase in penetrant uptake accompanied with large deformations, and weight loss due to irreversible chemical or physical degradation of the material. Fig. 2.7 shows typical Fickian and non-Fickian curves.

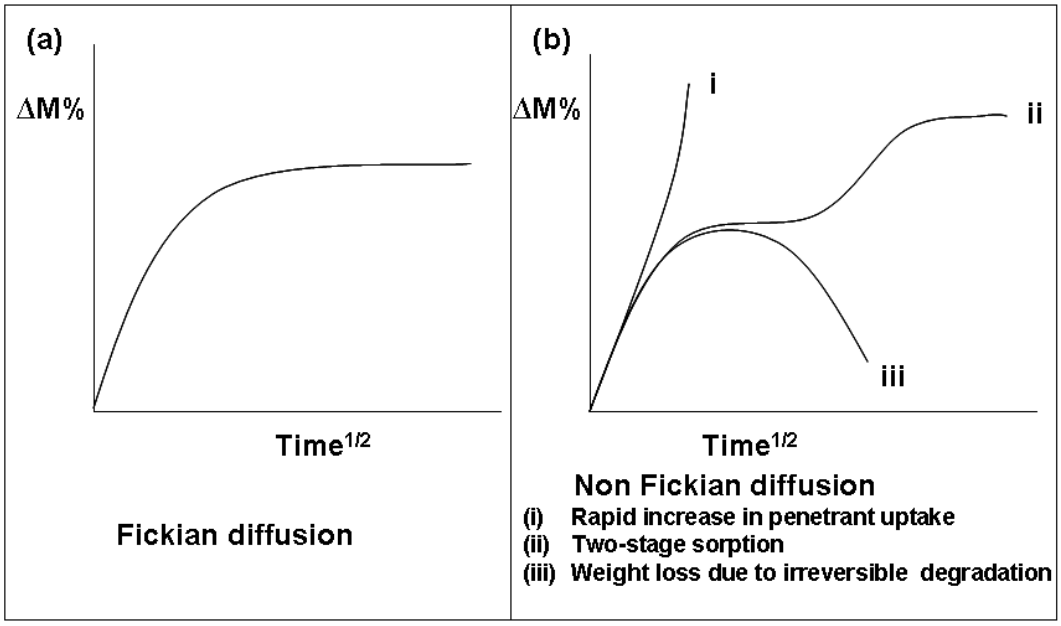

Fig. 2.7: Typical examples of diffusion behaviour curves: (a) Fickian and (b) non-Fickian.

2.2.3 Sorption in polymers

Sorption is a term that is used to describe the dissolution of penetrant in a membrane, including adsorption, absorption, trapping in microvoids, and clustering of aggregates.[46-48]

Sorption mechanisms in polymers are influenced by the forces on interactions between the polymer and the penetrant. Typical sorption isotherm curves are shown in Fig. 2.8, where the concentration is plotted as a function of pressure. Penetrant activity can be used instead of pressure and equilibrium penetrant uptake instead of concentration in obtaining these sorption isotherm curves.

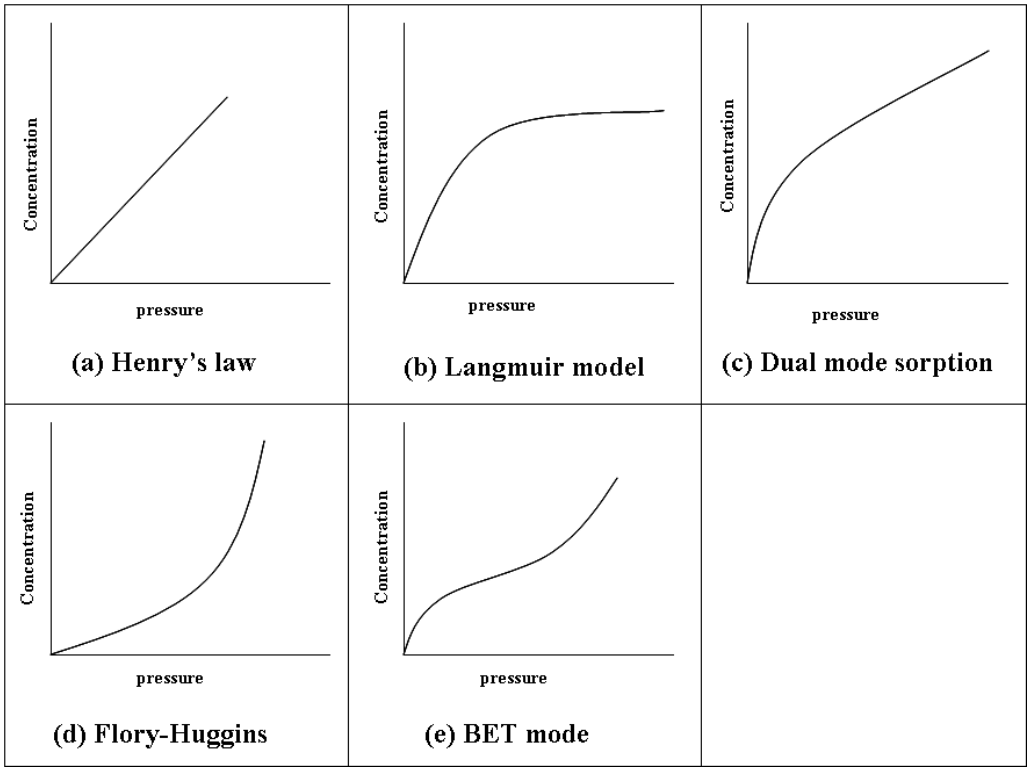

Fig. 2.8: Typical sorption isotherm curves.

2.2.3.1 Ideal sorption isotherm (Henry's law)

The sorbed penetrants are randomly dispersed within the polymer such that there is no polymer–penetrant or penetrant–penetrant interactions, hence Henry's law is observed.[47] The solubility coefficient is constant, independent of the sorbed concentration at any given temperature and the sorption isotherm is a linear relation of concentration and pressure (Fig. 2.8(a)), according to the equation:

$$C = k_D p \qquad \textbf{(2.4)}$$

where C is concentration, k_D is solubility coefficient of gas in polymer independent of concentration at a given temperature and p is the partial pressure.

2.2.3.2 Langmuir adsorption isotherm

The diffusing molecules occupy specific polymer sites, e.g. pre-existing voids or areas with high inorganic filler content,[47] hence the polymer–penetrant interactions are the dominant forces within the polymer–penetrant mixture. The diffusing penetrant will occupy all the voids and a small amount can solubilise in the polymer matrix when all sites are occupied. The penetrant concentration is then given by the eqution:

$$C_H = \frac{C'_H bp}{1+bp} \qquad \textbf{(2.5)}$$

where C'_H is a hole saturation constant and b is a hole affinity constant.

A typical Langmuir sorption isotherm curve is shown in Fig. 2.8(b).

2.2.3.3 Brunauer, Emmett and Teller sorption isotherm

The Brunauer, Emmett and Teller (BET) sorption model[55] represents a combination of the Langmuir and the Flory-Huggins, and is a characteristic model for water sorption in highly hydrophilic polymers. Initially the water molecules adsorb at specific sites and the clustering occurs at higher pressures.[56,57] The isotherm curve is sigmoidal, showing a concave shape at lower pressures and a convex shape at high pressures (see Fig. 2.8(e)).

2.2.3.4 Guggenheim-Anderson-de Boer sorption isotherm

The Guggenheim-Anderson-De Boer (GAB) sorption isotherm is considered to be a refinement of the Langmuir and the BET isotherms.[56,58] The theory behind this sorption isotherm assumes localized physical adsorption in multilayers without lateral interactions and that the sorption system consists of active sites which are identical.

2.2.3.5 Dual-mode sorption isotherm

The dual mode sorption model[47,59-61] (Fig. 2.8(c)) postulates the existence of two distinct populations of the diffusing penetrant molecules:

- Molecules dissolved in the polymer matrix by ordinary dissolution process with a concentration C_D.- the concentration of these molecules follows the Henry's law.
- Molecules trapped on specific sites, e.g. microvoids or holes, with a concentration C_H – the concentration of these molecules is given by the Langmuir equation.

The total concentration is therefore given by equation:

$$C = C_D + C_H = k_D p + \frac{C'_H bp}{1 + bp} \quad \textbf{(2.6)}$$

This model has been used extensively to explain the sorption behaviours in glassy polymers,[59-64] to explain the dependence of the solubility coefficient of glassy polymers on concentration. Recently, Feng[65] developed a new dual mode sorption model based on the (GAB) equation and the dual mode sorption because the dual mode sorption could not satisfactorily describe some of the sorption behaviours in glassy polymers, e.g. the (BET) type II sorption mode. Despite fitting well the BET type II water vapour sorption in food and natural materials, the GAB assumed all sites to be equivalent. This assumption is not applicable to glassy polymers, which are known to have two sorption sites. The new dual mode sorption fitted well the BET type II sorption in glassy polymers because it combined the dual mode sorption and the GAB equation.

2.2.3.6 Flory-Huggins sorption isotherm

The solubility coefficient increases continually with pressure because the penetrant–polymer interactions are smaller than the penetrant–penetrant interactions.[47,54] This results from either plasticisation of the polymers by the sorbed penetrant or cluster association in case of water-hydrophobic systems. The penetrant concentration in the polymer increases in a convex behaviour with increasing pressure, as shown in Fig. 2.8(d).

2.2.4 Determination of transport coefficients

2.2.4.1 Transmission measurement

The transmission measurement method measures the rate of movement of penetrant from a region of high pressure (p_1) across a membrane to a region of low pressure (p_2).[66-68] The two surfaces of the membrane are maintained at constant pressure p_1 and p_2, where $p_1 >> p_2$. After steady state is reached the amount of penetrant (Q) that crosses the membrane of area (A), and thickness (l) during time (t) can be measured and used to calculated P from the equation:

$$P = \frac{Ql}{tAp_1} \qquad \textbf{(2.7)}$$

2.2.4.2 Time lag method

The time lag method is used to calculate diffusion coefficient (D).

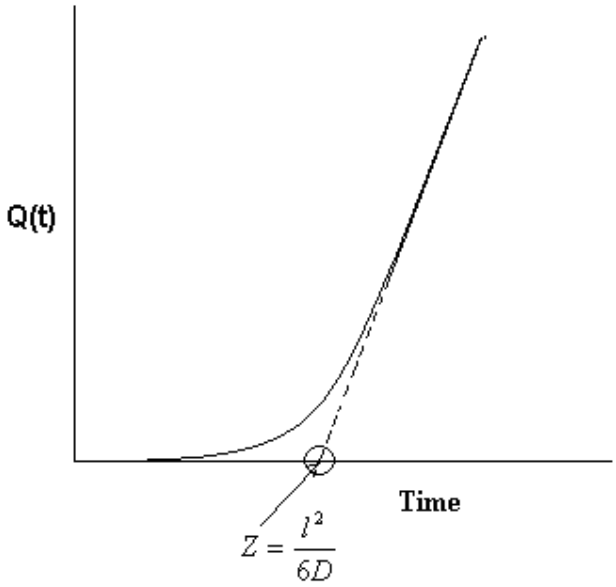

Fig. 2.9: Amount of absorbed penetrant as a function of time: Time lag method.

The penetrant is administered to one surface of the membrane and allowed to flow to the other side (p = 0) through the membrane.[66,69,70] Equation 2.8 can be used to used to calculate the amount of penetrant (Q) that passes through the membrane of thickness (l) at time (t).

$$\frac{Q(t)}{lp_1} = \frac{Dt}{l^2} - \frac{1}{6} - \frac{2}{\pi^2}\sum_{1}^{\infty}\frac{(-1)^n}{n^2}\exp\left(\frac{-Dn^2\pi^2 t}{l^2}\right) \quad \textbf{(2.8)}$$

Steady state conditions are approached as $t \to \infty$ and the exponential term of this equation becomes negligibly small so that the graph of Q(t) against time reduces to the line:

$$Q(t) = \frac{Dp_1}{l}\left(t - \frac{l^2}{6D}\right) \quad \textbf{(2.9)}$$

The time intercept of the line (Z), called the time lag, is:

$$Z = \frac{l^2}{6D} \quad \textbf{(2.10)}$$

2.2.4.3 Sorption-desorption test

A schematic representation of the sorption-desorption test is shown in Fig. 2.10.[66]

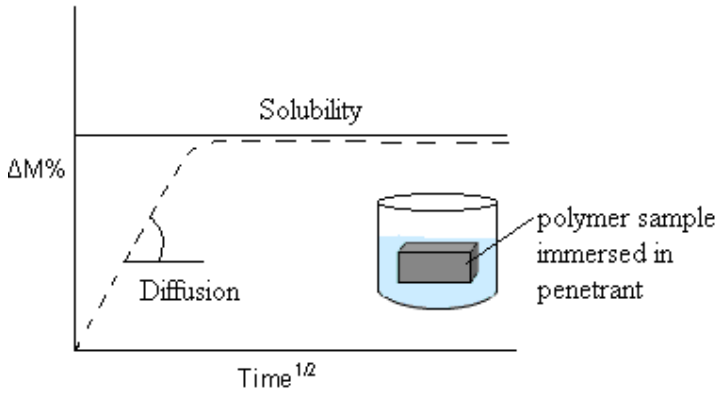

Fig. 2.10: Sorption-desorption method.

A sorption-desorption test is carried out by immersing the membrane in a penetrant.[45,66,71,72]

After a given time (t) the amount of penetrant absorbed by the sample is given by the equation: $\frac{M(t)}{M_\infty} = 1 - \sum_{n=0}^{\infty}\frac{8}{(2n+1)^2\pi^2}\exp\left[\frac{-D(2n+1)^2\pi^2 t}{l^2}\right]$ **(2.11)**

provided that D, temperature and pressure remain constant.

M_∞ is the mass of sample at equilibrium penetrant uptake

When $M(t)/M_\infty = ½$, t/l^2 is given by the equation:

$$\left(\frac{t}{l^2}\right)_{1/2} = \frac{1}{D}\left[\frac{-1}{\pi^2} In\left\{\frac{\pi^2}{16} - \frac{1}{9}\left(\frac{\pi^2}{16}\right)^9\right\}\right] \quad \textbf{(2.12)}$$

Solving this equation and expressing the final equation in terms of D we get:

$$D = \frac{0.04919}{\left[\frac{t}{l^2}\right]_{1/2}} \quad \textbf{(2.13)}$$

Using this equation we can calculate the diffusion coefficient.

The solubility coefficient is deduced using the equation:

$$S = \frac{M_\infty - M_0}{V_p.M.p} 22414 \quad \textbf{(2.14)}$$

M_0 is the initial mass of sample, M_∞ is the mass of sample at equilibrium penetrant uptake, V_p is the volume of sample, M is the molecular weight of penetrant, p is the partial pressure of penetrant and 22414 is the molar gas volume in cm^3).

In this study the transport parameters of water vapour and oxygen in poly(AN-co-MA)/clay nanocomposites were determined using the sorption-desorption test. The results were used to explain the diffusion and sorption behaviours of these penetrants in the PCNs.

2.2.5 Transport properties in PCNs

Polymers filled with nano-sized particles have been found to have lower permeability than the corresponding neat polymers.[43,70,73] The permeability decrease in nanocomposites is due to the impermeability of the clay platelets, which act as obstacles in the penetrant diffusion pathway thus creating a tortuous path.[3,69,73] The length of the tortuous path depends of the dispersion and orientation of the clay platelets within the polymeric material.[74]

Gorrasi *et al.*[43] studied the effect of clay dispersion on water vapour barrier properties of poly(ε-caprolactone)/Na-MMT nanocomposites. They prepared microcomposites using melt blending; intercalated nanocomposites using in-situ polymerisation or melt blending using modified clay; and exfoliated nanocomposites using in situ ring-opening of ε-caprolactone. They reported that the microcomposite and the intercalated had almost the same permeability parameters as those of the unfilled polymer, yet the exfoliated structure showed much lower

values. Their explanation was that in the intercalated samples the ordered structure of the inorganic component allows the diffusing molecules to jump from one site to another, whereas the exfoliated structure provides an actual barrier because there is no continuity in the inorganic phase as in the intercalated nanocomposites.

Gain *et al*. looked at the influence of morphology and polymer/clay interaction of the same polymer as that used by Gorrasi, and reported that the permeability coefficients of hydrogen, helium and carbon dioxide decreased when going from microcomposite to intercalated structure.[69]

In polypropylene/MMT nanocomposites studied by Osman *et al.*,[3] the relative permeability was found to decrease with increase in the d-spacing of the MMT. They suggest that a large d-spacing enhances exfoliation resulting in a decreased permeability coefficient. Their results were similar to those reported for polyethylene nanocomposites by Jacquelot *et al.*[70]

The decrease in the permeability value in PCNs is attributed mainly to the high decrease in diffusion due to the tortuosity factor of the clay platelets. Sorption is affected by the polymer-penetrant interaction, the amount of the amorphous material present, and the amount of clay content and its texture.

Muralidharan *et al.*[75] explained the diffusion through PCN by the free volume theory. They studied the free volume of poly(ethylene-co-vinyl acetate)/clay nanocomposites using positron annihilation and reported that the free volume in the copolymer decreases with the addition of the clay platelets, due to the restricted molecular movement of the polymer chains. However upon increasing the clay loading the relative free volume percentage increased, owing to the aggregation of the clay platelets taking place causing void formation. The reduced permeability values reported for the low clay loading were attributed to the reduced free volume available in the system.

PCNs may exhibit sorption isotherms which are either different or similar to those of neat polymers upon their incorporation.[76,77] Furthermore, clay was reported to be responsible for the increased sorption as the sorbed water increased with increasing clay content.[43]

2.3 PAN and PAN copolymers

Polyacrylonitrile (PAN) is a crystalline polymer produced by the polymerisation of acrylonitrile (AN) monomer. This polymer is a high barrier polymer; it shows remarkable barrier properties against oxygen and carbon dioxide. It has the lowest permeability of all polymers. The major drawback in its application is its poor melt processability. Its thermal degradation is reported to be 250–310 ºC, which is lower than its melting temperature of 320 ºC.[78] PAN undergoes cyclisation reactions to form a ladder structure, which is heat resistant before it melts hence, the melt processability is poor.[79-84]

2.3.1 Improving the melt processability of polyacrylonitrile

Two methods can be used to improve the melt processability of PAN: blending and copolymerization.

2.3.1.1 Blending

Blending involves the mixing of high molecular weight PAN polymers with 5–20% low molecular weight PAN which acts as plasticizers. Blending can also be done by mixing PAN with incompatible materials such as polyolefins. Although this method is effective in improving the melt processability of PAN, the desirable properties are often compromised in the process.[85]

2.3.1.2 Copolymerisation

The AN can be copolymerised with another monomer, e.g. styrene, butyl acrylate, methyl acrylate. The second monomer will alter the crystal morphology and the melting temperature of PAN by intercepting and shortening the crystallisable AN sequences, thus reducing the

number of and the average crystallite size. Simultaneously, comonomer improves the mobility by reducing close packing of the chains.

Rangarajan *et al*.[86] studied the effects of different comonomers, e.g. methyl acrylate, isobutyl acrylate and acrylamide, on the melt processability of PAN. They found that methyl acrylate enhanced the melt processability by widening the temperature and molecular weight range of processabilty. These achievements were attributed to the increased amorphous material in PAN, which disrupted its long range crystalline nature.

In 2003 Godshall *et al.*[87] reported a qualitative decrease in crystalline content with increasing methyl acrylate content in poly(acrylonitrile/methyl acrylate) copolymers. The incorporation of methyl acrylate was also found to push the stabilisation exotherm to higher temperatures while simultaneously reducing the melting temperatures, so that the temperature range over which melting and chemical transformation was sufficiently separated so that they did not overlap. Decrease in crystallinity with increasing comonomer content was also reported in the 1970s by Gupta *et al.* when they copolymerised acrylonitrile with HEMA.[88]

In the present study acrylonitrile was copolymerized with methyl acrylate, and the resulting copolymer was blended with clay to prepare nanocomposites.

References

1. Beyer, G. *Special Chemistry* **2002**, 1–11.
2. Fedullo, N.; Sorlier, E.; Sclavons, M.; Bailly, C.; Lefebvre, J. M.; Devaux, J. *Progress in Organic Coatings* **2007**, 58, (2–3), 87–95.
3. Osman, M. A.; Mittal, V.; Suter, U. W. *Macromolecular Chemistry and Physics* **2007**, 208, (1), 68–75.
4. Powell, C. E.; Beall, G. W. *Current Opinion in Solid State and Materials Science* **2006**, 10, 73–80.
5. Samakande, A.; Hartmann, P. C.; Cloete, V.; Sanderson, R. D. *Polymer* **2007**, 48, (6), 1490–1499.
6. Samakande, A.; Juodaityte, J. J.; Sanderson, R. D.; Hartmann, P. C. *Macromolecular Materials and Engineering* **2008**, 293, (5), 428–437.
7. Choi, Y. S.; Xu, M. Z.; Chung, I. J. *Polymer* **2005**, 46, (2), 531– 538.
8. Meneghetti, P.; Qutubuddin, S. *Thermochimica Acta* **2006**, 442, (1–2), 74–77.
9. Messersmith, P. B.; Giannelis, E. P. *Chemistry of Materials* **1994**, 6, (10), 1719–1725.
10. Moraes, R. P.; Santos, A. M.; Oliveira, P. C.; Souza, F. C. T.; Amaral, M.; Valera, T. S.; Demarquette, N. R. *Macromolecular Symposia* **2006**, 245–246, 106–115.
11. Sinha Ray, S.; Okamoto, M. *Progress in Polymer Science* **2003**, 28, 1539–1641.
12. Kim, T. H.; Jang, L. W.; Lee, D. C.; Choi, H. J.; John, M. S. *Macromolecular Rapid Communication* **2002**, 23, (3), 191–195.
13. Meincke, O.; Hoffmann, B.; Dietrich, C.; Friedrich, C. *Macromolecular Chemistry and Physics* **2003**, 204, (5-6), 823–830.
14. Park, B. J.; Kim, T. H.; Choi, H. J.; Lee, J. H. *Journal of Macromolecular Science: Part B: Physics* **2007**, 46, (2), 341–354.
15. Solomon, M. J.; Almusallam, A. S.; Seefeldt, K. F.; Somwangthanaroj, A.; Varadan, P. *Macromolecules* **2001**, 34, (6), 1864–1872.

16. Choi, Y. S.; Choi, M. H.; Wang, K. H.; Kim, S. O.; Kim, Y. K.; Chung, I. J. *Macromolecules* **2001**, 34, 8978–8985.

17. Choi, Y. S.; Xu, M.; Wang, K. H.; Chung, I. J. *Chemistry of Materials* **2002**, 14, 2936–2939.

18. Greesh, N.; Hartmann, P. C.; Cloete, V.; Sanderson, R. D. *Journal of Colloid and Interface Science* **2008**, 319, (1), 2–11.

19. Xu, M. Z.; Choi, Y. S.; Kim, Y. K.; Wang, K. H.; Chung, I. J. *Polymer* **2003**, 44, (20), 6387–6395.

20. Xu, M. Z.; Choi, Y. S.; Wang, K. H.; Kim, J. H.; Chung, I. J. *Macromolecular Research* **2003**, 11, (6), 410–417.

21. Choi, Y. S.; Chung, I. J. *Polymer* **2004**, 45, (11), 3827–3834.

22. Choi, Y. S.; Xu, M. Z.; Chung, I. J. *Polymer* **2003**, 44, (22), 6989–6994.

23. Voorn, D. J.; Ming, W.; van Herk, A. M. *Macromolecules* **2006**, 39, 4654–4656.

24. Wheeler, P. A.; Wang, J. Z.; Mathias, L. J. *Chemistry of Materials* **2006**, 18, 3937–3945.

25. Austin Samakande, P. C. H., Valeska Cloete and Ronald D. Sanderson. *Polymer* **2007**, 48, (6), 1490-1499.

26. T.D. Fornes, P. J. Y. H. K., D. R. Paul. *Polymer* **2001**, 42, 9929-9940.

27. Lim, Y. T.; Park, O. O. *Rheologica Acta* **2001**, 40, (3), 220–229.

28. Gunister, E.; Pestreli, D.; Unlu, C. H.; Atici, O.; Gungor, N. *Carbohydrate Polymers* **2007**, 67, (3), 358-365.

29. Bongiovanni, R.; Mazza, D.; Ronchetti, S.; Turcato, E. A. *Journal of Colloid and Interface Science* **2006**, 296, (2), 515–519.

30. Gorrasi, G.; Tortora, M.; Vittoria, V.; Pollet, E.; Alexandre, M.; Dubois, P. *Journal of Polymer Science: Part B: Polymer Physics* **2004**, 42, (8), 1466–1475.

31. Agag, T.; Koga, T.; Takeichi, T. *Polymer* **2001**, 42, (8), 3399–3408.

32. Alexandre, B.; Marais, S.; Langevin, D.; Mederic, P.; Aubry, T. *Desalination* **2006**, 199, (1–3), 164–166.

33. Li, J.; Zhou, C. X.; Wang, G.; Zhao, D. L. *Journal of Applied Polymer Science* **2003**, 89, (13), 3609–3617.

34. Zong, R.; Hu, Y.; Wang, S.; Song, L. *Polymer Degradation and Stability* **2004**, 83, (3), 423–428.

35. Zhong, W.; Qiao, X.; Sun, K.; Zhang, G.; Chen, X. *Journal of Applied Polymer Science* **2006**, 99, 1523–1529.

36. M.S. Hedenqvist, A. B., M. Ga¨llstedt, R.H. Boyd , U.W. Gedde *Composites Science and Technology* **2006**, 66, 2350–2359.

37. Wang, S. J.; Liu, L. M.; Fang, P. F.; Chen, Z.; Wang, H. M.; Zhang, S. P. *Radiation Physics and Chemistry* **2007**, 76, (2), 106–111.

38. Lee, H. M.; Park, B. J.; Choi, H. J.; Gupta, R. K.; Bhattachary, S. N. *Journal of Macromolecular Science: Part B: Physics* **2007**, 46, (2), 261–273.

39. Park, J. H.; Lee, H. M.; Chin, I. J.; Choi, H. J.; Kim, H. K.; Kang, W. G. *Journal of Physics and Chemistry of Solids* **2008**, 69, (5–6), 1375–1378.

40. Lotti, C.; Isaac, C. S.; Branciforti, M. C.; Alves, R. M. V.; Liberman, S.; Bretas, R. E. S. *European Polymer Journal* **2008**, 44, (5), 1346–1357.

41. Picard, E.; Vermogen, A.; Gerard, J. F.; Espuche, E. *Journal of Membrane Science* **2007**, 292, (1–2), 133–144.

42. Kumar, S. A.; He, Y. L.; Ding, Y. M.; Le, Y.; Kumaran, M. G.; Thomas, S. *Industrial and Engineering Chemistry Research* **2008**, 47, (14), 4898–4904.

43. Gorrasi, G.; Tortora, M.; Vittoria, V.; Pollet, E.; Lepoittevin, B.; Alexandre, M.; Dubois, P. *Polymer* **2003**, 44, (8), 2271–2279.

44. Gorrasi, G.; Vittoria, V.; Murariu, M.; Ferreira, A. D. S.; Alexandre, M.; Dubois, P. *Biomacromolecules* **2008**, 9, (3), 984–990.

45. Barr, C. D.; Giacin, J. R.; Hernandez, R. J. *Packaging Technology and Science* **2000**, 13, (4), 157–167.

46. Pino, M.; Duckett, R. A.; Ward, I. M. *Polymer* **2005**, 46, (13), 4882–4890.

47. Klopffer, M. H.; Flaconnèche, B. *Oil & Gas Science and Technology* **2001**, 56, (3), 223–244.

48. Scheichl, R.; Klopffer, M. H.; Benjelloun-Dabaghi, Z.; Flaconneche, B. *Journal of Membrane Science* **2005**, 254, (1-2), 275–293.

49. Sorrentino, A.; Gorrasi, G.; Tortora, M., *Polymer Nanocomposites.* Woodhead Publishing Limited: Cambridge, 2006.

50. Crank, J.; Park, G. S., *Diffusion in Polymers*. Academic Press: London and New York, 1968.

51. Patton, C. J.; Felder, R. M.; Koros, W. J. *Journal of Applied Polymer Science* **1984**, 29, 1095–1110.

52. Alentiev, A.; Semenova, S. I.; Sanopoulou, M. *Journal of Applied Polymer Science* **2005**, 95, 226–230.

53. Sun, Y.-M. *Polymer* **1996**, 37, (17), 3921–3928.

54. Sun, Y.-M.; Lee, H.-L. *Polymer* **1996**, 37, (17), 3915–3919.

55. Brunauer, S.; Emmett, P. H. *Journal of American Chemical Society* **1937**, 59, 1553–1564.

56. Kachrimanis, K.; Noisternig, M. F.; Griesser, U. J.; Malamataris, S. *European Journal of Pharmaceuticals and Biopharmaceuticals* **2006**, 64, 307-315.

57. Kohler, R.; Alex, R.; Brielmann, R.; Ausperger, B. *Mocromolecular symposia* **2006**, 244, 89–96.

58. Quirijns, E. J.; van Boxtel, A. J. B.; van Loon, W. K. P.; van Straten, G. *Journal of the Science of Food and Agriculture* **2005**, 85, 1805–1814.

59. Huang, J.; Cranford, R. J.; Matsuura, T.; Roy, C. *Journal of Applied Polymer Science* **2003**, 87, 2306–2317.

60. Xing, B.; Pignatello, J. *Environmental Science and Technology* **1997**, 31, 792–799.

61. Fredrickson, G. H.; Helfand, E. *Macromolecules* **1985**, 18 (11), 2201–2207.

62. Motamedian, S.; Pusch, W.; Tanioka, A.; Becker, F. *Journal of Colloid and Interface Science* **1998**, 204, (1), 135–142.

63. Tsujita, Y. *Progress in Polymer Science* **2003**, 28, (9), 1377–1401.

64. Watari, T.; Wang, H.; Kuwahara, K.; Tanaka, K.; Kita, H.; Okamoto, K. *Journal of Membrane Science* **2003**, 219, (1–2), 137–147.

65. Feng, H. D. *Polymer* **2007**, 48, (10), 2988–3002.

66. Flaconneche, B.; Martin, J.; Klopffer, M. H. *Oil & Gas Science and Technology* **2001**, 56, (3), 245–259.

67. Schult, K. A.; Paul, D. R. *Journal of Applied Polymer Science* **1996**, 61, (11), 1865–1876.

68. Sekelik, D. J.; Stepanov, E. V.; Nazarenko, S.; Schiraldi, D.; Hiltner, A.; Baer, E. *Journal of Polymer Science: Part B: Polymer Physics* **1999**, 37, (8), 847–857.

69. Gain, O.; Espuche, E.; Pollet, E.; Alexandre, M.; Dubois, P. *Journal of Polymer Science: Part B: Polymer Physics* **2005**, 43, (2), 205–214.

70. Jacquelot, E.; Espuche, E.; Gerard, J.-F.; Duchet, J.; Mazabraud, P. *Journal of Polymer Science: Part B: Polymer Physics* **2006**, 44, 431–440.

71. Ban, H.; Gui, J.; Duan, L.; Zhang, X.; Song, L.; Sun, Z. *Fluid Phase Equillibria* **2005**, 232, 149–158.

72. Dubey, V.; Kuthe, S.; Saxena, C.; Jaiswal, D. K. *Journal of Applied Polymer Science* **2003**, 88, (7), 1760–1767.

73. Arunvisut, S.; Phummanee, S.; Somwangthanaroj, A. *Journal of Applied Polymer Science* **2007**, 106, (4), 2210–2217.

74. Xu, B.; Zheng, Q.; Song, Y. H.; Shangguan, Y. *Polymer* **2006**, 47, (8), 2904–2910.

75. Muralidharan, M. N.; Kumar, S. A.; Thomas, S. *Journal Membrane Science* **2008**, 315, (1–2), 147–154.

76. Murase, S.; Inoue, A.; Miyashita, Y.; Kimura, N.; Nishio, Y. *Journal of Polymer Science: Part B: Polymer Physics* **2002**, 40, 479–487.

77. Gorrasi, G.; Tortora, M.; Vittoria, V.; Galli, G.; Chiellini, E. *Journal of Polymer Science: Part B: Polymer Physics* **2002**, 40, (11), 1118–1124.

78. Korte, S., *Polymer handbook*. John Wiley & Sons: New Jersey, 1999.

79. Saufi, S. M.; Ismail, A. F. *Membrane Science and Technology* **2002**, 24, 843–854.

80. Martin, S. C.; Liggat, J. J.; Snape, C. E. *Polymer Degradation and Stability* **2001**, 74, (3), 407–412.

81. Gupta, A. K.; Paliwal, D. K.; Bajaj, P. *Journal of Applied Polymer Science* **1998**, 70, (13), 2703–2709.

82. Guyot, A.; Bert, M.; Hamoudi, A. *European Polymer Journal* **1977**, 14, 101–107.

83. Grassie, N.; McGuchan, R. *European Polymer Journal* **1971**, 8, 257–269.

84. Bajaj, P. *Review on Macromolecular Science: Chemistry and Physics* **1997**, 37, 97.

85. Percec, E. S. *Blends of high nitrile polymers and polyolefins and method of preparation thereon*. United States Patent (4914138), 1990.

86. Rangarajan, P.; Yang, J.; Bhanu, V.; Godshall, D.; McGrath, J.; Wilkes, G.; Baird, D. *Journal of Applied Polymer Science* **2002**, 85, (1), 69–83.

87. Godshall, D.; Rangarajan, P.; Baird, D. G.; Wilkes, G. L.; Bhanu, V. A.; McGrath, J. E. *Polymer* **2003**, 44, (15), 4221–4228.

88. Gupta, A. K.; Chad, N. *European Polymer Journal* **1979**, 15, 899–902.

CHAPTER 3

Poly(acrylonitrile/methyl acrylate) copolymers: Correlation between copolymer composition and free volume properties, as determined by positron annihilation lifetime spectroscopy

3.1 Introduction

Polyacrylonitrile (PAN) exhibits remarkable properties such, as low permeability to gases, resistance to most chemicals and the ability to orient. However, it has few applications because the homopolymer has poor processability, which results from its high melting point and a high melt viscosity.[1] Copolymerisation has become the most widely used method to improve the melt processability of PAN without significantly compromising its desirable properties.[1] During copolymerization, a non crystallisable comonomer is randomly inserted along the PAN chains so that it alters the close chain packing and the long crystallisable acrylonitrile (AN) sequences, resulting in improved chain mobility and reduced crystallite size. These AN based copolymers have found applications as fiber precursors (e.g. acrylonitrile-methyl acrylate copolymers)[1-4] and packing material (e.g. styrene-acrylonitrile, acrylonitrile-methyl acrylate copolymers).[1] Copolymerisation affords materials with properties (e.g crystallinity, molecular relaxation) that are different from those of homopolymers of the respective monomers used in the copolymerisation.

Many physical properties of polymers have been related to their free volume properties, hence efforts have been made to evaluate and quantify these free volume properties in polymers.[5-9] Positron annihilation lifetime spectroscopy (PALS) has become one of the commonly used techniques to study the free volume of polymers, due to its high sensitive to sub-nanometer holes.[6,10-15] The average size of the free volume holes can be determined from the ortho positronium (o-Ps) lifetime using a simple relationship, while the o-Ps intensity can be related

to the free volume concentration. When a positronium is formed it occupies the free volume holes because they have a lower electron density and they annihilate by combination with electrons. o-Ps lifetime is the time the positronium exists in the free volume hole before it picks up an electron and annihilates. While PALS provides unique information on the polymer free volume, is not an information rich technique. It is therefore necessary to correlate PAL parameters to other polymer properties, such as crystallinity and chain mobility, in order to obtain a better understanding of the microstuctural properties of the polymer. PALS has been used extensively in the miscibility studies of polymer blends,[11,16-20] but there are only a few reports of its use for on systematic copolymers.[21-24] These reports on positron parameters in copolymers focused mainly on weakly polar polymers, emphasising the effect of polarity on positron parameters (o-Ps lifetime and o-Ps intensity). It was concluded that polarity affects o-Ps lifetime through quenching and o-Ps intensity through inhibition. These effects can lead to misleading free volume parameters. These effects were, however, not observed in strongly polar polymers like polymethyl methacrylate (PMMA).[25-27] In the present study, poly(acrylonitrile-co-methyl acrylate) (poly(AN-co-MA)), of various comonomer compositions were synthesised and their positron parameters were studied and correlated to molecular structure, crystallinity and chain mobility in terms of T_g. Earlier reports[18,19,26,28] on the use of positron parameters focused mainly on commercial polymers, but here a systematic copolymer series was synthesised and the respective samples characterised in terms of their positron parameters.

3.2 Synthesis of poly(AN/MA) random copolymers

3.2.1 Materials

Acrylonitrile and methyl acrylate monomers, both 99.5% purity, were supplied by Merck. These monomers were passed through an alumina column to remove the inhibitor prior to use. Sodium dodecyl sulphate (SDS) was supplied by Aldrich and was used without any purification. Potassium persulphate (KPS) was obtained from Aldrich and was used as received.

3.2.2 Preparation methods

Copolymers with different compositions, varying from 90% AN:10% MA to 10% AN:90% MA (mol:mol ratio) were prepared according to the procedure outlined below.

A three neck flask was charged with 150ml water and the two monomers were added in the quantities shown in Table 3.1, according to the targeted copolymer composition. For example, for sample A90 the target was a copolymer containing 90% AN and 10% MA. SDS (0.76 g; 2.6×10^{-3} mol) was added, the mixture stirred for 30 min under nitrogen. The temperature was increased to 70 ºC and, after equilibration, KPS (10 ml: 3.7×10^{-4} mol) was added to initiate the reaction. The reaction was run for 2 h at 70 °C. The resultant copolymer was precipitated in methanol and then washed with ethanol and water. Finally, the copolymer was dried under vacuum at 60 ºC to constant weight.

For all the copolymers, the SDS, water and KPS components were kept constant, but the monomer compositions were varied, as shown in Table 3.1.

3.3 Characterisation

3.3.1 Proton nuclear magnetic resonance spectroscopy

The copolymer compositions were determined using proton nuclear magnetic resonance spectroscopy (^{1}H NMR). The ^{1}H NMR spectra were determined using a Varian VXR-Unity 400 MHz instrument. The copolymers were dissolved in deuterated dimethyl sulphoxide (DMSO-d_6) and the chemical shifts were reported in parts per million (ppm), using tetramethylsilane (TMS) as a reference.

Table 3.1: Formulations used to prepare poly(AN/MA) copolymers with varying comonomer compositions.

Sample	Reagents				
	Acrylonitrile (mol)	Methyl acrylate (mol)	SDS (mol)	KPS (mol)	Water (ml)
A100	0.16	0.00	2.6×10^{-3}	3.7×10^{-4}	150
[a]A90	0.16	0.01	2.6×10^{-3}	3.7×10^{-4}	150
A80	0.13	0.03	2.6×10^{-3}	3.7×10^{-4}	150
A70	0.11	0.05	2.6×10^{-3}	3.7×10^{-4}	150
A60	0.09	0.06	2.6×10^{-3}	3.7×10^{-4}	150
A50	0.08	0.08	2.6×10^{-3}	3.7×10^{-4}	150
A40	0.06	0.10	2.6×10^{-3}	3.7×10^{-4}	150
A30	0.04	0.11	2.6×10^{-3}	3.7×10^{-4}	150
A20	0.03	0.13	2.6×10^{-3}	3.7×10^{-4}	150
A10	0.02	0.15	2.6×10^{-3}	3.7×10^{-4}	150
A00	0.00	0.16	2.6×10^{-3}	3.7×10^{-4}	150

[a] Copolymer with feed composition of 90% AN and 10% MA (mol:mol ratio)

3.3.2 Size exclusion chromatography

Size exclusion chromatography (SEC) measurements of copolymers with 60%–100% MA content were carried out on a SEC instrument comprising a Waters 717 plus autosampler,

Waters 600E system controller and Water 610 fluid unit. A Waters 410 differential refractometer was used for detection. Two PLgel 5 μm Mixed-C columns and a PLgel 5 μm guard column were used. The sample volume injected into the column was 100 μL . The oven temperature was kept at 30 ºC. THF (HPLC grade, BHT stabilised), containing 0.1 M lithium chloride (LiCl) was used as an eluent at a flow rate of 1 ml/min. Calibrations were done using narrow polystyrene standards with a molecular range of 800–2 x 10^6 g/mol, and the SEC data are reported as polystyrene equivalents.

The SEC measurements of a copolymer with 40% MA content were carried out using a Waters 150 ºC ALC/GPC chromatograph and a GRAM column. Copolymer weighing 0.02 g was dissolved in N-methyl-2-pyrrolidinone (NMP) and 0.1 M LiCl. A temperature of 70 °C and a flow rate of 1 ml/min were used.

3.3.3 Dynamic mechanical analysis

Dynamic mechanical analysis (DMA), used to determine the storage modulus (G'), loss modulus (G'') and damping factor (tan (δ)) of the copolymer films, was carried out using a MCR 501Anton Paar Rheometer in oscillatory mode, from 180 ºC to 45 ºC, at a heating rate of – 4 ºC/min, using a 25 mm diameter plate-plate geometry. All tests were done under 0.1% deformation and 10 N normal force at a frequency of 1 Hz. The samples were moulded into disk shaped films by compression at 150 ºC. The thickness of all samples was in the range 0.8–1.0 mm.

3.3.4 Positron annihilation lifetime spectroscopy measurements

All positron annihilation lifetime spectroscopy (PALS) measurements were performed at room temperature using a conventional fast-fast coincidence system with 250 ps time resolution. A 20-μCi ^{22}Na positron source, sealed in an aluminium foil, was sandwiched between two circular sample disks of 15 mm diameter and 1 mm thickness. This sample-

source sandwich was placed between two detectors of the spectrometer to acquire the lifetime spectrum. Each spectrum contained approximately a million counts accumulated, over 1–1.5 h. All spectra were analysed in three lifetime components with the help of the PATFIT programme.[29] The o-Ps lifetime results were used to obtain the mean free volume hole radius, using the empirical equation:[15]

$$\tau_3^{-1} = 2\left[1 - RR_0^{-1} + (2\pi)^{-1}\sin\left(\frac{2\pi R}{R_0}\right)\right]\left(ns^{-1}\right) \quad \textbf{(3.1)}$$

where $R_0 = R + \Delta R$ *, where* ΔR *= 1.66 Å is the thickness of the homogeneous electron layer in which the positron annihilates;* τ_3 *(ns) is the o-Ps lifetime; and R (Å) is the hole radius.*

Assuming that the probability of o-Ps formation is proportional to the low electron density regions, the o-Ps intensity (I_3) can be related to the number of free volume holes in the matrix and the fractional free volume can be determined by using the equation:

$$f_v = C \times I_3 \times V_f \quad \textbf{(3.2)}$$

where C is a constant that can be determined from independent experiment and the free volume hole size is given by: $V_f = \frac{4}{3}\pi R^3$.

The author, however, did not determine the constant C, hence the relative fractional free volume (F_{vR}) was used:

$$F_{vR} = V_f \times I_3 \quad \textbf{(3.3)}$$

The use of positron parameters in relation to free volume parameters has been reported to be justified only if there are no other chemical processes that come into play to inhibit the formation of the o-Ps.[15,24,30] This is due to the fact that if o-Ps inhibition or quenching, these processes affect the o-Ps intensity.

3.4 Results and discussion

3.4.1 Copolymer composition

^{1}H NMR data were used to calculate the copolymer composition over the entire composition range used. Fig. 3.1 shows the ^{1}H NMR spectrum of a 60% AN:40% MA copolymer (mol:mol). The spectra of some other selected copolymers are shown in Appendix A. The peak in the region 3.6–3.8 ppm is due to the resonance of the protons of the methoxy group of the MA units only, while the protons of the methylene units from both comonomer units (AN and MA) yield the broad peak at 1.6–2.2 ppm. The protons of the methine units of both comonomers yield peak in the region 2.6–3.2 ppm. The single peak at 3.3 ppm is due to traces of water in DMSO-$_{d6}$.

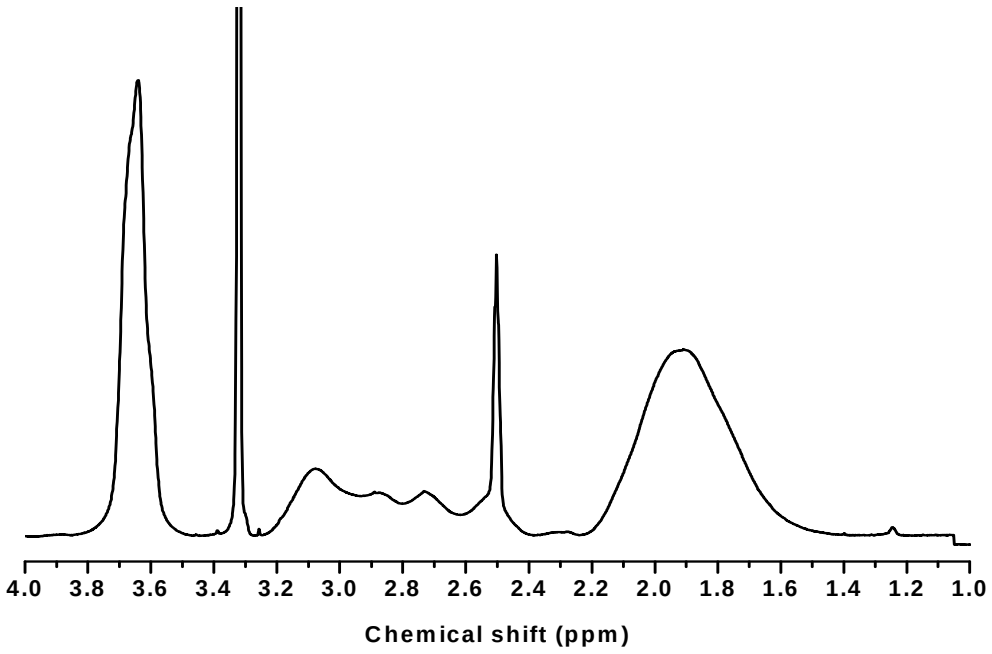

Fig. 3.1: ^{1}H NMR spectrum of poly(AN-co-MA) containing 40% MA content.

The AN compositions in different copolymers were determined [Using the calculation procedure described in Appendix B]. The results are tabulated in Table 3.2 as F_{AN}.

Table 3.2 shows that the number average molecular weight (Mn) values of the copolymers were high; they were in the range of $3.2 \times 10^5 - 4.0 \times 10^5$ g/mol and are typical of products of emulsion polymerisations. High AN content copolymers were not soluble in THF, hence their Mn values were difficult to obtain via SEC. Their Mn values are omitted, except that of the copolymer with 60% AN, the Mn of which was obtained with help from another laboratory that had the facilities to use NMP as a mobile phase in the analysis. However, because we were unable to determine all the Mn values of all high AN copolymers, the Mn value of the copolymer with 60% AN only is reported here.

Table 3.2: Poly(AN-co-MA): acrylonitrile feed composition (f_{AN}) and copolymer composition (F_{AN}), number average molecular weight (Mn), polydispersity index (PDI), particle size and Tg of copolymers of different copolymer compositions.

Sample	f_{AN}	[a]F_{AN}	Mn x 10^5 (g/mol)	[b]PDI	[c]Tg onset °C	[d]Tg (°C)
A100	1.00	1.00	-	-	101.3	101.5
A90	0.90	0.85	-	-	90.8	91.6
A80	0.80	0.77	-	-	75.0	77.6
A70	0.70	0.68	-	-	70.4	73.3
A60	0.60	0.58	3.29	5.84	67.9	70.9
A50	0.50	0.46	-	-	49.6	52.4
A40	0.40	0.36	3.82	2.76	42.7	45.7
A30	0.30	0.28	4.00	2.55	31.1	33.9
A20	0.20	0.16	3.80	3.59	24.9	26.7
A10	0.10	0.08	3.20	2.67	19.4	23.3
A00	0.00	0.00	-	-	12.3	12.5

[a]Determined using NMR, [b]PDI: Mw/Mn, [c]Temperature corresponding to the extrapolated onset of storage decrease, [d]Temperature corresponding to the extrapolated peak maximum of the loss modulus (according to ASTM D4065).

3.4.2 Glass transition temperature

The ASTM glass transition (T_g) values of the copolymers were taken from the temperatures corresponding to the maximum of the loss modulus (see Appendix C). The T_g of the copolymers decreases linearly with increasing comonomer (MA) content, as shown in Table 3.2 and Fig 3.3. The MA is randomly inserted along the AN chain thus, enhancing the molecular motions of the chains. The AN chains are stiff due to the intermolecular dipole–dipole interactions between the CN groups of monomer units causing helical conformations of the chains.[31,32] The main chains of PAN are tightly packed so that the intermolecular spaces in the amorphous regions are reduced and the triple bond of the cyanide group restricts free rotation, leading to molecular stiffness, and hence a high T_g for PAN. The introduction of the methoxy pendant group of the MA in the AN polymer chain results in disruption of the AN chain helix, causing an improvement in the chain mobility and hence the observed reduction in the T_g of the copolymer.

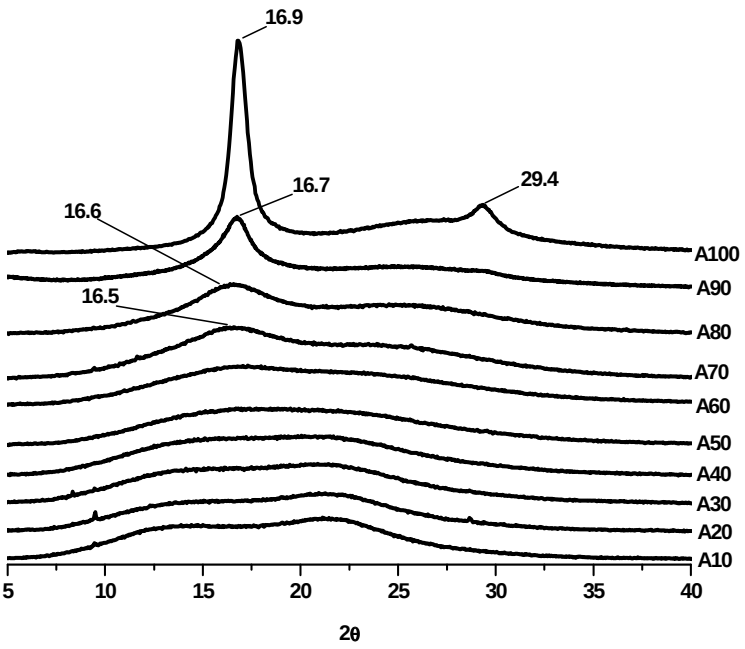

Fig. 3.2: WAXD spectroscopy results of poly(acrylonitrile-co-methyl acrylate) copolymer of different compositions (key: A90 = 90% AN:10% MA copolymer).

3.4.3 Crystallinity

The crystallinity of the copolymers was also found to decrease with increasing MA content, as is expected.[33,34] Fig. 3.2 shows the WAXD spectra of the copolymers. The homopolymer PAN shows two crystalline peaks, at $2\theta = 17°$ and $2\theta = 29°$, as is reported elsewhere.[31,33,35] The crystallinity of the PAN has been attributed to parallel alignment of molecular rods, which results from the irregular helical conformation of PAN macromolecular chains through intermolecular dipole–dipole interactions between nitrile groups.[31,32] Upon incorporation of MA these two crystalline peaks decrease in intensity and became broader until they completely diffuse. The MA causes changes in the crystalline lattice when a critical MA content is reached through interruption of the long range AN sequences as the MA becomes randomly inserted along the AN chain, due to imperfections at crystalline boundaries produced by the bulkier comonomer. As the comonomer (MA) content increases the average length of uninterrupted AN sequence decreases and so does the crystallinity of the copolymer.

3.4.4 Positron annihilation lifetime parameters and free volume

Fig. 3.3(a) is a 3D plot relating o-Ps lifetime (τ_3), T_g and MA content while Fig 3.3(b) shows a correlation between T_g and o-Ps lifetime. The positron annihilation lifetime spectra were recorded for PAN and PMA homopolymers and copolymers of different comonomer compositions at 25 ºC. The spectra could only be resolved into three components for all samples not four components as reported for other crystalline polymers[6,36]

It was found that upon addition of the MA content the ASTM T_g of the copolymers decrease while the o-Ps lifetime increase. Although the o-Ps lifetime values of the copolymers fall between those of the homopolymers, deviation from linearity (solid line) was observed. The general increase in the o-Ps lifetime followed a sigmoidal curve with increasing MA content as shown by the dotted graph in Fig. 3.3(b) whose equation was calculated using the Origin 7.5 programme ($R^2 = 0.995$).

Below 50% MA content there was a positive deviation from linearity with increasing MA content, while above 50% MA a negative deviation was observed with increasing MA content.

o-Ps lifetime shows a sharp increase with increasing MA content from 0% MA to 30% MA. This is considered to be due to the enhanced mobility of molecular chains in the amorphous regions as well as the disruption of the crystalline structure of the long range AN chain. The PAN homopolymer chains are known to be closely packed due to the polarity of the cyano group and the incorporation of MA disrupts this close packing, causing an increase in the hole size.[32,33] The crystalline phases in the crystalline copolymers are dominated by AN units so that the amorphous phase contain more MA relative to the crystalline phases. The o-Ps lifetime come from the amorphous phase hence a positive deviation in o-Ps lifetime is observed in crystalline polymers.

Between 40% and 60% MA content the increment gradient in o-Ps lifetime is reduced so that an inflection point from positive to negative deviation from linearity is observed in this region. The onset of inflection in the τ_3–T_g curve corresponds to the point at which the disappearance of crystalline peaks begins to be observed in the WAXD spectra of the copolymers. In this region it seems that the incorporation of MA has a larger effect on free volume hole number rather than the hole size since o-Ps intensity shows a positive linearity while o-Ps lifetime plateaus in this region (compare Fig 3.3 and Fig 3.4). This could be a result of the larger volume methoxy group which is incorporated randomly along the AN chain, causing an increase in the hole number rather than hole size, due to the steric hindrance effects. The loss of crystallinity at this juncture could also contribute to the increase in hole number.

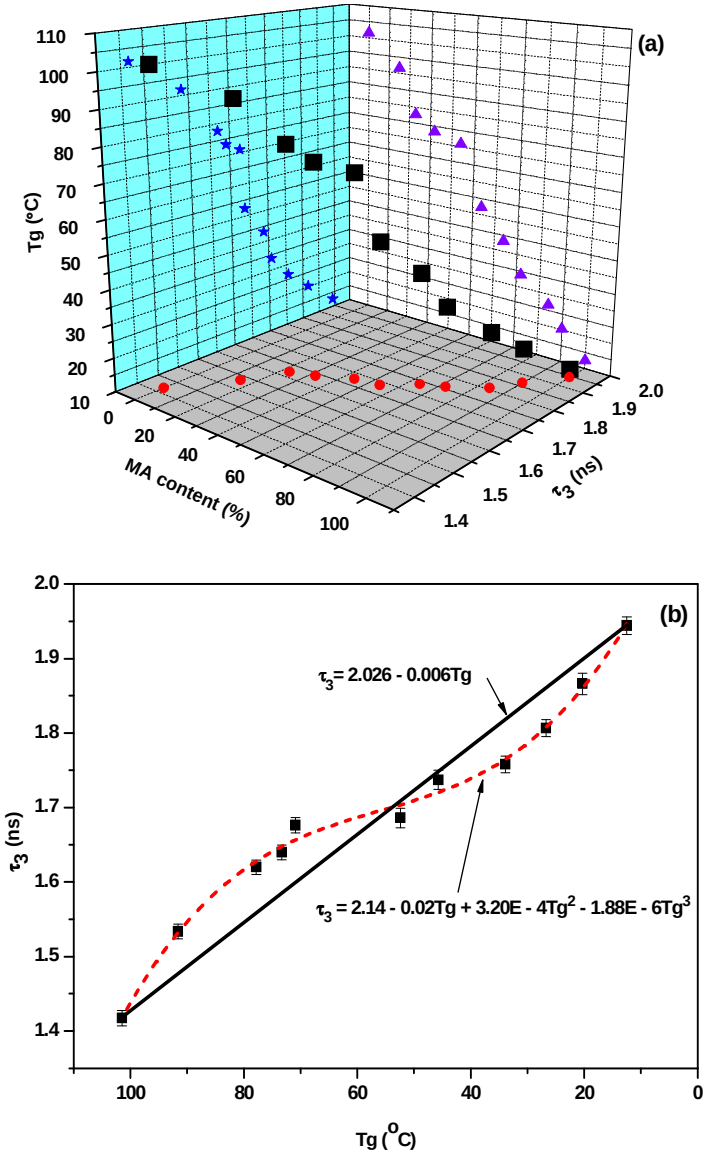

Fig. 3.3: (a) The effect of MA content on Tg and o-Ps lifetime, (b) relationship between T_g and o-Ps lifetime in different poly(acrylonitrile-co-methyl acrylate) copolymers.

From 70% to 100% MA content a negative deviation from linearity in the τ_3 value was observed. Similar negative deviations have been reported in polymer blends and attributed to the miscibility of the blends[37] due to changes in the molecular packing interactions[9] and favourable segmental conformations.[8] The negative deviation observed here could result from intermolecular interactions between the polymer chain pendant groups, which would cause enhanced molecular packing and hence a smaller free volume hole size than expected.

However, there was a sharp increase in o-Ps lifetime with increasing MA content. This is as a result of increased steric hindrances and repulsions, with an increasing number of methoxy groups having a more significant effect on the hole size. With increasing MA content the intermolecular repulsions dominate the intermolecular interactions due to decreasing cyano groups with increasing MA content, hence there is an increased distance between the chains, which might be responsible for the sharp increase in the o-Ps lifetime.

The o-Ps intensity shows a more positive linear dependence on the MA and T_g, as shown in Fig 3.4(a) and 3.4(b), up to 80% MA, after which it starts to show a slight deviation from linearity (indicated by the dotted line). However, this linear relationship deviates from the theoretical linearity (indicated by the solid line). The equations of both lines were calculated using the Origin 7.5 program ($R^2 = 0.997$).

Most of the copolymers studied here are glassy and the experiments were done below their T_g values except for the copolymer with 90% MA and polymethyl acrylate (PMA) homopolymer. It could be expected that the changes in chemical composition that enhance chain mobility would have the same effect on o-Ps intensity as those reported for temperature variations below T_g.[5] An increase in temperature in the regions of restricted mobility ($T<T_g$) results in increase in free volume hole number rather than increasing free volume hole radius. In the copolymer system used here the addition of the MA monomer caused an increase in the hole number (I_3) in the 40–60% MA content region, where the o-Ps lifetime value remained almost constant. Above 80% MA the PAL measurements were conducted above the T_g of these copolymers. As reported earlier,[5] increased temperature above T_g result in increased hole size rather than hole number hence this deviation from linearity in o-Ps volume intensity at higher MA content yet an increase in o-Ps lifetime value

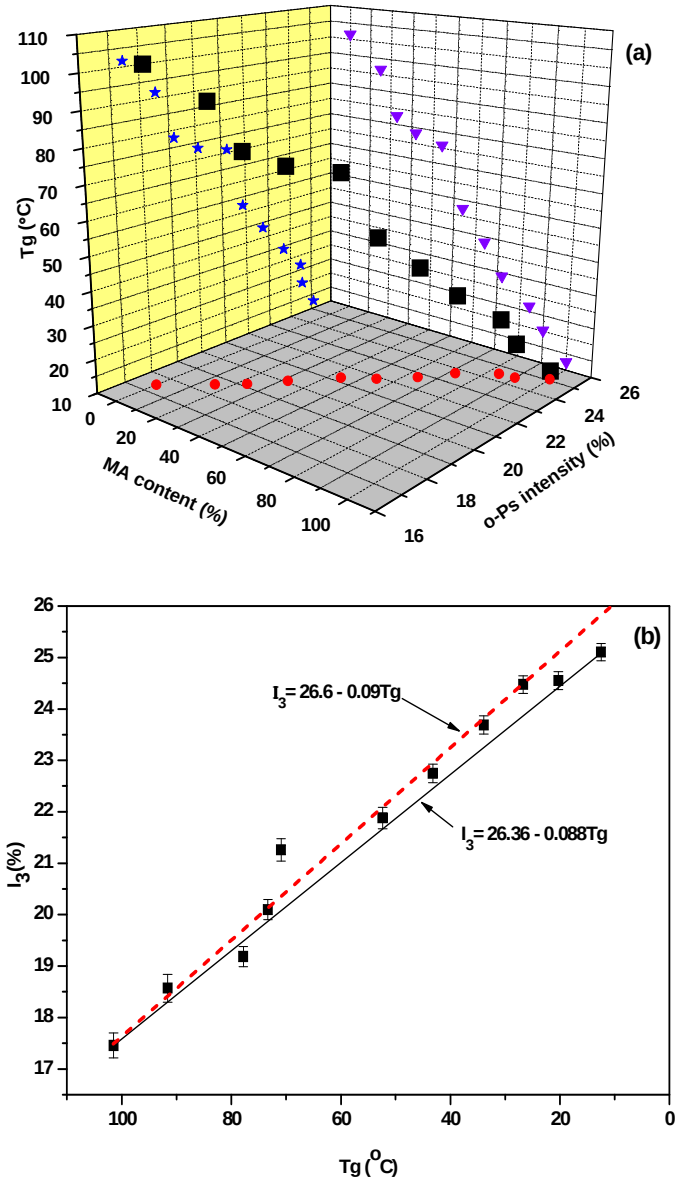

Fig. 3.4: (a) The effect of MA content on T_g and o-Ps intensity, (b) relationship between T_g and o-Ps lifetime in different poly(acrylonitrile-co-methyl acrylate) copolymers.

Equation 3 was used to calculate the relative fractional free volume in the different copolymers and the results were plotted against T_g, as shown in Fig 3.5.

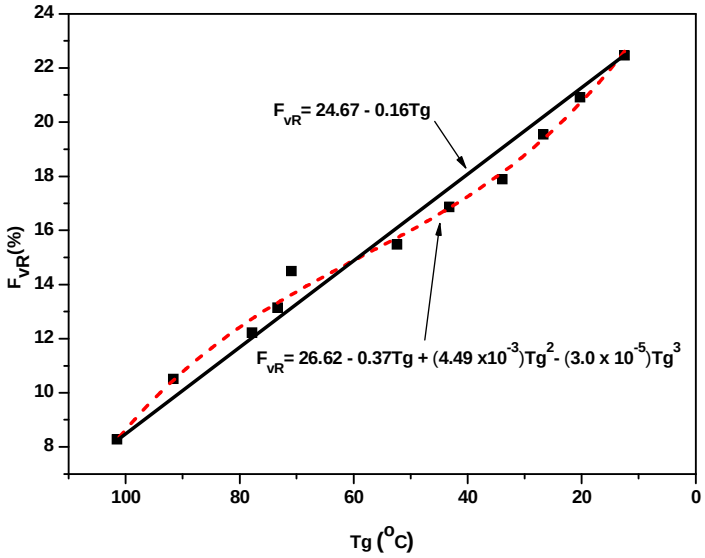

Fig. 3.5: Variation of relative free volume in poly(AN-co-MA) as a function of increasing MA content.

The fractional free volume also follows a sigmoidal curve with decreasing T_g. Below 50% MA content the fractional free volume shows a slight positive deviation from linearity while above 50% MA a negative deviation from linearity was observed for much the same reasons stated earlier.

3.5 Conclusions

The free volume properties, the crystallinity and the T_g of poly(AN-co-MA) copolymers are dependant on the copolymer compositions. WAXD spectra showed that copolymers containing more than 60% AN had a crystalline reflection peak while those with less than 60% did not exhibit any crystalline peak, thus showing total disruption of crystallinity in copolymers with high MA content. The ASTM T_g linearly decreased with increasing MA content due to the enhancement of chain mobility. The o-Ps lifetime followed a sigmoidal increase with decreasing T_g. There is a positive deviation at low MA contents and a negative deviation at high MA content. The positive deviation resulted from the differences in MA content between the amorphous and the crystalline phases. The onset of inflection coincides with the disappearance of the crystalline peak. The negative deviation could be due intermolecular interactions. This deviation of o-Ps lifetime with regard to T_g exists despite the linear relationship between the MA content and the T_g. However, there was a linear dependence between o-Ps intensity and T_g of copolymers with T_g values below measurement temperature, but the fractional free volume showed a sigmoidal increase with decreasing T_g. The increases in o-Ps lifetime (related to the free volume hole size), o-Ps intensity (related to free volume hole number), and the fractional free volume are a result of improved chain mobility and reduced packing brought about by disruptions in the AN sequence in the poly(AN/MA) copolymers upon MA incorporation.

References

1. Wu, M. M., *Encyclopedia of Polymer Science and Technology*. John Wiley and Sons: New Jersey, 2003.
2. Bortner, M. J.; Bhanu, V.; McGrath, J. E.; Baird, D. G. *Journal of Applied Polymer Science* **2004**, 93, (6), 2856–2865.
3. Bortner, M. J.; Bhanu, V. A.; McGrath, J. E.; Baird, D. G. *Polymer* **2004**, 45, (10), 3413–3422.
4. Soulis, S.; Simitzis, J. *Polymer International* **2005**, 54, (11), 1474–1483.
5. Kobayashi, Y.; Zheng, W.; Meyer, E. F.; McGervey, J. D.; Jamieson, A. M.; Simha, R. *Macromolecules* **1989**, 22, 2302–2306.
6. Dlubek, G.; Stejny, J.; Lupke, T. H.; Bamford, D.; Petters, K.; Hubner, C. H.; Alam, M. A.; Hill, M. J. *Journal of Polymer Science: Part B: Polymer Physics* **2002**, 40, 65–81.
7. Wastlund, C.; Schmidt, M.; Schantz, S.; Maurer, F. H. J. *Polymer Engineering and Science* **1998**, 38, (8), 1286–1294.
8. Liu, J.; Jean, Y. C.; Yang, H. J. *Macromolecules* **1995**, 28, (17), 5774–5779.
9. Zipper, M. D.; Simon, G. P.; Tant, M. R.; Small, J. D.; Stack, G. M.; Hill, A. J. *Polymer International* **1995**, 36, (2), 127–136.
10. Pethrick, R. A. *Progress in Polymer Science* **1997**, 22, 1–47.
11. Ranganathaiah, C.; Kumaraswamy, G. N. *Journal of Applied Polymer Science* **2009**, 111, 577–588.
12. Bamford, D.; Dlubek, G.; Lupke, T.; Kilburn, D.; Stejny, J.; Menke, T. J.; Alam, M. A. *Macromolecular Chemistry and Physics* **2006**, 207, 492–502.
13. Wang, S. J.; Liu, L. M.; Fang, P. F.; Chen, Z.; Wang, H. M.; Zhang, S. P. *Radiation Physics and Chemistry* **2007**, 76, (2), 106–111.

14. Dlubek, G.; Gupta, A. S.; Pionteck, J.; Hibler, R.; Krause-Rehberg, R.; Kaspar, H.; Lochhaas, K. H. *Polymer* **2005**, 46, 6075–6089.

15. Jean, Y. C.; Mallon, P. E.; Schrader, D. M., *Principles and Applications of Positron and Positronium Chemistry*. World Scientific: Singapore, 2003.

16. Jiang, Z. Y.; Jiang, X. Q.; Yang, Y. X.; Huang, Y. J.; Huang, H. B.; Hsia, Y. F. *Nuclear Instruments & Methods in Physics Research: Section B: Beam Interactions with Materials and Atoms* **2005**, 229, (2), 309–315.

17. Fang, Z. P.; Xu, Y. Z.; Tong, L. F. *Journal of Applied Polymer Science* **2006**, 102, (3), 2463–2469.

18. Gnther-Schade, K.; Schubert, D. W.; Faupel, F. *Macromolecules* **2002**, 35, (24), 9074–9078.

19. Gomaa, E.; Mostafa, N.; Mohsen, M.; Mahommed, M. *Journal of Materials Engineering and Perfomance* **2004**, 13, (5), 583–587.

20. Wastlund, C.; Berndtsson, H.; Maurer, F. H. J. *Macromolecules* **1998**, 31, (10), 3322–3327.

21. Qi, C. Z.; Zhang, S. H.; Wu, Y. J.; Li, H. M.; Wang, G.; Huai, G.; Wang, T. M.; Ma, J. T. *Journal of Polymer Science: Part B: Polymer Physics* **1999**, 37, (17), 2476–2485.

22. Qi, C. Z.; Zhang, S. H.; Wu, Y. J.; Zhong, Y. R.; Song, D. K.; Wang, T. M. *Journal of Polymer Science: Part B: Polymer Physics* **1999**, 37, (5), 465–472.

23. Wastlund, C.; Maurer, F. H. J. *Polymer* **1998**, 39, (13), 2897–2902.

24. Wastlund, C.; Maurer, F. H. J. *Positron Annihilation* **1997**, 255–257, 363–365.

25. Qi, C. Z.; Wei, W.; Wu, Y. J.; Zhang, S. H.; Wang, H. J.; Li, H. M.; Wang, T. M.; Yan, F. Y. *Journal of Polymer Science: Part B: Polymer Physics* **2000**, 38, (3), 435–442.

26. Wang, C. L.; Hirade, T.; Maurer, F. H. J.; Eldrup, M.; Pedersen, N. J. *Journal of Chemical Physics* **1998**, 108, (11), 4654–4661.

27. Wang, C. L.; Maurer, F. H. J.; Eldrup, M.; Pedersen, N. J. *Positron Annihilation* **1997**, 255–257, 387–389.

28. Ravindrachary, V.; Chandrashekara, A.; Sreepad, H. R.; Sreeramalu, V.; Ranganathaiah, C.; Gopal, S. *Physics Letters A* **1993**, 174, (5–6), 428–432.

29. Kirkegaard, P.; Pedersen, N. J.; Eldrup, M. *Rosie National Laboratory* **1989**, M-2740.

30. Wang, C. L.; Kobayashi, Y.; Zheng, W.; Zhang, C.; Nagai, Y.; Hasegawa, M. *Physical Review B* **2001**, 63, 1–9.

31. Gupta, A. K.; Singhal, R. P. *Journal of Polymer Science: Polymer Physics Edition* **1983**, 21, 2243–2262.

32. Henric-Olive, G.; Olive, S. *Advances in Polymer Science* **1979**, 32, 123–152.

33. Godshall, D.; Rangarajan, P.; Baird, D. G.; Wilkes, G. L.; Bhanu, V. A.; McGrath, J. E. *Polymer* **2003**, 44, (15), 4221–4228.

34. Rangarajan, P.; Yang, J.; Bhanu, V.; Godshall, D.; McGrath, J.; Wilkes, G.; Baird, D. *Journal of Applied Polymer Science* **2002**, 85, (1), 69–83.

35. Gupta, A. K.; Chad, N. *European Polymer Journal* **1979**, 15, 899–902.

36. Cheng, M.-L.; Sun, Y.-M. *Physica Status Solidi C: Current Topics in Solid State Physics* **2007**, 4, (10), 3916–3919.

37. Mostafa, N. *Journal of Applied Polymer Science* **2008**, 108, (5), 3001–3008.

CHAPTER 4

Synthesis of poly(acrylonitrile-co-methyl acrylate)/clay nanocomposites via emulsion polymerisation and their characterisation

4.1 Introduction

The enhanced mechanical properties reported for Nylon 6/clay nanocomposites,[1] relative to the neat polymer, prompted increased interest in the field of nanocomposites because of their interesting morphological structures and mechanical properties.[2,3-6] Numerous types of polymer clay nanocomposites (PCNs) have since been prepared and their properties studied in an effort to enhance the properties of the neat polymer.[7-14]

PCNs are made by dispersing nanosized clay in a polymer matrix. Incorporated clay nanofillers add value to the properties of the materials they are incorporated in, without compromising the processibility and mechanical properties of the material, due to the strong interaction occurring between the clay and the polymer matrix itself.[15]

PCNs have been reported to be lighter in weight, have enhanced flame retardancy,[11] and thermal stability,[8] as well as enhanced gas barrier properties,[16] relative to the corresponding neat polymer material.[8,9,17]

In order obtain a homogeneous system, clay is usually modified by organic modifiers, such as quartenary ammonium compounds, before polymerisation takes place. This improves compatibility between the highly hydrophilic clay and the hydrophobic polymer chains, as well as increasing the basal spacing between the clay platelets, thus promoting the penetration of monomers and polymer chains between the platelets. Choi *et al*.[18,19] reported the use of 2-acrylamido-2-methyl-1-propanesulphonic acid (AMPS) as both a reactive surfactant and a clay modifier to obtain nanocomposities with exfoliated morphology, using in situ

polymerisation methods. They reported that AMPS adsorbs on the surface of the galleries through ion exchange, by a mechanism similar to that reported for alkylammonium compounds.[20,21] In a recent paper, Greesh *et al*.[22] disagree with this mechanism, but agree that AMPS is able to penetrate the clay galleries and adsorb on the clay surface, thus increasing the basal spacing, to promote exfoliation during polymerisation.

Copolymers of acrylonitrile (AN) and methyl acrylate (MA) are commonly used as carbon fibre precursors. They are also used in packaging applications because of their outstanding gas barrier properties. Currently, poly(acrylonitrile-co-methyl acrylate) (poly(AN-co-MA)) based packaging films are readily available under the trade name Barex,[23] but no reports have been found on the preparation of nanocomposites of this copolymer.

This study focuses on the preparation of poly(AN-co-MA)/clay nanocomposites via emulsion polymerisation using AMPS as clay modifier, sodium dodecyl sulphate (SDS) as surfactant and the water soluble initiator potassium persulphate (KPS). Nanocomposites of different clay content were prepared from copolymers made using a comonomer feed ratio of 60% AN and 40% MA (mol:mol). The conversions, copolymer compositions and particle sizes of the nanocomposites were investigated as a function of clay content. Morphological characteristics, thermomechanical properties and thermal stability of these nanocomposites were also investigated with respect to clay content.

4.2 Synthesis of poly(AN-co-MA)/clay nanocomposites

4.2.1 Materials

Sodium-montmorillonite (Na-MMT) with a cationic exchange capacity (CEC) of 92.6 mequiv/100 g clay was obtained from Southern Clay Products, USA. The monomers AN and MA were supplied by Merck, and passed through an alumina column to remove the inhibitor

prior to use. The surfactant, SDS, the initiator, KPS, and the clay modifier, AMPS, were supplied by Aldrich, and used as received.

4.2.2 Preparation of nanocomposites

4.2.2.1. Preparation procedure

The procedure for the preparation of the neat copolymer was described in Section 3.2.2. An example of typical procedure used to prepare the nanocomposites is described here for the nanocomposite with 7% clay content.

Na-MMT (1.08 g) and AMPS (0.21 g: 1.0 x 10^{-3} mol) were dispersed in water and stirred for 24 h in a three-neck flask, connected to a condenser and a nitrogen inlet. A mixture of monomer (AN and MA) (3.70 ml, 1:1 v/v) was then added to the clay dispersion. The resultant mixture was stirred for 30 min, then sonicated at 30 ^{o}C for 30 min at 90% amplitude (the average sonication energy was 30000 KJ). The remaining comonomer mixture (AN/MA) (8.6 ml) was added to the sonicated mixture together with SDS (0.76 g: 2.6 x 10^{-3} mol) and the resultant emulsion stirred at room temperature for a further 30 min, under nitrogen, before increasing the reaction temperature to 70 ºC. After temperature equilibration, degassed KPS solution (10 ml: 3.7 x 10^{-4} mol) was added and the polymerisation was carried out at 70 ºC for 2 h. Formulations used for all samples that were prepared for use in this study are shown in Table 4.1 The resultant nanocomposites were precipitated in methanol and then washed with ethanol and with water. Finally, the copolymer nanocomposites were then dried under vacuum at 60 ºC to constant weight.

4.2.2.2 Polymer recovery

Samples of the nanocomposites to be used for SEC and NMR analyses were recovered from the PCNs by removing the clay as follows.

A sample of precipitated polymer (1.00 g) was dissolved in a DMF/LiCl (80 g/0.3 g) solution in a three-neck round bottom flask fitted with a condenser and nitrogen inlet. The mixture was stirred at 80 ºC under nitrogen for two days. The mixture was then centrifuged at 4400 rpm

for 60 min to separate the clay platelets from the polymer solution. The supernatant was filtered using a 0.45 μm membrane to remove any silicates and unwanted aggregates. The filtrate was then precipitated in methanol. The recovered polymer was washed with ethanol and with water, and then vacuum dried at 60 ºC.

Table 4.1: Formulations used in the preparation of AN/MA copolymer nanocomposites of varying clay content.

Reagent	Clay content				
	0%	1%	3%	5%	7%
Acrylonitrile (mol)	0.09	0.09	0.09	0.09	0.09
Methyl acrylate (mol)	0.06	0.06	0.06	0.06	0.06
Clay (g)	0	0.11	0.32	0.54	1.08
AMPS (mol)	0	9.7×10^{-5}	2.9×10^{-4}	4.8×10^{-4}	1.0×10^{-3}
SDS (mol)	2.6×10^{-3}	2.6×10^{-3}	2.6×10^{-3}	2.6×10^{-3}	2.6×10^{-3}
KPS (mol)	3.7×10^{-4}	3.7×10^{-4}	3.7×10^{-4}	3.7×10^{-4}	3.7×10^{-4}
Water (ml)	150	150	150	150	150

4.3 Characterisation

4.3.1 Dynamic light scattering

Particle sizes of the resultant emulsions were determined using dynamic light scattering (DLS). A Malvern Zetasizer ZS90 apparatus was used. The samples were first diluted to a five times dilution using deionised water before being analysed.

4.3.2 Size exclusion chromatography

The molecular masses of the neat copolymer and copolymer recovered from the nanocomposites were determined using size exclusion chromatography (SEC). This was done using a Waters 150C ALC/GPC chromatograph and a GRAM column. A copolymer sample

weighing 0.02 g was dissolved in N-methyl-2-pyrrolidinone (NMP) and 0.1 M lithium chloride (LiCl). A temperature of 70 °C and a flow rate of 1 ml/min were used.

4.3.3 Proton nuclear magnetic resonance spectroscopy

The copolymer compositions were determined using proton nuclear magnetic resonance (^{1}H NMR) spectroscopy. The NMR spectra were obtained using a Varian VXR-Unity 400 MHz instrument. The copolymers were dissolved in deuterated dimethyl sulphoxide ($DMSO_6$). The chemical shifts are reported in parts per million (ppm), using tetramethylsilane (TMS) as a reference.

4.3.4 Fourier transform infrared spectroscopy

Fourier transform infrared (FTIR) spectra were recorded using a Perkin Elmer 1650 Fourier transform infrared spectrophotometer. Thirty two scans were recorded for each sample.

4.3.5 Transmission electron microscopy

The morphology of the clay particles in the nanocomposites was directly visualized using transmission electron microscopy (TEM). Bright TEM images for the latex and the microtomed samples were recorded on a JEM 200 CX transmission electron microscope at an accelerating voltage of 120 kV. Latex samples were diluted with water and then placed on a 300-mesh copper grid. The latexes on the grids were stained using acetylaldehyde before being placed in the TEM apparatus for analysis. Thin films were made by compressing the precipitated polymer, and embedding these samples into epoxy resin, followed by curing at 55 ºC for 48 h. They were then microtomed to 100 nm thick slices with a diamond knife on a Reichert Ultra cut S ultra microtome, at room temperature. The microtomed sections were then transferred onto a 300 mesh copper grid.

4.3.6 Small angle X-ray scattering

The dispersion of the clay platelets was analysed using small angle X-ray scattering (SAXS). SAXS measurements were recorded using a rotating copper anode X-ray source (functioning at 4 kW) with a multilayer focusing 'Osmic' monochromator giving high flux (10^8 photons/s) and punctual collimation. Analyses were performed in a transmission configuration at 298 K using a 2D 'image plate' for detection. Diffraction patterns were obtained, giving the intensity as a function of the diffraction angle.

4.3.7 Dynamic mechanical analysis

Dynamic mechanical analysis (DMA), to determine the storage modulus (G'), loss modulus (G") and tan (δ) of the copolymer films, was carried out using an Anton Paar Rheometer in oscillatory mode, from 50 ºC to 120 ºC, at a heating rate of 4 ºC/min, using a 25 mm diameter plate geometry. All tests were done under 0.1% deformation and 10 N normal force at a frequency of 1 Hz. The samples were moulded into disk shaped films by compression at 150 ºC. The thickness of all samples was in the range 0.8–1.0 mm.

4.3.8 Thermogravimetric analysis

Thermogravimetric analysis (TGA) was used to determine the thermal stability of both the nanocomposites and the neat copolymers. A Perkin Elmer TGA 7 instrument was used for TGA analyses. The experiments were carried out under a nitrogen atmosphere, at a flow rate of 5 ml/min. Using a heating rate of 15 °C/min, the temperature was increased from 25 °C to 590 °C. Powder samples were used here.

4.4 Results and discussion

The results from the different analyses were use to compare the nanocomposites of different clay contents. The effect of clay incorporation was investigated by comparing the results of the nanocomposites with the results of the neat copolymer.

4.4.1 Monomer to polymer conversion

The conversions of monomer to polymer, over time were obtained using a gravimetric method. Conversions at different time intervals were monitored at, 10, 30, 60 and 90 min, by first drying the polymer latex and the weighing it. The mass of the dried yield was used to calculate conversion using equation 4.1.

$$\text{Conversion (at time t) (\%)} = \frac{Yield}{Expected} \times 100 \qquad \textbf{(4.1)}$$

$$Yield = \frac{P_D}{L}$$

where P_D is the mass of dry polymer and L is mass of latex

The neat copolymer and the nanocomposites showed relatively fast polymerisation rates and the maximum conversion was obtained after 90 min. Fig. 4.1 shows a graph of the conversion against time of the different nanocomposites. High comonomer conversions of up to 80% were obtained at all clay loadings. The comonomer conversions were similar to the conversion of the neat copolymer, meaning that the incorporation of clay did not affect the final comonomer conversion. Moraes *et al*.[24] prepared polystyrene-montmorillonite nanocomposites in miniemulsion using conventional free radical polymerisation and reported similar results, but did not give explain the results. On the other hand, results obtained here differ from those reported by Samakande *et al*.[17] for poly(styrene-co-butyl acrylate)/clay nanocomposites. They observed a decrease in the overall conversion with increasing clay loading. They reported on the use of controlled polymerisations and attributed the decrease in conversion to polymerisation to the presence of RAFT agents.

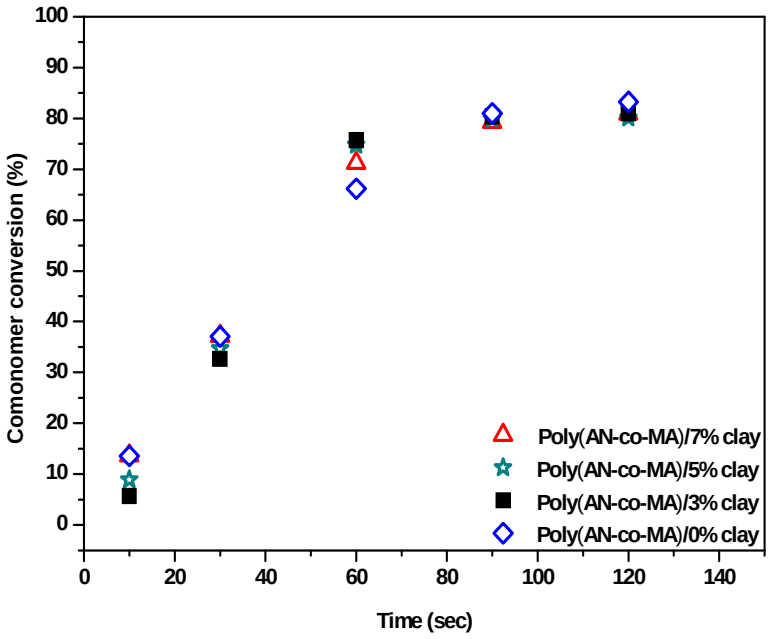

Fig. 4.1: Percentage conversion of monomer in the neat copolymer and nanocomposites as a function of reaction time.

4.4.2 Particle size

The particle sizes of the nanocomposite latexes were found to increase with increasing clay loading, as illustrated by DLS and TEM results in Fig. 4.2(a) and Fig. 4.2(b), respectively. However, particle sizes determined by TEM (approximate average particle size 48 nm for 5% clay nanocomposite) were found to be lower than those obtained by DLS (approximate average particle size 88.3 nm for 5% clay nanocomposite). This variation is due to the differences in mode of operation of the two analytical techniques. The increase in particle size with increasing clay loading could be a result of the incorporation of clay platelets inside the copolymer particles. The TEM results (Fig. 4.2(b)) suggest that the clay is incorporated into the copolymer particles even at high clay loadings because no clay platelets were observed in the aqueous continuous phase. The effect of the amount of the AMPS on the particle size was considered to be negligible due to the small amounts utilised, relative to the other monomers (see Appendix D).

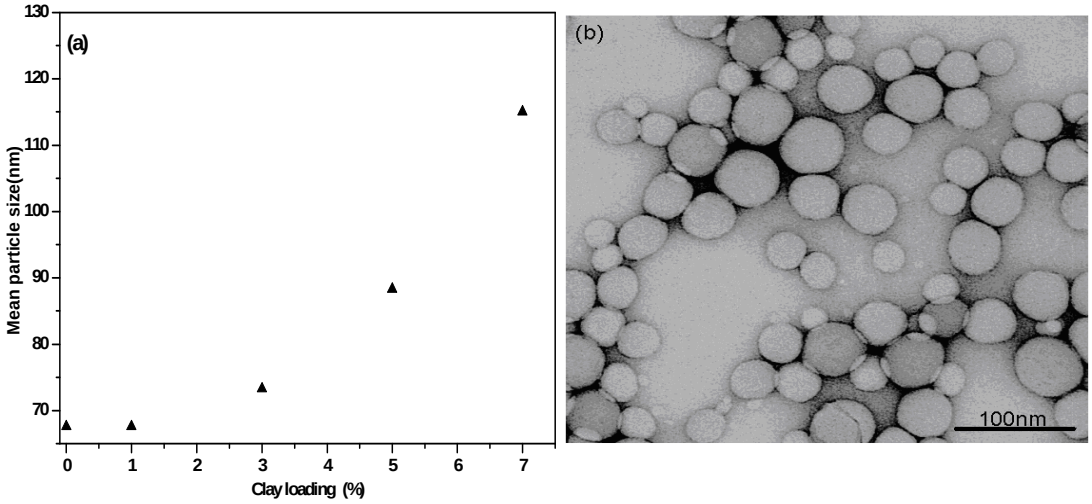

Fig. 4.2: (a) Average particle size of poly(AN-co-MA) latexes with increasing clay loadings, determined by DLS, (b) TEM image of poly(AN-co-MA)/5% clay emulsion latex.

4.4.3 Copolymer composition

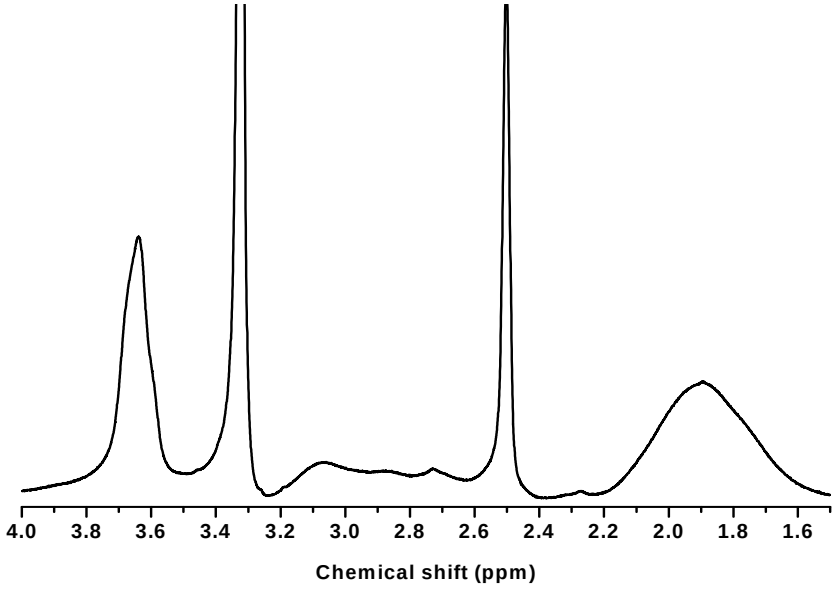

Fig. 4.3: ^{1}H NMR spectrum of the organic copolymer fraction recovered from poly(AN-co-MA)/3% clay nanocomposite (Solvent: *DMSO-$_{d6}$*)

A series of nanocomposites with different clay loadings was prepared using the same monomer feed composition of AN:MA (60%:40%, mol:mol) in all cases. Fig. 4.3 shows a ^{1}H

NMR spectrum of the polymer recovered, through reverse ion exchange, from the nanocomposite containing 3% clay. The results of the nanocomposites containing 1%, 5% and 7% clay are shown in Appendix E.

The copolymerisation of the monomers, AN and MA ($r_{AN} = 0.78 \pm 0.02$, $r_{MA} = 1.04 \pm 0.02$),[25] is known to produce random copolymers with the MA distributed along a polymer chain that is dominated by AN units in high AN containing copolymers.[26] Despite the different clay loadings used in the study for the preparation of the nanocomposites the spectra were similar. The ^{1}H NMR spectra here agree with that for random poly(AN-co-MA) reported by Wiles,[27] thus confirming that copolymerisation took place. The copolymer composition was calculated using the method outlined in Appendix B. The calculated copolymer compositions at different clay loadings are shown in Table 4.2. Fig. 4.3 shows that the peak in the region 3.6–3.8 ppm (x) was due to the resonance of the protons of the methoxy group of the MA units only while the protons of the methylene units from both comonomer units gave the broad peak at 1.6–2.2 ppm (y). The protons of the methine units of both comonomers gave a peak in the region 2.6–3.2 ppm (z). The single peak at 3.3 ppm is due to traces of water in DMSO-$_{d6}$.

The content of MA was found to be slightly higher in the copolymer than in the feed composition. A similar but unexplained result was reported by Izumi and Kitagawa.[25] It is proposed that this could be due to the slight difference in the water solubility of the two monomers. Since the AN solubility (7.2 g/100 g water) is slightly higher than that of MA (5.2 g/100 g water) the copolymer particle would contain more MA relative to AN, and hence the copolymer will contain more MA than AN.

The number average molecular weight (Mn) values decrease with increasing clay loading. Similar results are reported elsewhere.[18,28-30] Xu *et al.*[31] and Kim *et al.*[32] reported no change in the Mn value with increasing clay loading. They attributed this to crowding of the AMPS and monomers around the clay so that the overall rate of polymerisation is decreased. On the contrary, the impurities in the clay galleries are thought cause a reduction in the molecular

weight. The poly(AN-co-MA)/clay nanocomposites showed high PDI values. This could be because the propagation in clay-free micelles yields very high molecular weight products, while micelles with clay yield low molecular weight products in the clay galleries.[33] This is in agreement with the impurity proposal.

Table 4.2: Molar ratios for the copolymer compositions (F_{AN} and F_{MA}), number average molecular weight (Mn), polydispersity index (PDI), glass transition temperature (T_g), temperature at 50% weight loss (T_{50}) and the residual mass of the poly(AN-co-MA) nanocomposites.

Clay content (%)	AN units ratio in copolymers F_{AN}	MA units ratio in copolymers F_{MA}	Mn x 10^5 (g/mol)	[a]PDI	[b]Tg onset (°C)	[c]Tg (°C)	T_{50} (°C)	Residual mass (%)
7.0	0.552	0.448	1.45	8.62	68.3	71.6	409	29
5.0	0.574	0.426	1.35	9.12	68.2	71.3	407	26
3.0	0.580	0.420	1.32	6.84	68.1	70.9	404	25
1.0	0.585	0.415	1.90	9.84	68.4	71.0	401	24
0.0	0.583	0.417	3.29	5.84	67.9	70.9	400	21

[a]PDI = Mw/Mn, [b]Temperature from extrapolated onset of storage modulus decrease, [c]Temperature from the loss modulus peak (according to ASTM D4065)

4.4.4 Clay dispersion in nanocomposites

The clay dispersion in the polymer matrix and the morphologies of the different nanocomposites were studied using FTIR, SAXS and TEM.

FTIR was used to monitor the presence of inorganic clay filler and the organic polymer matrix in the nanocomposites. Fig. 4.4 shows the FTIR spectra of pure AMPS, neat poly(AN-co-MA) copolymer, a nanocomposite with 7% clay loading, and pure Na-MMT clay. Appendix F includes the FTIR spectra of the other nanocomposites with different clay loadings. The Na-

MMT spectrum exhibited typical absorption bands at 623 cm^{-1} (Al-O bending), 1046 cm^{-1} (Si-O stretching) and 3632 cm^{-1} (O-H stretching). The neat copolymer spectrum showed bands at 1167cm^{-1} (C-O stretching), 1447 cm^{-1} (C-H bending), 1738 cm^{-1} (C=O stretching), 2242 cm^{-1} (C≡N stretching),[18] and 2960 cm^{-1} (C-H stretching). The AMPS spectrum shows bands at 1550 cm^{-1} (N-H bending) and 1622 cm^{-1} (C=S vinylic stretching).[22]

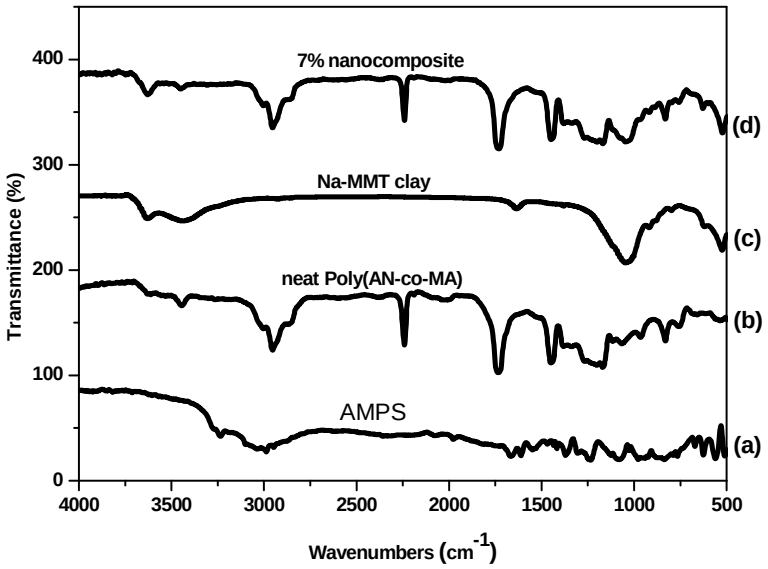

Fig. 4.4: FTIR spectra of (a) AMPS, (b) neat poly(AN-co-MA), (c) pristine clay and (d) poly(AN-co-MA)/7% nanocomposite.

The nanocomposites exhibited characteristic peaks of both the neat copolymer and the Na-MMT clay, hence demonstrating the presence of both clay and polymer matrix in the PCN. In the spectrum of the 7% nanocomposite, absorption bands at 522 cm^{-1}, 1046 cm^{-1}, 3425 cm^{-1} and 3632 cm^{-1} originated from the Na-MMT, while those at 1167 cm^{-1}, 1447 cm^{-1}, 1738 cm^{-1}, 2242 cm^{-1} and 2960 cm^{-1} originated from the copolymer. However, no typical absorption bands of the AMPS were visible in the nanocoposites because only a small quantity of AMPS was utilised. AMPS is however believed to have been incorporated in the nanocomposites, as has been reported elsewhere.[18,29]

TEM images (see Fig. 4.2(b)) of the nanocomposites' aqueous dispersions did not show any free clay particles in the aqueous phase, even at high clay loadings. These results qualitatively indicated that the clay was incorporated in the polymer particles. Microtomed samples of films of the precipitated nanocomposites confirmed that clay was incorporated into the copolymer matrix.

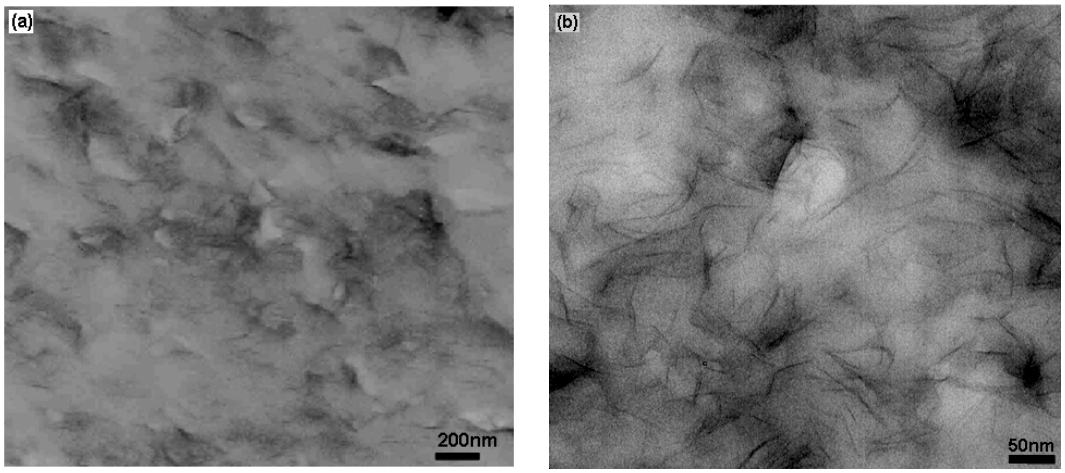

Fig. 4.5: TEM images of the extracted poly(AN-co-MA)/7% clay nanocomposite: (a) at low magnification (bar = 200 nm), showing uniform dispersion of the clay in the polymer matrix and (b) at high magnification (bar = 50 nm), showing partial exfoliation.

TEM results (Fig. 4.5(a), (b)) of the microtomed films showed that there was a homogeneous dispersion of clay in the copolymer matrix. There was no major difference in the morphology when the clay loading was increased as all samples showed partially exfoliated structures (Fig. 4.5 and Appendix G). Choi *et al.*,[18,19] on the other hand, reported exfoliated structures for nanocomposites containing up to 20% clay when excess (well above 100% cationic exchange capacity (CEC) of clay) AMPS was used as both a modifier and a reactive surfactant. Although AMPS equivalent o 100% CEC was used in this study, exfoliated PCNs were expected since it is reported that the amount of AMPS that intercalates between the clay galleries before polymerisation is independent of quantity above 100% CEC.[22] The differences between the morphological results found in the study and those reported by Choi

indicate that the morphology is dependent on the quantity of AMPS used and the polymerisation technique used.

The degree of order within the nanocomposites was measured by SAXS. The MMT clay showed a diffraction peak at 2θ = 7.7° corresponding to a d-spacing of 1.14 nm. In the nanocomposites this peak was shifted to lower diffraction peaks and the peak intensities significantly decreased, as shown in Fig. 4.6.

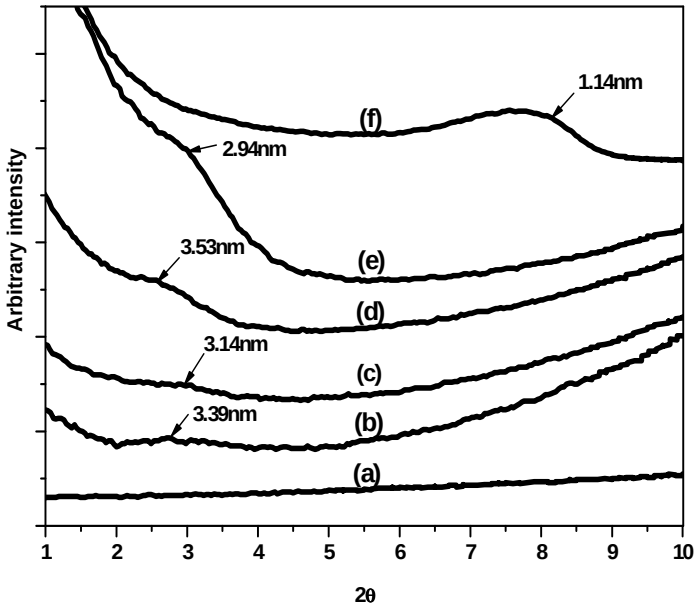

Fig. 4.6: SAXS patterns of poly(AN-co-MA)/Na-MMT nanocomposites with different clay loadings: (a) 0%, (b) 1%, (c) 3%, (d) 5%, (e) 7% and (f) pristine clay.

The SAXS results showed that the extent of exfoliation remained fairly constant regardless of the clay loading. The change in peak intensities of the nanocomposites with different clay loadings was attributed to the differences in clay content within the nanocomposites. The d-spacing of the nanocomposites showed that polymer chains were intercalated between the clay platelets although they did not cause total exfoliation.[30,34,35] This confirmed the results obtained from TEM analysis, which showed partial exfoliation in all the nanocomposites.

4.4.5 Thermomechanical properties

The dependence of storage modulus, loss modulus and damping factor on temperature is shown in Fig. 4.7(a), 4.7(b) and 4.7(c), respectively. In Fig. 4.7(a) the DMA results show enhanced storage moduli for the PCN materials compared to the pure copolymer, over the entire temperature range explored (50–120 °C), i.e. above and below the T_g. The effect of clay loading on the storage modulus was however found to be more pronounced above the T_g, as shown in Fig. 4.7(a). An increase in storage modulus is generally observed in PCNs.[18,36,37] This is attributed to the strong interaction taking place between the clay platelets and the polymer chain constituting the matrix because platelets act as rigid links between the polymer chains. The polymer chains thus confined in the vicinity of the clay platelets become immobilised. Choi *et al.*[19] and Kodgire *et al.*[37] also reported that the degree of intercalation and clay dispersion affect the storage modulus.

The onset of T_g and the (ASTM) T_g were taken from the extrapolated onset of storage modulus decrease and the extrapolated maximum loss modulus peak, respectively (see Appendix 3). The results in Fig. 4.7(b) and Table 4.2 show no major change in T_g with increasing clay loading, similar to the results reported by Moraes *et al.*[24] This is however contrary to what was reported by Agag *et al.*[38,39] for the clay nanocomposites of polyimide and polybenzoxazine. They reported that T_g increases with increasing clay loading due to the maximised adhesion between the polymer chains and the clay platelets and the polymer is more immobilised.

Fig. 4.7(c) shows that the temperature taken at the maximum damping factor peak did not shift towards higher temperatures, as could have been expected.[40] A peak shift towards high temperature with increasing clay loading is attributed to an increase in T_g caused by the hindered cooperative motion of the polymer chains.[40] However, in the present study the temperature at the maximum tan (δ) value was found to decrease with increasing clay content, as is reported elsewhere for poly(vinyl alcohol)/laponite nanocomposites.[41,42]

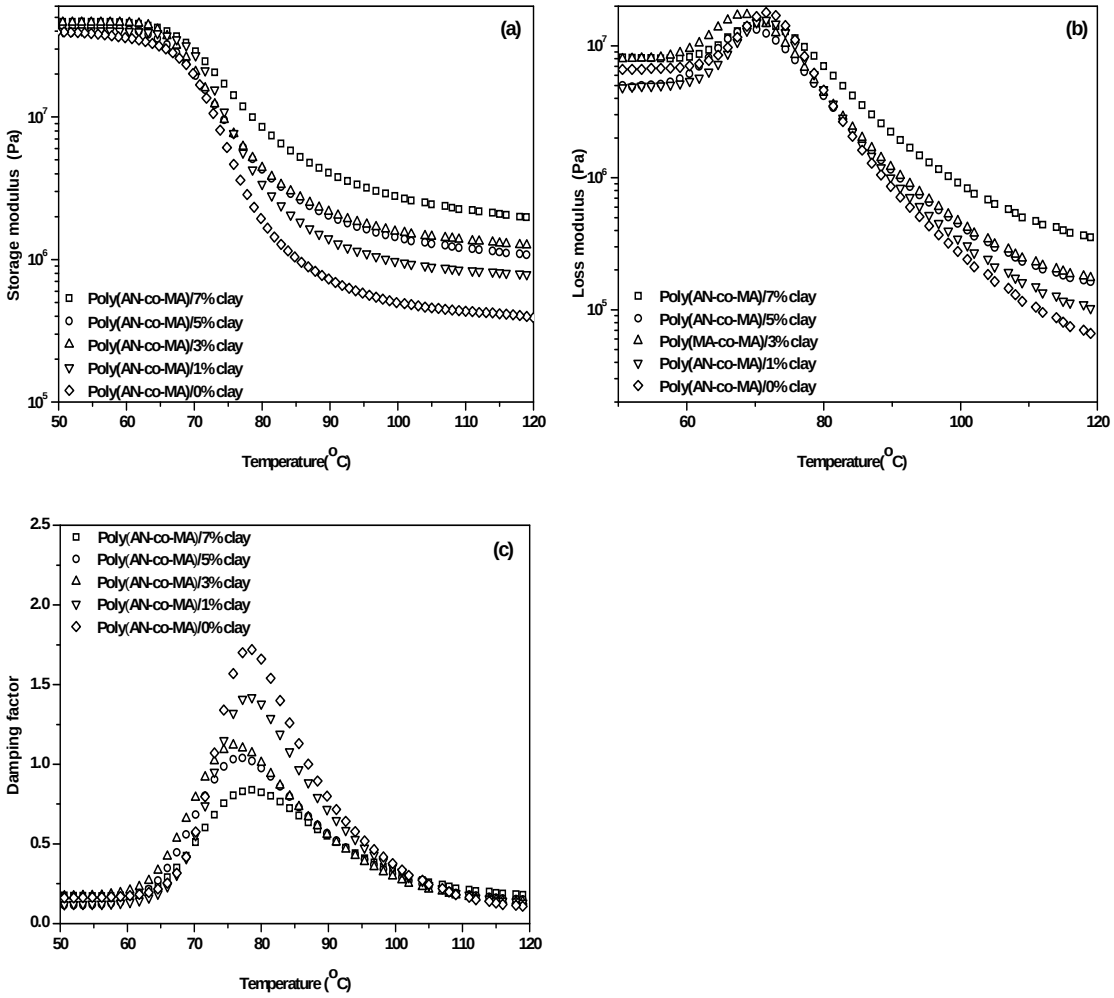

Fig. 4.7: Dynamic mechanical properties of the copolymer recovered from the nanocomposites as a function of temperature: (a) storage modulus, (b) loss modulus and (c) damping factor.

4.4.6 Thermal stability

The neat copolymer and the nanocomposites show similar thermal decomposition behaviour. The neat copolymer does not completely decompose as observed in other polymer systems.[30,34] This is due to the intra- and inter-molecular cyclisation that takes place upon heating to form ring structures, which are resistant to thermal degradation. For this reason it has been reported that pure PAN yields residue of up to 70%.[18,43] In the present study a residual mass of up to 21% for the neat copolymer was observed, indicating that the

cyclisation process does indeed take place. The probability of cyclisation decreases with increasing MA content as MA hinders the cyclisation process.[44,45]

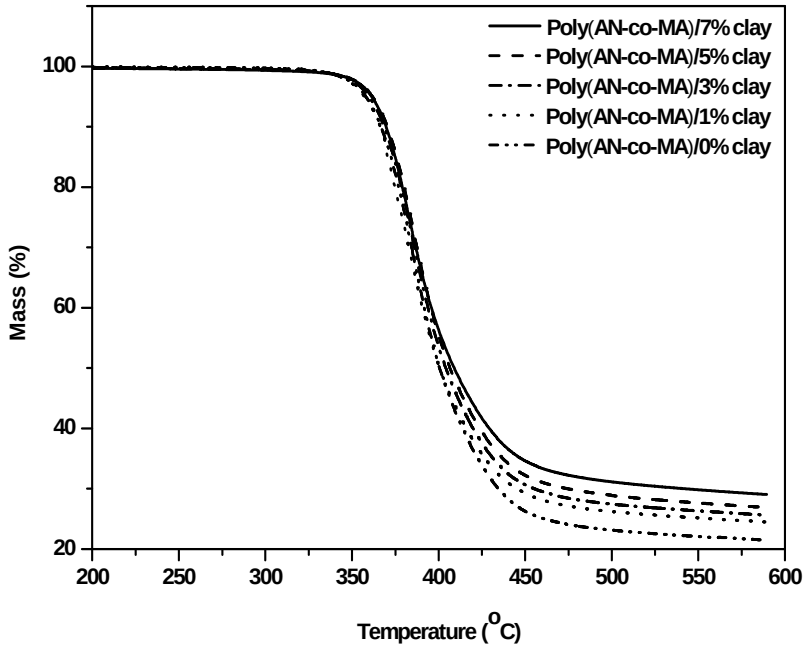

Fig. 4.8: TG thermograms for copolymer nanocomposites and neat copolymer.

Fig. 4.8 shows that the nanocomposites were slightly more thermally stable than the neat copolymer, which is in agreement with other literature reports.[8,18,29,31] The temperature at which 50% weight loss occurred increased with increasing clay loading, as shown in Table 4.2. This is explained in terms of the clay's ability to act as an insulator between the polymer and the decomposing zone. It also forms a char that acts as a mass transport barrier and restricts thermal motion of the polymer localised in the clay galleries.[8]

The residual amount of the nanocomposites also increased with increasing clay loading from 21.5% for the neat copolymer to 29.0% for the 7% nanocomposite, as shown in Table 4.2. This is due to the increasing content of the thermally stable nanosilicates that are dispersed within the polymer matrix.

4.5 Conclusions

Poly(AN-co-MA)/clay nanocomposites with up to 7% clay content were successfully prepared via batch emulsion polymerisation, using AMPS as a compatibiliser. Stable PCN latexes were obtained and the incorporation of clay showed an increase in the particle size. On the other hand, the clay did not affect the overall conversion and the copolymer composition remained fairly constant with increasing clay content. SAXS and TEM results showed that the PCNs were partially exfoliated and the morphology was found to be rather invariable with the clay loading. The PCNs produced exhibited enhanced properties, such as an increase in storage modulus and thermal stability. These improvements are due to mainly the variation in clay content in the different copolymers rather than morphological variations. The T_g values of the nanocomposites remained fairly constant, and were similar to the T_g of the neat copolymer.

References

1. Usuki, A.; Koiwai, A.; Kojima, Y.; Kawasumi, M.; Okada, A.; Kurauchi, T.; Kamigaito, O. *Journal of Applied Polymer Science* **1995**, 55, (1), 119–123.
2. Lan, T.; Pinnavaia, T. J. *Chemistry of Materials* **1994**, 6, (12), 2216–2219.
3. Jeon, H. G.; Jung, H. T.; Lee, S. W.; Hudson, S. D. *Polymer Bulletin* **1998**, 41, (1), 107–113.
4. Jacquelot, E.; Espuche, E.; Gerard, J.-F.; Duchet, J.; Mazabraud, P. *Journal of Polymer Science: Part B: Polymer Physics* **2006**, 44, 431–440.
5. Choi, Y. S.; Xu, M. Z.; Chung, I. J. *Polymer* **2005**, 46, (2), 531– 538.
6. Alexandre, B.; Marais, S.; Langevin, D.; Mederic, P.; Aubry, T. *Desalination* **2006**, 199, (1–3), 164–166.
7. Sinha Ray, S.; Okamoto, M. *Progress in Polymer Science* **2003**, 28, 1539–1641.
8. Samakande, A.; Hartmann, P. C.; Cloete, V.; Sanderson, R. D. *Polymer* **2007**, 48, (6), 1490–1499.
9. Powell, C. E.; Beall, G. W. *Current Opinion in Solid State and Materials Science* **2006**, 10, 73–80.
10. Osman, M. A.; Mittal, V.; Suter, U. W. *Macromolecular Chemistry and Physics* **2007**, 208, (1), 68–75.
11. Gilman, J. W. *Applied Clay Science* **1999**, 15, 31–49.
12. Gacitua, E. W.; Ballerini, A. A.; Zhang, J. *Maderas: Ciencia y Technologia* **2005**, 7, (3), 159–178.
13. Fedullo, N.; Sorlier, E.; Sclavons, M.; Bailly, C.; Lefebvre, J. M.; Devaux, J. *Progress in Organic Coatings* **2007**, 58, (2–3), 87–95.
14. Beyer, G. *Special Chemistry* **2002**, 1–11.
15. Meneghetti, P.; Qutubuddin, S. *Thermochimica Acta* **2006**, 442, (1–2), 74–77.

16. Tortora, M.; Gorrasi, G.; Vittoria, V.; Galli, G.; Ritrovati, S.; Chiellini, E. *Polymer* **2002**, 43, (23), 6147–6157.

17. Samakande, A.; Juodaityte, J. J.; Sanderson, R. D.; Hartmann, P. C. *Macromolecular Materials and Engineering* **2008**, 293, (5), 428–437.

18. Choi, Y. S.; Xu, M.; Wang, K. H.; Chung, I. J. *Chemistry of Materials* **2002**, 14, 2936–2939.

19. Choi, Y. S.; Xu, M. Z.; Chung, I. J. *Polymer* **2003**, 44, (22), 6989–6994.

20. Fischer, H. *Materials Science and Engineering* **2003**, 23, 763–772.

21. Leszczynska, A.; Njuguna, J.; Pielichowski, K.; Banerjee, J. R. *Thermochimica Acta* **2007**, 453, (2), 75–96.

22. Greesh, N.; Hartmann, P. C.; Cloete, V.; Sanderson, R. D. *Journal of Colloid and Interface Science* **2008**, 319, (1), 2–11.

23. Park, H. C. *Mobil Chemical Company (U.S.A)* **1985**.

24. Moraes, R. P.; Santos, A. M.; Oliveira, P. C.; Souza, F. C. T.; Amaral, M.; Valera, T. S.; Demarquette, N. R. *Macromolecular Symposia* **2006**, 245–246, 106–115.

25. Izumi, Z.; Kitagawa, H. *Journal of Polymer Science: Part A-1* **1967**, 5, 1967–1975.

26. Bhanu, V. A.; Bortner, M.; Mukundan, T.; Glass, T. E.; Baird, D. G.; McGrath, J. E. *Polymer Preprints* **2003**, 44, (1), 1067–1068.

27. Wiles, K. B.; Bhanu, V. A.; Pasquale, A. J.; Long, T. E.; McGrath, J. E. *Journal of Polymer Science: Part A: Polymer Chemistry* **2004**, 42, (12), 2994–3001.

28. Krishnamoorti, R.; Giannelis, E. P. *Macromolecules* **1997**, 30, (14), 4097–4102.

29. Xu, M. Z.; Choi, Y. S.; Kim, Y. K.; Wang, K. H.; Chung, I. J. *Polymer* **2003**, 44, (20), 6387–6395.

30. Choi, Y. S.; Choi, M. H.; Wang, K. H.; Kim, S. O.; Kim, Y. K.; Chung, I. J. *Macromolecules* **2001**, 34, 8978–8985.

31. Xu, M. Z.; Choi, Y. S.; Wang, K. H.; Kim, J. H.; Chung, I. J. *Macromolecular Research* **2003**, 11, (6), 410–417.

32. Kim, T. H.; Jang, L. W.; Lee, D. C.; Choi, H. J.; John, M. S. *Macromolecular Rapid Communication* **2002**, 23, (3), 191–195.

33. Choi, Y. S.; Chung, I. J. *Polymer* **2004**, 45, (11), 3827–3834.

34. Lee, H. M.; Park, B. J.; Choi, H. J.; Gupta, R. K.; Bhattachary, S. N. *Journal of Macromolecular Science: Part B: Physics* **2007**, 46, (2), 261–273.

35. Wu, D.; Wu, L.; Wu, L.; Zang, M. *Polymer Degradation and Stability* **2006**, 91, 3149–3155.

36. Hambir, S.; Bulakh, N.; Kodgire, P.; Kalgaonkar, R.; Jog, J. P. *Journal of Polymer Science: Part B: Polymer Physics* **2001**, 39, (4), 446–450.

37. Kodgire, P.; Kalgaonkar, R.; Hambir, S.; Bulakh, N.; Jog, J. P. *Journal of Applied Polymer Science* **2001**, 81, (7), 1786–1792.

38. Agag, T.; Koga, T.; Takeichi, T. *Polymer* **2001**, 42, (8), 3399–3408.

39. Agag, T.; Takeichi, T. *Polymer* **2000**, 41, (19), 7083–7090.

40. Priya, L.; Jog, J. P. *Journal of Polymer Science: Part B: Polymer Physics* **2003**, 41, (1), 31–38.

41. Ogata, N.; Kawakage, S.; Ogihara, T. *Journal of Applied Polymer Science* **1997**, 66, (3), 573–581.

42. Nair, S. H.; Pawar, K. C.; Jog, J. P.; Badiger, M. V. *Journal of Applied Polymer Science* **2007**, 103, (5), 2896–2903.

43. Xue, T. J.; McKinney, M. A.; Wilkie, C. A. *Polymer Degradation and Stability* **1997**, 58, 193–202.

44. Bang, Y. H.; Lee, S.; Cho, H. H. *Journal of Applied Polymer Science* **1998**, 68, (13), 2205–2213.

45. Bhanu, V. A.; Rangarajan, P.; Wiles, K.; Bortner, M.; Sankarpandian, M.; Godshall, D.; Glass, T. E.; Banthia, A. K.; Yang, J.; Wilkes, G.; Baird, D.; McGrath, J. E. *Polymer* **2002**, 43, (18), 4841–4850.

CHAPTER 5

Rheological properties of poly(acrylonitrile-co-methyl acrylate)/clay nanocomposites

5.1 Introduction

Polymer/clay nanocomposites (PCNs)[1] are relatively new materials, and have attracted great interest, both industrially and academically. Studies on properties of PCNs in comparison to their neat polymers[2-6] have revealed that the PCNs have enhanced properties, and that the morphological properties of the PCNs also contribute to the observed enhanced properties.[7] The focus in PCN studies to date has been mainly on two morphological features,[8,9] i.e. the exfoliated structure and the intercalated structure. Materials with such morphologies exhibit improved properties when compared to the neat polymers and conventional microcomposites.[10-12] In the exfoliated structure the clay platelets are finely dispersed in the polymer matrix so that there is no order within the platelets, and they exist independently. However, in the intercalated structure the polymer chains diffuse between the clay galleries but the platelets remain orderly stacked, although the spaces between the platelets increase slightly.[8,13] Since these morphological structures contribute significantly to the mechanical properties of the resultant material, various techniques have been used to characterise the morphology of PCNs, particularly transmission electron microscope (TEM) and X-ray diffraction (XRD).

Rheological properties have been correlated to the microstructure, the particle size and dispersion of the nanofiller within the polymer matrix.[14,15] Hence the rheological properties have also been used to obtain indications of the morphological structure of PCNs.[15,16] The dependence of the slope of the storage modulus curve (in log) plotted as a function of the oscillation frequency (in log) indicates the degree of dispersion of the clay nanofillers with the

polymer matrix.[17,18] At low frequencies the slopes for molten homopolymers have been found to be equal to 2.0, and equal to 0 or 1 for the solid homopolymers.[16,19,20]

Rheological properties of PCNs such as storage modulus, viscosity, and loss modulus in the molten state provide useful information on the melt properties of the PCNs. Lotti *et al.*[19] studied the rheological properties of HDPE/clay nanocomposites and found that the nanocomposites exhibited early shear thinning and an increase in the storage modulus, which improved the elasticity of the material, resulting in a stable inflated bubble during film blowing. An increase in shear thinning behaviour with increasing clay content has also been reported.[19,21] The increased shear thinning and the shifting of the onset of shear thinning to lower frequencies in nanocomposites have been attributed to the ability of the clay platelets to align along the direction of shear under high shear rates.[3,21,22]

This study describes rheological studies of poly(acrylonitrile-co-methyl acrylate)/clay nanocomposites (poly(AN-co-MA/clay) with different clay contents, prepared via emulsion polymerization, using 2-acrylamido-2-methyl-1-propanesulphonic acid (AMPS) as the clay compatibiliser. Although some rheological properties have been reported for the neat poly(AN-co-MA) copolymer, they focused on low molecular weight products made via solution polymerisation.[23-25] The focus is now on the impact of clay incorporation on the melt flow properties such as storage modulus, complex viscosity, relaxation behaviour and shear thinning, as well as evaluating the thermal stability of these PCNs.

5.2 Synthesis of poly(AN-co-MA)/clay nanocomposites

5.2.1 Materials

The materials used for the preparation of these nanocomposites were described in Section 4.2.1.

5.2.2 Preparation of nanocomposites

The procedure used for the preparation of the poly(AN-co-MA)/clay nanocomposites was described in Section 4.2.2 and the preparation of the neat copolymer in Section 3.2.2.

5.3 Analyses

Most of the details pertaining to the characterisation of the nanocomposites used in this study were described in Chapter 4. The procedures used in linear rheology and Fourier transform infrared (FTIR) analyses are described here.

5.3.1 Frequency sweep test

Frequency sweep measurements were performed using a Physica MCR 501 in oscillatory mode, with parallel plate geometry (25 mm diameter). The measurements were carried out at 180 °C, using an angular frequency range of 100–0.01 rad/sec, under a 10 N normal force. A constant strain of 0.1% was used, which is within the linear viscoelastic (LVE) range. Before conducting the measurements the samples were moulded into circular discs at 150 °C. The disc samples were 40 mm in diameter and the sample thickness in the range 0.8–1.2 mm.

5.3.2 Fourier transform infrared

Fourier transform infrared (FTIR) spectra were recorded using a Perkin Elmer 1650 Fourier transform infrared spectrophotometer. Thirty two scans were recorded for each sample. Circular disc samples, approximately 10 mm in diameter, made by pressing the polymer samples at 150 ºC, were used in this analysis.

5.4 Results and discussion

5.4.1 Characteristics of nanocomposites

The nanocomposites produced were partially exfoliated, as evident from TEM and SAXS results in Fig. 5.1(a) and Fig. 5.1(b), respectively

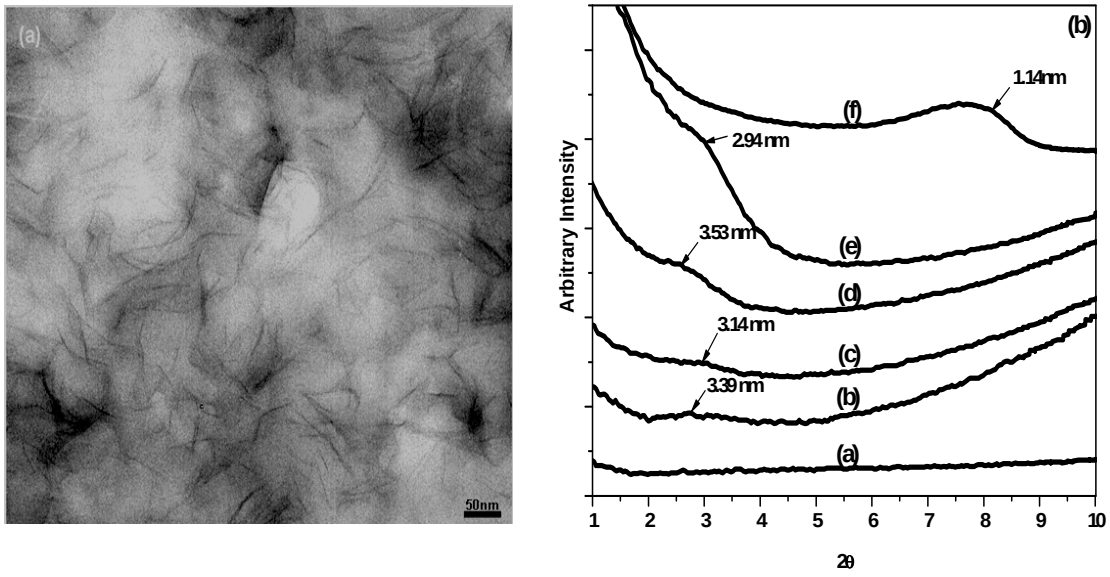

Fig. 5.1: (a) TEM image of a poly(AN-co-MA)/7% clay nanocomposite and (b) SAXS results for: (a) neat poly(AN-co-MA), (b) 1% clay nanocomposite, (c) 3% nanocomposite, (d) 5% nanocomposite, (e) 7% nanocomposite, and (f) pristine clay.

TEM images give a visual representation of the dispersion of the clay platelets within the polymer matrix. The platelets are clearly seen as dark stripes, showing the extent of exfoliation. Fig. 5.1(a) and Appendix 7 show that the platelets are partially exfoliated within the polymer matrix and finely dispersed throughout the polymer matrix irrespective of the clay content. TEM results are supported by SAXS results. Fig. 5.1(b) shows that the peak in the Na-MMT ($2\theta = 7.7°$, $d = 1.14$ nm) shifts to smaller angles, indicating an increase in the d-spacing between the clay sheets, up to 3.5 nm. The increase in peak intensity in the

nanocomposites with increasing clay content was attributed to the increase in clay content, while the extent of exfoliation remained almost the same for the different clay contents studied. Both the TEM results and the SAXS results showed that the PCNs were only partially exfoliated.

Table 5.1 tabulates the number average molecular weight, the storage modulus and complex viscosity at angular frequency of 100 s^{-1}, for poly(AN-co-MA) copolymer with different clay loadings.

Table 5.1: Number average molecular weight (Mn), polydespersity index (PDI), storage modulus (G') and the complex viscosity at 100 s^{-1}, of poly(AN-co-MA)/clay nanocomposites

Sample	Mn x 10^5 (g/mol)	[a]PDI	G' (Pa) at 100 s^{-1}	Complex viscosity at 100 s^{-1}
Poly(AN-co-MA)/7% clay	1.45	8.62	2.96 x 10^6	3.20 x 10^4
Poly(AN-co-MA)/5% clay	1.35	9.12	2.31 x 10^6	2.30 x 10^4
Poly(AN-co-MA)/3% clay	1.32	6.84	1.49 x 10^6	1.50 x 10^4
Poly(AN-co-MA)/1% clay	1.90	9.84	6.88 x 10^5	8.20 x 10^3
Poly(AN-co-MA)/0% clay	3.29	5.84	3.68 x 10^5	5.30 x 10^3

[a]PDI: Mw/Mn

The Mn values decreased significantly upon the addition of clay. This indicates that the clay plays a significant role in the propagation step during the polymerisation reaction. As expected from emulsion polymerisations, products with relatively higher molecular weights were obtained compared to products from solution polymerisations.[24]

5.4.2 Rheology results

5.4.2.1 Linear viscoelastic range

In order to determine the oscillation amplitude, i.e. the range within which the polymer structure is unaffected by the deformation applied (the LVE range), an amplitude sweep was performed at a constant frequency of 5 Hz. The LVE range is described by a constant storage modulus before the storage modulus shows a gradual but steep decrease. Fig. 5.2 depicts the effect that the oscillation amplitude has on the G', from 0.01 to 100% strain.

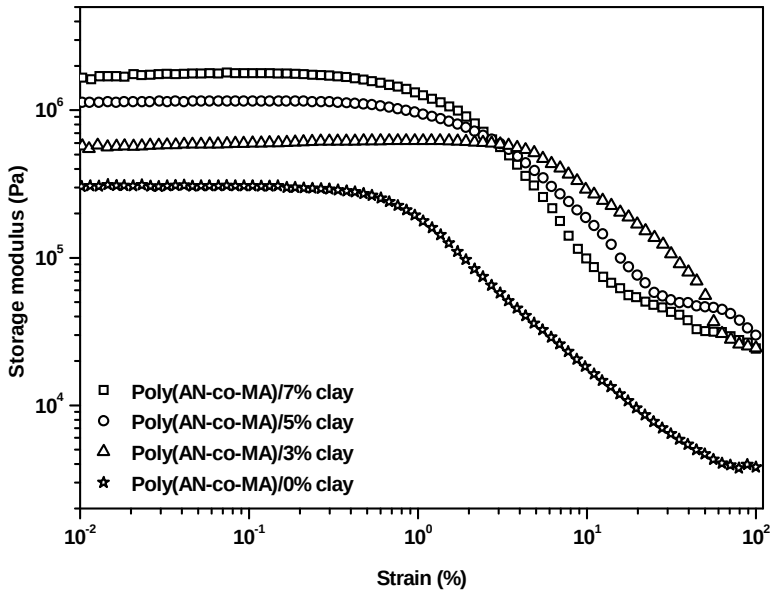

Fig. 5.2: Strain amplitude sweeps for neat poly(AN-co-MA) and 3%, 5% and 7% clay nanocomposites at a constant oscillation frequency of 5 Hz.

It is interesting to note that the LVE upper boundary increased from 1% for the neat copolymer to 5% upon incorporation of 3% clay into the polymer matrix. However, as the clay loading increased the LVE upper boundary decreased monotonically, probably due to the increased restriction of polymer chain motion. On the other hand the G' within the LVE range increased with increasing clay content, as is reported elsewhere.[26,27]

Despite this behaviour, the LVEs of the samples studied here were within the 0.01-1% strain range, except for the sample with 3% clay content. The frequency sweep measurements were therefore carried out at 0.1% strain, which is within the LVE of the nanocomposites and the neat copolymer.

5.4.2.2 Frequency sweep

Fig. 5.3 shows the relationship between the G' and the oscillation frequency for the nanocomposites with various clay loadings. G' was found to increase monotonically with increasing clay content over the entire frequency range. G' values at high angular frequency, tabulated in Table 5.1, showed a sharp increase with increasing clay content. This is attributed to the strong interaction between the polymer and the clay.[22]

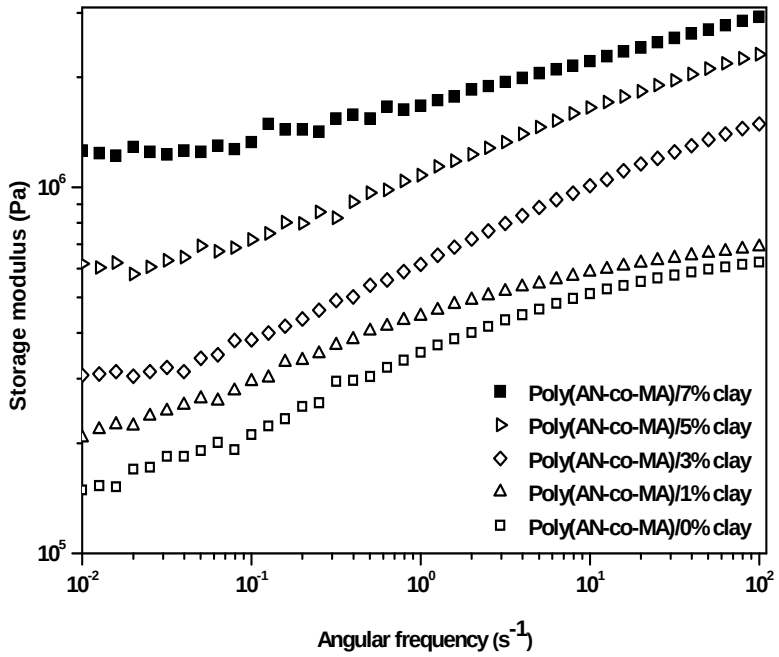

Fig. 5.3: Storage modulus versus frequency sweep for neat poly(AN-co-MA) and 1%, 3%, 5% and 7% clay nanocomposites.

The G' values of the neat copolymer and the 1% nanocomposite did not show any low frequency plateaus as did the samples with higher clay loadings. This indicates that in the 1%

nanocomposite the polymer matrix dominates the viscoelastic properties rather than the clay.[19,28] Since PCNs with a clay content as low as 3% exhibited a plateau at low frequencies, one can speculate that the percolation threshold is in the region of 1.5–2.5% clay content.[18,27,28] At this clay content the polymer and the clay begin to form an interconnected 3-dimensional network structure.[19,22,28] The 3-D network structure is a characteristic of highly filled polymers in which a percolated structure is formed. The plateau behaviour has been reported to be an indication that the PCNs act as solid-like viscoelastic materials in the frequency domain considered, or as viscoelastic fluids with infinitely long relaxation times.[29]

Fig. 5.4(a) and 5.4(b) shows plots for G' and loss modulus (G") as a function of the angular frequency for the neat copolymer and the nanocomposite with 7% clay, respectively. The G' and G" vs angular frequency curves of nanocomposites with 1%, 3% and 5% clay content are shown in Appendix H. Throughout the frequency range the G' values are higher than the G" values for both the nanocomposites and the unfilled copolymer. No crossover point between G' curves and the G" curve was observed, (see Fig. 5.4), as would be expected for a conventional viscoelastic material shifting from solid-like to liquid-like behaviour at frequencies below the relaxation time of the polymer chains at a given temperature in the molten state. When G'>G" a material exhibits solid-like behaviour and when G'<G" a material exhibits liquid-like behaviour.[22] The results obtained here show that all samples showed typical solid-like behaviour throughout the frequency range, despite all measurements being recorded at a temperature above the T_g of all the samples. The poly(AN-co-MA) and its nanocomposites exhibit relaxation times much longer than the domain of frequencies evaluated.

Poly(AN-co-MA) and its nanocomposites exhibited high complex viscosities. Table 5.1 includes the complex viscosity values for the different nanocomposites at 100 s^{-1}. These values were taken to represent the initial complex viscosity (complex viscosity at t_0). The high values observed were attributed to the high molecular weights of the polymer matrix.

Furthermore, an increase in viscosity with increasing clay content was observed, as shown in Fig. 5.5, although the nanocomposites had lower molecular weights than the neat copolymer. This demonstrated that the melt flow properties were dominated by the clay filler rather than the continuous polymeric matrix. Such an increase in the complex viscosity with incorporation of clay is reported to be caused by the occurrence of interactions between the dispersed clay filler and the polymeric matrix.[22] This hinders chain motion.

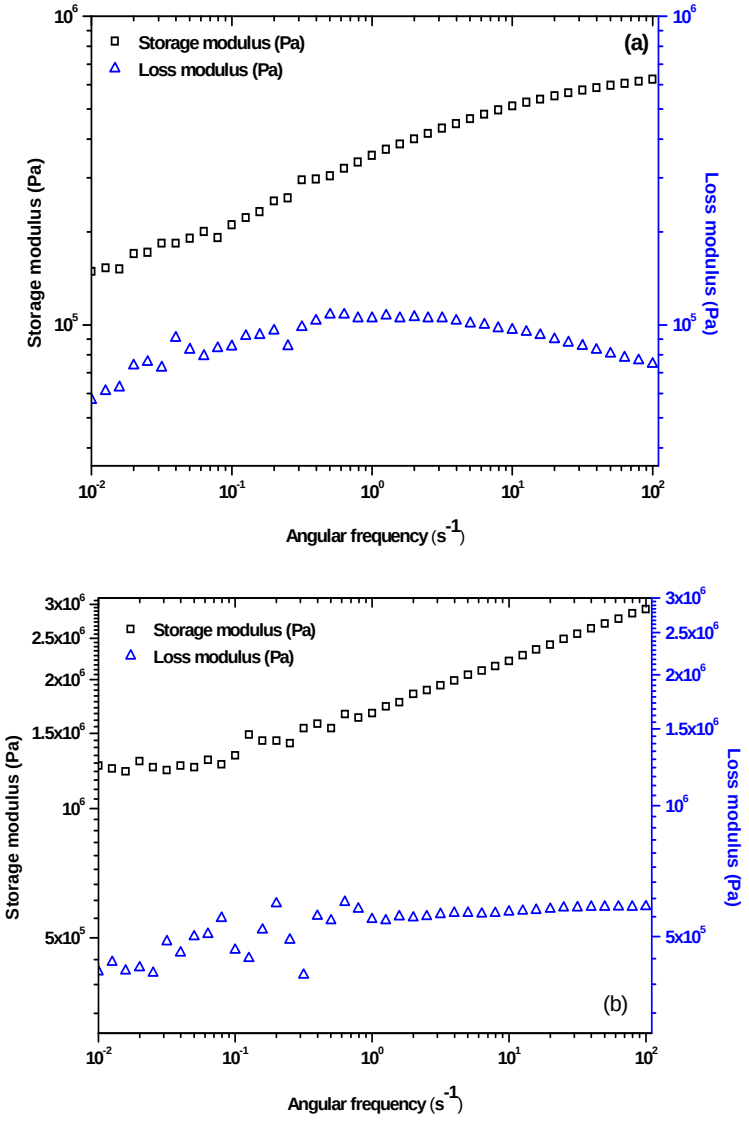

Fig. 5.4: Storage and loss modulus of (a) neat poly(AN-co-MA) and (b) poly(AN-co-MA)/7% clay nanocomposites as a function of angular frequency.

Fig. 5.5 shows that all samples exhibit shear thinning behaviour, even the neat copolymer. The shear thinning in nanocomposites is a result of clay's ability to align in the direction of shear at high frequencies.[3,21,22] However, none of the samples showed a Newtonian plateau within the frequency range studied, as was also reported by Rangarajan *et al.*[30] for poly(acrylonitrile-co-methyl acrylate) prepared via solution polymerisation (they did not however comment on this behaviour). Although the author recorded an increase in shear thinning with increasing clay content, as is reported elsewhere,[3,21,22] the onset of shear thinning was not observed within the angular frequency range studied in this present study. The more pronounced shear thinning characteristic with increasing clay content is attributed to the ability of the clay to orient in the direction of shear under high angular frequencies.[21,22,31]

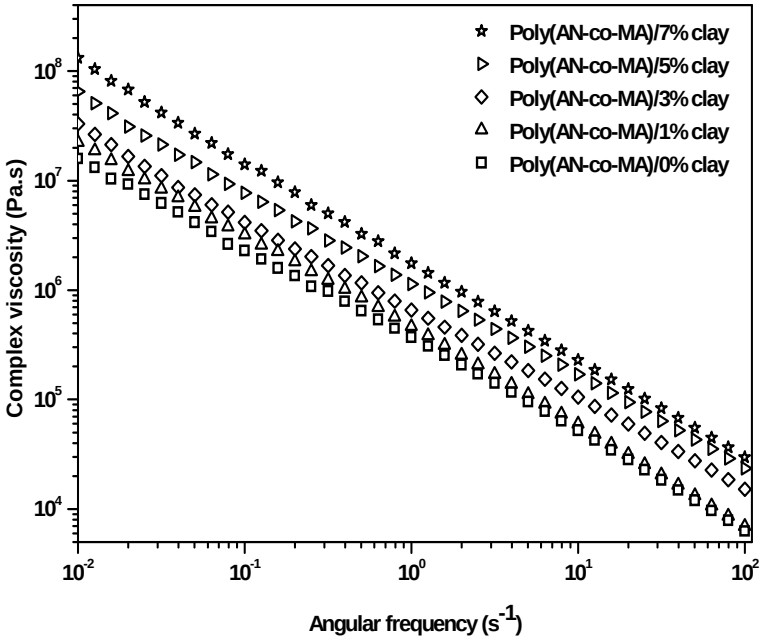

Fig. 5.5: Complex viscosity of various poly(AN-co-MA)/clay nanocomposites as a function of angular frequency.

After the frequency sweep measurements the samples were analysed using TEM to confirm the orientation of clay platelets in the direction of shear during the test. The results, Fig 5.6(b)

and Appendix I, show a reorganisation and enhanced exfoliation of the clay platelets after the frequency sweep measurement. Fig. 5.6 shows the cross sectional TEM images of the poly(AN-co-MA)/7%clay nanocomposite film before and after frequency sweep measurement.

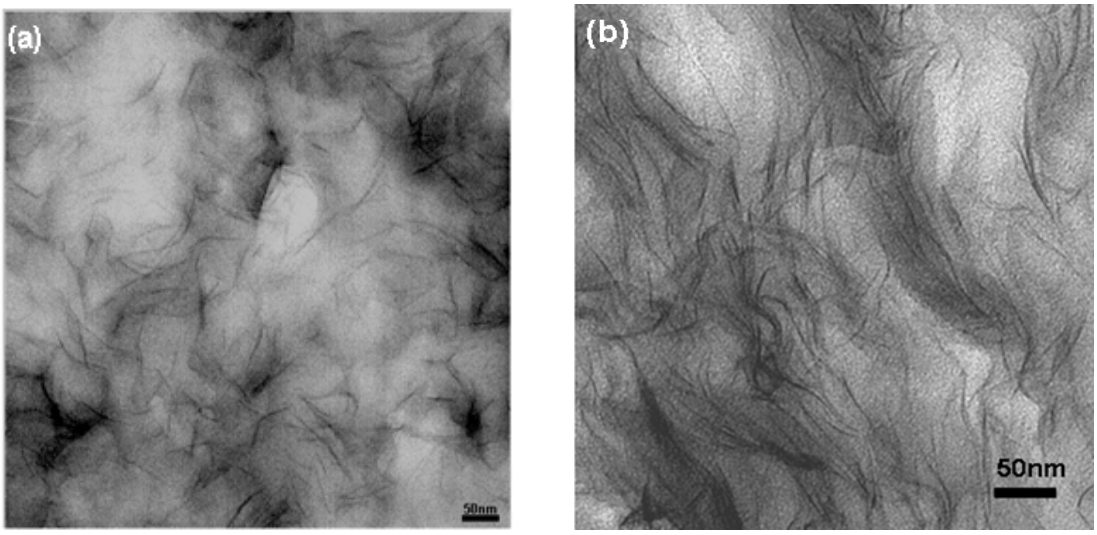

Fig. 5.6: TEM images of poly(AN-co-MA)/7% clay (a) before frequency sweep measurement and (b) after frequency sweep measurement.

5.4.2.3 Melt stability

The solid-like behaviour observed in all samples could be due to thermal instability of the samples occurring at the temperature of the frequency sweep test. The melt stability of the neat copolymer and PCN with 7% clay content was studied over 20 h (the approximate time taken to perform a frequency sweep test). The time dependence of the complex viscosity of these samples at constant strain (0.1%) and frequency (5 Hz) was plotted. The results are shown in Fig. 5.7(a) and 5.7(b). The complex viscosity of both the neat copolymer and the nanocomposite increases sharply with time within the first 4 h. Beyond 4 h the extent to which complex viscosity increases seems to be dependent on the clay loading. The 7% nanocomposite showed a steeper gradient than the neat copolymer, meaning that the rate at

which the complex viscosity of PCN with 7% clay content increased was higher than that of the neat copolymer. These results indicate that the chemical structures of both the neat copolymer and the nanocomposite undergo changes upon prolonged heating at 180 °C.

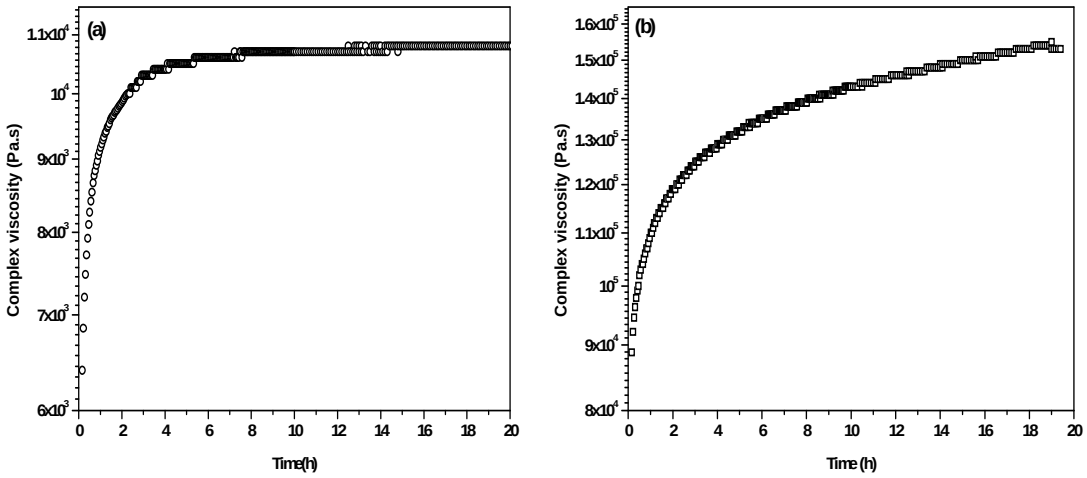

Fig. 5.7: Results of the dynamic time sweeps: (a) poly(AN-co-MA) and (b) poly(AN-co-MA)/7% clay nanocomposites at 180 ℃ and 0.1% strai n.

FTIR was used to analyse the neat copolymer samples before and after exposure to the frequency sweep test in order to monitor any chemical changes that may take place during the test. Fig. 5.8 shows the FTIR spectra of the neat copolymer sample before and after the frequency sweep measurements.

The FTIR spectrum of the copolymer sample after the frequency sweep test shows a new band at 1621 cm^{-1}, representative of =C=C= and –C=N– conjugated bonds. This indicates a small detectable amount of products from cyclisation reactions,[32,33] which took place during the frequency sweep measurement. The copolymer was soluble in DMF before the frequency sweep tests but after the test it only swells in DMF. This change in solubility indicates that crosslinking reactions took place during the test. This melt instability may hence be responsible for the solid-like character observed in these materials, even at low frequencies, were the materials were expected to shift to liquid-like character.

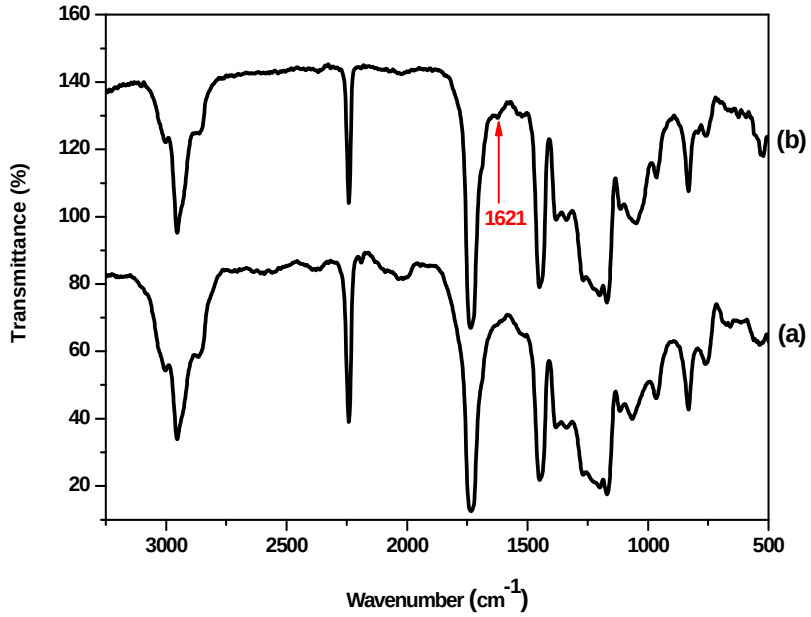

Fig. 5.8: FTIR spectra of poly(AN-co-MA): (a) before frequency sweep measurement and (b) after frequency sweep measurement.

5.5 Conclusions

Poly(AN-co-MA)/clay nanocomposites were successfully prepared via emulsion polymerisation. These nanocomposites were of high molecular weight and exhibited high complex viscosities, typically in the 10^3–10^4 range at 100 s^{-1}. Shear thinning behaviour was observed in these nanocomposites due to the ability of clay platelets to align in the direction of shear stress at high angular frequencies. The incorporation of clay monotonically led to an increase in the storage modulus thoroughout the angular frequency range studied, and up to 500% increase was observed at 100 s^{-1} for copolymers with the maximum clay content used (7%). However, the nanocomposites and the neat copolymer showed typical behaviour of material with long relaxation times: the G' values were greater than the G" values throughout the angular frequency range studied. This phenomenon could have resulted from the cyclisation reactions which took place during the oscillatory tests. Results of dynamic time sweeps and FTIR indicated that cyclisation reactions probably took place during these tests. The incorporation of clay fillers dominated the rheological properties more than molecular weight did, especially in terms of the complex viscosity.

References

1. Usuki, A.; Koiwai, A.; Kojima, Y.; Kawasumi, M.; Okada, A.; Kurauchi, T.; Kamigaito, O. *Journal of Applied Polymer Science* **1995**, 55, (1), 119–123.
2. Messersmith, P. B.; Giannelis, E. P. *Chemistry of Materials* **1994**, 6, (10), 1719–1725.
3. Kim, T. H.; Jang, L. W.; Lee, D. C.; Choi, H. J.; John, M. S. *Macromolecular Rapid Communication* **2002**, 23, (3), 191–195.
4. Choi, Y. S.; Choi, M. H.; Wang, K. H.; Kim, S. O.; Kim, Y. K.; Chung, I. J. *Macromolecules* **2001**, 34, 8978–8985.
5. Osman, M. A.; Mittal, V.; Suter, U. W. *Macromolecular Chemistry and Physics* **2007**, 208, (1), 68–75.
6. Zeng, C.; Lee, L. J. *Macromolecules* **2001**, 34, 4098–4103.
7. Gorrasi, G.; Tortora, M.; Vittoria, V.; Pollet, E.; Lepoittevin, B.; Alexandre, M.; Dubois, P. *Polymer* **2003**, 44, (8), 2271–2279.
8. Paul, D. R.; Robeson, L. M. *Polymer* **2008**, 49, (15), 3187–3204.
9. Kawasumi, M.; Hasegawa, N.; Kato, M.; Usuki, A.; Okada, A. *Macromolecules* **1997**, 30, (20), 6333–6338.
10. Park, J. H.; Lee, H. M.; Chin, I. J.; Choi, H. J.; Kim, H. K.; Kang, W. G. *Journal of Physics and Chemistry of Solids* **2008**, 69, (5–6), 1375–1378.
11. Natu, A. A.; Lofgren, E. A.; Jabarin, S. A. *Polymer Engineering Science* **2005**, 45, (3), 400–409.
12. Muralidharan, M. N.; Kumar, S. A.; Thomas, S. *Journal Membrane Science* **2008**, 315, (1–2), 147–154.
13. Gacitua, E. W.; Ballerini, A. A.; Zhang, J. *Maderas: Ciencia y Technologia* **2005**, 7, (3), 159–178.
14. Gelfer, M. Y.; Burger, C.; Chu, B.; Hsiao, B. S.; Drozdov, A. D.; Si, M.; Rafailovich, M.; Sauer, B. B.; Gilman, J. R. W. *Macromolecules* **2005**, 38, (9), 3765–3775.

15. Wagener, R.; Reisinger, T. J. G. *Polymer* **2003**, 44, (24), 7513–7518.

16. Li, J.; Zhou, C. X.; Wang, G.; Zhao, D. L. *Journal of Applied Polymer Science* **2003**, 89, (13), 3609–3617.

17. Galgali, G.; Ramesh, C.; Lele, A. *Macromolecules* **2001**, 34, (4), 852–858.

18. Krishnamoorti, R.; Giannelis, E. P. *Macromolecules* **1997**, 30, (14), 4097–4102.

19. Lotti, C.; Isaac, C. S.; Branciforti, M. C.; Alves, R. M. V.; Liberman, S.; Bretas, R. E. S. *European Polymer Journal* **2008**, 44, (5), 1346–1357.

20. Li, J.; Zhou, C. X.; Wang, G.; Zha, D. L. *Journal of Applied Polymer Science* **2003**, 89, (2), 318–323.

21. Park, B. J.; Kim, T. H.; Choi, H. J.; Lee, J. H. *Journal of Macromolecular Science: Part B: Physics* **2007**, 46, (2), 341–354.

22. Lee, H. M.; Park, B. J.; Choi, H. J.; Gupta, R. K.; Bhattachary, S. N. *Journal of Macromolecular Science: Part B: Physics* **2007**, 46, (2), 261–273.

23. Park, H. C. *Mobil Chemical Company (U.S.A)* **1985**.

24. Bortner, M. J.; Bhanu, V.; McGrath, J. E.; Baird, D. G. *Journal of Applied Polymer Science* **2004**, 93, (6), 2856–2865.

25. Bhanu, V. A.; Rangarajan, P.; Wiles, K.; Bortner, M.; Sankarpandian, M.; Godshall, D.; Glass, T. E.; Banthia, A. K.; Yang, J.; Wilkes, G.; Baird, D.; McGrath, J. E. *Polymer* **2002**, 43, (18), 4841–4850.

26. Zhong, W.; Qiao, X.; Sun, K.; Zhang, G.; Chen, X. *Journal of Applied Polymer Science* **2006**, 99, 1523–1529.

27. Wang, K.; Liang, S.; Deng, J. N.; Yang, H.; Zhang, Q.; Fu, Q.; Dong, X.; Wang, D. J.; Han, C. C. *Polymer* **2006**, 47, (20), 7131–7144.

28. Wu, D.; Wu, L.; Wu, L.; Zang, M. *Polymer Degradation and Stability* **2006**, 91, 3149–3155.

29. Xu, M. Z.; Choi, Y. S.; Wang, K. H.; Kim, J. H.; Chung, I. J. *Macromolecular Research* **2003**, 11, (6), 410–417.

30. Rangarajan, P.; Yang, J.; Bhanu, V.; Godshall, D.; McGrath, J.; Wilkes, G.; Baird, D. *Journal of Applied Polymer Science* **2002**, 85, (1), 69–83.

31. Solomon, M. J.; Almusallam, A. S.; Seefeldt, K. F.; Somwangthanaroj, A.; Varadan, P. *Macromolecules* **2001**, 34, (6), 1864–1872.

32. Soulis, S.; Simitzis, J. *Polymer International* **2005**, 54, (11), 1474–1483.

33. Devasia, R.; Nair, C. P. R.; Sadhana, R.; Babu, N. S.; Ninan, K. N. *Journal of Applied Polymer Science* **2006**, 100, (4), 3055–3062.

CHAPTER 6

Sorption and transport properties of water vapour in poly(acrylonitrile-co-methyl acrylate)/clay nanocomposites

6.1 Introduction

Transport of small molecules (penetrants) in and through polymeric materials is described by three parameters: permeability coefficient (P), diffusion coefficient (D) and solubility coefficient (S). The permeability coefficient describes the ease with which the penetrant moves in and through the polymer membrane, the diffusion coefficient gives an indication of the mobility of penetrants, and S gives an indication on the polymer–penetrant and penetrant–penetrant interactions.[1-3]

The diffusion of penetrants within a polymer matrix is associated with the rate at which polymer structural changes takes place in response to the motion of the penetrant molecules.

The solubility of a penetrant in a polymer matrix is described by the sorption isotherm which correlates the amount of sorbed penetrant in a polymer to the pressure or penetrant activity. Sorption isotherms show considerable differences depending on the polymer–penetrant system.[1-3] In glassy polymers the dual-mode sorption model is a well accepted model to describe sorption in many penetrant/polymer systems.[4-8] The dual-mode sorption assumes the existence of two penetrant populations, those immobilised in the polymer matrix and those entrapped in microvoids.

The transport properties of different penetrants through a polymer membrane are affected by, among other factors, the presence of fillers in the polymer. The transport properties of water vapour in polymers filled with clay platelets, polymer clay nanocomposites (PCNs), have been studied,[9-17] and a reduction in the permeability coefficient in PCNs compared to the neat copolymers has been reported. This has been attributed to a tortuous path model where the

high aspect ratio platelets act as physical barriers for the diffusing penetrant because they are impermeable to the penetrant.[12,17-21] Nielsen[18] proposed the tortuous path model to explain the permeability coefficient reduction in filled polymers. This models assumes that the fillers are impermeable to the diffusing penetrant but have no effect on the mobility of the polymer chains, and that the plates are oriented parallel to the polymer film surface, perpendicular to the direction of diffusion.

Different numerical models have since been developed to explain permeability and diffusion coefficient reduction in polymer/clay nanocomposites based on the tortuous models. Various considerations, such filler–polymer interface,[22] polymer constrains around fillers, and filler orientation[22,23] were taken into account during the development of these different models. The decrease in diffusion coefficient in PCNs compared to neat polymers is attributed to the tortuous path introduced by the clay platelets, which are impermeable to the penetrant so that the penetrant travels a longer distance in filled polymer than in neat polymers.[21,23,24] The effectiveness of clay in decreasing the diffusion coefficient of water in poly(ε-caprolactone) was found to be dependent on its degree of dispersion in the polymer matrix with the exfoliated nanocomposites having a significantly reduced diffusion coefficient, while the intercalated nanocomposites and microcomposites did not show any changes compared to the neat polymer.[12]

Solubility in PCNs is influenced by both the matrix and the clay platelets. Gorrasi et al.[10] reported an increase in the equilibrium water uptake with increasing clay content due to the hydrophilicity of clay. Burnside and Giannelis[25] proposed that strong interacting fillers reduce swelling while non-reinforcing fillers result in a solvent uptake that might be higher than that of the unfilled polymer. The nanocomposites can exhibit sorption isotherms which are either different or similar to those of neat polymers upon their incorporation.[10,26]

This Chapter describes the study of the transport properties of water vapour in poly(AN-co-MA)/clay nanocomposites. Two of the four nanocomposites described in Chapter 4 were used

in this study, namely poly(AN-co-MA)/1% clay and poly(AN-co-MA)/5% clay). The neat copolymer was used as a comparison. Transport properties in the other two samples are still under investigation. The transport properties of water vapour in these nanocomposites were determined from sorption-desorption measurements. The aim was to investigate the sorption isotherms and determine the solubility, diffusion and permeability coefficients of water vapour in these nanocomposites.

6.2 Materials

The poly(AN-co-MA)/clay nanocomposites used in this study were synthesised and characterised as reported in Chapter 4.

6.3 Analyses

6.3.1 Sorption measurements

The sorption measurements were carried out using by the sorption-desorption methods, using an intelligent gravimetric analyser (IGA). An IGA microbalance (Hiden Analytical Ltd., Warrington, UK) was used to accurately measure the sorption rate of water vapour by the films. The IGA apparatus is an ultrahigh vacuum system which allows the sorption-desorption isotherms and the corresponding kinetics of sorption or desorption at various pressures to be determined. The IGA consists of a fully computerised microbalance (with a weighing resolution of ±1 μg), which automatically measures the weight of the sample as a function of time while the gas vapour pressure and the sample temperature are accurately controlled. The equilibrium pressures were determined by Baratron pressure transducers and maintained at the set point by active computer control of the admittance/exhaust valves throughout the experiment. The sample temperature was also monitored throughout the measurement and regulated to ± 0.1ºC using a water bath.

Sorption measurements were done at 23 ºC, with the reactor thermostated by means of a water bath. The films were degassed in the electrobalance under a vacuum of $<10^{-5}$ until a constant weight was reached (approximately 16 h). The vapour was introduced at a rate of 100 mbar/min until the desired pressure was achieved and the weight gain was recorded until equilibrium was reached. The pressure was increased in the same manner to move to the next set point, and a new sorption kinetic determination was carried out. This step was repeated until the isotherm was completed. The sorption and desorption isotherms were measured by increasing or decreasing the equilibrium pressure in small steps. Correction of the buoyancy effect was done online.

The poly(acrylonitrile-co-methyl acrylate)/clay nanocomposites used in this study were first pressed into cubic films (1 cm x 1 cm x 0.03 cm) using a hot press at 150 ºC. The masses of the resultant films were approximately 35 μg.

6.3.2 Positron annihilation lifetime spectroscopy

The procedure used for positron annihilation lifetime spectroscopy (PALS) measurements of the nanocomposites is as described in Section 3.3.4.

6.4 Results and discussion

The samples used in this study were prepared via free radical polymerisation in emulsion, as detailed in Chapter 4. These samples were of high molecular mass, although the molecular mass decreased upon incorporation of clay, while the PDIs increased with increasing clay content (Section 4.4.3). All samples (the neat copolymer and the nanocomposites) used in this study have high glass transition temperatures (T_g values), as determined by DMA (Section 4.4.5). The nanocomposites exhibited T_g values similar to those of the neat copolymer regardless of the clay content. Despite the different clay loadings used in the preparation of the nanocomposites, they all exhibited partially exfoliated morphologies (Section 4.4.4). The

sorption-desorption measurements were done at a temperature well below the samples' glass transition temperatures, at which the neat copolymer and nanocomposites were in their glassy state.

6.4.1 Sorption-desorption results

During the sorption-desorption measurements the partial pressure of water vapour within the IGA reactor was changed in a stepwise manner, Fig 6.2(a), and the sorption kinetics were recorded as time dependent mass gain or loss at each water activity (a_w), as shown in Fig. 6.1(b).

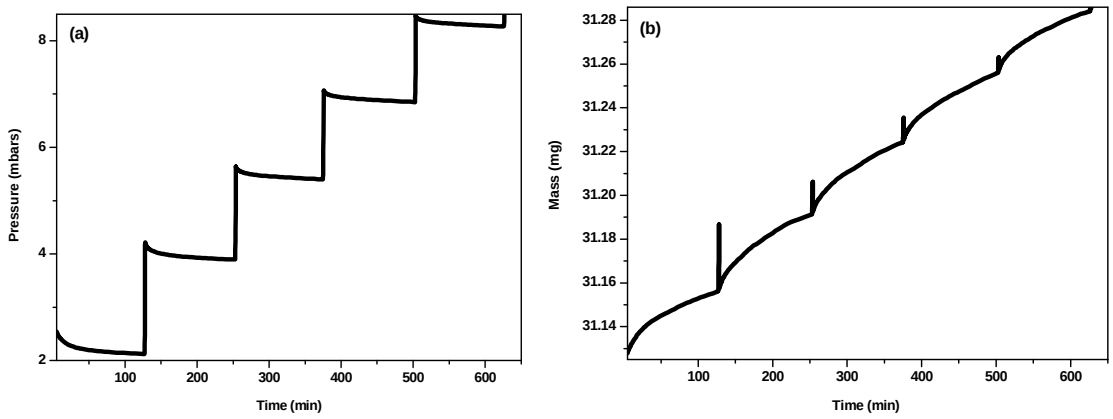

Fig. 6.1: (a) The first five sorption pressure steps and (b) the corresponding sorption kinetics of water vapour in neat poly(AN-co-MA) for the first five pressure steps.

The water vapour sorption isotherms were obtained after plotting the equilibrium mass uptake versus the corresponding a_w of each pressure step. The results are shown in Fig. 6.2.

6.4.1.1 Sorption behaviour of water vapour in poly(AN-co-MA)/clay nanocomposites.

Fig 6.2 shows the sorption isotherms of water vapour in neat poly(AN-co-MA) and its nanocomposites of different clay content. The equilibrium water vapour uptake was dependent on both a_w as well as the clay content. The changes in equilibrium water vapour uptake could not be attributed to the polymer matrix because all the nanocomposites had

similar compositions. As the a_w increased the equilibrium water vapour uptake also increased in all the samples, and the equilibrium water vapour uptake was found to be higher in the nanocomposites compared to the neat copolymer at each given a_w. This has been previously attributed to the hydrophilic nature of the clay.[12] However, the equilibrium uptake in the nanocomposites increased significantly with increasing clay content, especially at the high a_w values. The partially exfoliated morphology of these nanocomposites could act as extra absorbing sites so that the nanocomposites could absorb more water compared to the neat copolymer.

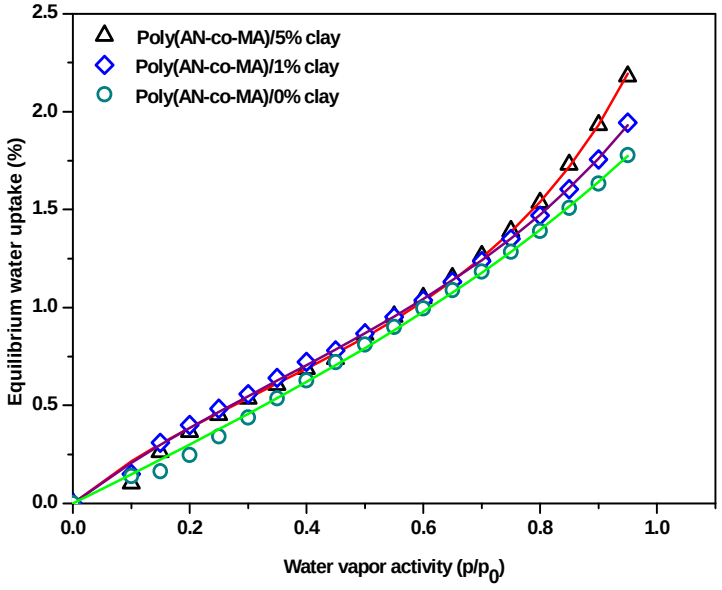

Fig. 6.2: Sorption isotherms of poly(acrylonitrile-co-methyl acrylate) of different clay content.

The equilibrium water vapour uptake of neat poly(AN-co-MA) and its nanocomposites follows a sigmoidal increase with increasing a_w, as shown in Fig. 6.2 - typical dual sorption behaviour (BET type II mode). The dual mode sorption, a widely accepted model to explain sorption in glassy polymers,[5,8,12,27-29] cannot satisfactorily describe the BET type II mode. The Guggenheim-Anderson-de Boer (GAB) equation,[30] on the other hand, has been used to

simulate sorption isotherms showing BET type II behaviour after it fitted well to the water vapour sorption data of food and natural materials.[8,31-33] Although it fits well to this behaviour its required assumption, namely that all sorption sites are equivalent, is inconsistent with glassy polymers, which have been widely accepted to have two sorption sites. Feng[6] developed a new dual-mode sorption model based on the conventional dual-mode sorption and the GAB equation. This model fits the BET type II sorption mode well.

According to the new dual-mode sorption model the penetrant concentration in the polymer is given by the Equation 6.1:

$$c = \bar{C}_p \frac{k'a}{1-k'a} + \bar{C}_p \frac{(A'-1)k'a}{1+(A'-1)k'a} \qquad \textbf{(6.1)}$$

$\bar{C}_p$ *-The weighted mean value of sorption capacity of a polymer to penetrant*

k' *- A measure of the interaction between the penetrant molecule and the polymer*

a *- Penetrant activity*

A' *- A measure of the interaction of penetrant molecule and the microvoid*

Since the new model fits well with the BET type II sorption mode it was adopted here. The parameters obtained from fitting this model to experimental data are given in Table 6.1. The fitting was done using the regression method. The fitting curves are shown in Fig. 6.2 as solid lines and R^2 was utilised to estimate the goodness of fit. The new dual-mode sorption fitted well all the sorption data obtained here, as shown in Fig 6.2. The sorption parameters show that the water vapour–polymer interaction and water vapour–microvoid increases with increasing clay content.

Table 6.1: New dual-mode sorption parameters of poly(AN-co-MA) nanocomposites with different clay content.

Sample	$\bar{C}_p$ (wt%)	k'	A'	R^2

Poly(AN-co-MA)/0% clay	1.71	0.45	1.95	0.999
Poly(AN-co-MA)/1% clay	0.93	0.62	4.01	0.999
Poly(AN-co-MA)/5% clay	0.74	0.77	4.67	0.999

A significant upswing was observed at $a_w > 0.65$. This could be due to water liquefication which results from capillary condensation into microvoids.[34] The neat copolymer and the nanocomposites show similar sorption behaviour, as was also reported by Murase *et al.*[26] for nylon 6/clay films, but contrary to what was reported by Gorrasi *et al.*[12] who reported different water vapour sorption isotherm behaviours between the neat syndiotactic polypropylene and its nanocomposites.

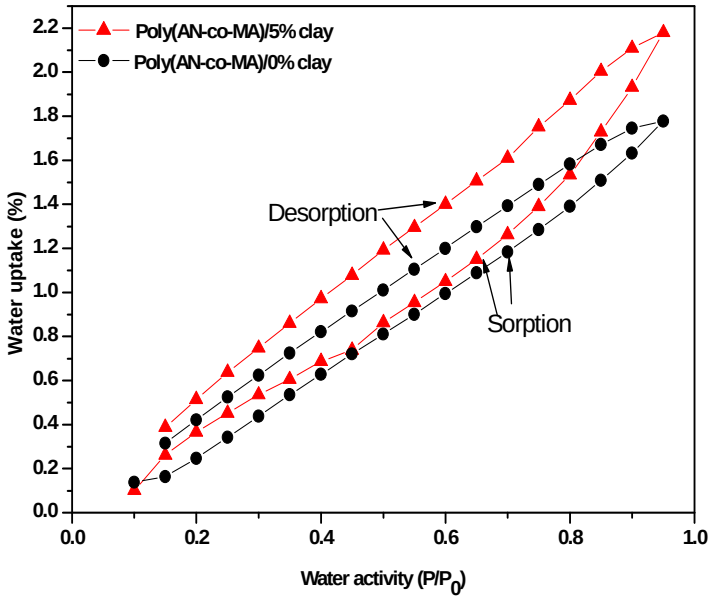

Fig. 6.3: The sorption-desorption isotherms of neat poly(AN-co-MA) and the poly(AN-co-MA)/5% clay nanocomposite.

The sorption-desorption isotherms of all samples exhibited hysteresis feature (Fig. 6.3) as is reported for other glassy polymer/water mixtures.[35,36] Hysteresis is typified by a higher equilibrium penetrant uptake during desorption than during sorption. Fig. 6.3 shows the sorption-desorption isotherms of neat copolymer and the copolymer with 5% clay content.

The equilibrium water uptake during desorption was higher than the equilibrium water uptake during sorption at any given a_w value. This phenomenon is due to a slower movement of clustered water molecules during desorption. Clustering of water molecules in microvoids makes them less mobile than individual molecules, resulting in a decreased rate of desorption.[37] The hysteresis could be due to different internal stresses developing in the polymer as a result of the penetration of water vapour through the polymer matrix at the sorption and desorption stages.[38]

The solubility coefficient was calculated using the following equation:[39,40]

$$S = \frac{M_\infty - M_0}{V_p.M.p} 22414 \qquad \textbf{(6.2)}$$

where M_0 is the initial mass of sample, M_∞ is the mass of sample at equilibrium water vapour uptake, V_p is the volume of the film, M is the molecular weight of water, p is the partial pressure of water, and 22414 is the molar gas volume in cm^3.

The solubility coefficient results at a_w = 0.8 are given in Table 6.2. The solubility was found to increase with increasing clay content. This is due to the hydrophilic nature of the clay platelets.

6.4.1.2 Diffusion of water vapour in poly(AN-co-MA)/clay nanocomposites

IGA software was used to calculate the diffusion coefficient, based on the Fick's law, as outlined in the IGA manual.[41]

The total amount of penetrant uptake by thin films, such as those used in this study, with negligible diffusion from the edges can be described by Equation 6.3 under a constant pressure atmosphere, assuming that D is constant:

$$\frac{M(t)}{M_\infty} = 1 - \sum_{n=0}^{\infty} \frac{8}{(2n+1)^2 \pi^2} \exp\left[\frac{-D(2n+1)^2 \pi^2 t}{l^2}\right] \qquad \textbf{(6.3)}$$

Taking long times approximations into account (50-90% M_∞), this equation reduces to:

$$\frac{M_t}{M_\infty} = 1 - \left(\frac{8}{\pi^2}\right) \exp\left(-\frac{D\pi^2 t}{l^2}\right) \qquad \textbf{(6.4)}$$

The IGA software fits Fickian kinetics by the following equation:

$$\frac{M_t}{M_\infty} = 1 - \exp\left(-\frac{t}{k}\right) \quad \textbf{(6.5)}$$

where k is a time exponential constant.

D is defined by the long time approximation, and be calculated from the k parameter given by the IGA software from the equation:

$$D = \frac{l^2}{\pi^2 k} \quad \textbf{(6.6)}$$

where l is the sample thickness

Table 6.2 gives the transport parameter of water vapour in poly(AN-co-MA)/clay nanocomposites at 0.8 p/p_0. The diffusion coefficient was calculated using the IGA software, the solubility coefficient was calculated as described in Section 6.4.1.1, and the permeability coefficient as described Section 6.4.1.3.

Table 6.2: The transport parameters of water vapour in poly(AN-co-MA) nanocomposites of different clay loadings.

Sample	D x 10^{-9} (cm^2 s^{-1})	S (cm^3(STP)/cm^3mbar)	P x 10^{-7} (cm^3(STP) cm/cm^2 s, mbar)
Poly(AN-co-MA)/0% clay	7.29	55.47	4.04
Poly(AN-co-MA)/1% clay	6.05	58.16	3.52
Poly(AN-co-MA)/5% clay	3.38	60.42	2.04

The diffusion coefficient decreased considerably upon incorporation of clay, as is also reported elsewhere.[16] This is because the impermeable clay platelets cause the diffusing molecules to follow a tortuous path.[22,24] The rate of diffusion in filled polymer is understood to be strongly affected by filler orientation, concentrations, as well as interactions between filler and the polymer matrix.[22]

6.4.1.3 Permeability of water vapour in poly(AN-co-MA)/clay nanocomposites

The permeability coefficients were calculated using the equation

$$P = D.S \quad \textbf{(6.7)}$$

where D is diffusion coefficient and S is the solubility coefficient

The results are as given in Table 6.2. The decrease in the permeability of the nanocomposites is due to the high aspect ratio of the platelets, which increases the contact surface area between the filler and the matrix.[42]

6.4.2 Free volume properties of poly(AN-co-MA)/clay nanocomposites

Free volume and molecular theories can be used to describe the diffusion of penetrants through polymers. Cohen and Turnbull[43] developed the free volume model which states that the diffusion of a molecule takes place when the molecule moves into a void that is larger than its critical size. The free volume theory assumes that diffusion is a result of random redistribution of voids inside the polymer matrix.

The free volume parameters of samples used in the sorption study were measured by PALS and the results are tabulated in Table 6.3. The effect of clay content on o-Ps lifetime (related to free volume hole radius), o-Ps intensity (related to free volume concentration) and the relative fractional free volume (F_vR) were studied in relation to the transport properties of the poly(AN-co-MA)/clay nanocomposites.

The lifetime spectra of the neat copolymer and the nanocomposites were resolved into three lifetimes only, similar to the poly(AN-co-MA) copolymers described in Section 3.4.4. The o-Ps lifetime of the neat copolymer remained fairly constant but a decrease in o-Ps intensity and fractional free volume with increasing clay content was observed. Similar results were reported by Ammala *et al.*[44] for poly(m-xylene adipamide)/MMT nanocomposites. The decrease in relative fractional free volume can be attributed to restricted mobility of chain segments.[17,42] The free volume results also indicate that there was no significant agglomeration in the nanocomposites, as was observed from TEM and the SAXS results

(Section 4.4.4). Agglomeration would have caused an increase in the o-Ps intensity, and consequently fractional free volume upon incorporation of clay, due to additional void formation,[44] but o-Ps intensity decreased instead.

Table: 6.3 Free volume properties of poly(AN-co-MA)/clay nanocomposites of different clay content, as determined by PALS.

Clay content (%)	o-Ps lifetime $\tau_3 \pm 0.02$ ns	o-Ps intensity $I_3 \pm 0.02$ %	F_{vR} (%)
Poly(AN-co-MA)/0% clay	1.68	20.9	14.49
Poly(AN-co-MA)/1% clay	1.66	21.1	14.19
Poly(AN-co-MA)/5% clay	1.66	20.4	13.63

The decrease in diffusion coefficient observed can be due to two factors: the decrease in available free volume resulting from the nanoscale homogeneous dispersion of the clay platelets and the polymer matrix, and the increased turtousity brought by the platelet structure of clay and its high aspect ratio.[17] This decrease in diffusion coefficient had a major influence on the permeability coefficient, which decreased significantly despite an increase in the solubility coefficient.

6.5 Conclusions

The water vapour sorption in poly(AN-co-MA) and its clay nanocomposites follows dual mode (BET type II) sorption behaviour and the sorption behaviour was not affected by the incorporation of clay. The sorption-desorption isotherms exhibit hysteresis due to slow rate of desorption, as a result of water clustering in the microvoids. Using the new dual sorption model, it was found that the water vapour interaction with the polymer matrix and the microvoids increased with increasing clay content. Although the solubility poly(AN-co-MA)/clay nanocomposites increased with increasing clay content the permeability and diffusion coefficients decreased with increasing clay content due to the tortuous path introduced by the impermeable clay platelets. The increase in the solubility with increasing clay content is due to hydrophilic nature of clay.

Despite the decrease in diffusion coefficients with increasing clay content the average free volume hole size remained almost constant while the average free volume hole number and the relative fractional free volume decrease slightly with increasing clay content, so that the decrease in diffusion is attributed to the tortuous path and a decrease in relative fractional free volume. The platelet structure of clay and its high aspect ratio enhanced the polymer/clay interaction, hence the decrease in free volume. The free volume parameters indicate that there was no significant agglomeration in clay nanocomposites despite the clay content.

References

1. Comyn, J., *Polymer Permeability*. Elsevier Applied Science Publishers: New York, 1986.
2. Crank, J.; Park, G. S., *Diffusion in Polymers*. Academic Press: London and New York, 1968.
3. Klopffer, M. H.; Flaconnèche, B. *Oil & Gas Science and Technology* **2001**, 56, (3), 223–244.
4. Xing, B.; Pignatello, J. *Environmental Science and Technology* **1997**, 31, 792–799.
5. Fredrickson, G. H.; Helfand, E. *Macromolecules* **1985**, 18 (11), 2201–2207.
6. Feng, H. D. *Polymer* **2007**, 48, (10), 2988–3002.
7. Motamedian, S.; Pusch, W.; Tanioka, A.; Becker, F. *Journal of Colloid and Interface Science* **1998**, 204, (1), 135–142.
8. Huang, J.; Cranford, R. J.; Matsuura, T.; Roy, C. *Journal of Applied Polymer Science* **2003**, 87, 2306–2317.
9. Gorrasi, G.; Tammaro, L.; Tortora, M.; Vittoria, V.; Kaempfer, D.; Reichert, P.; Mulhaupt, R. *Journal of Polymer Science: Part B: Polymer Physics* **2003**, 41, (15), 1798–1805.
10. Gorrasi, G.; Tortora, M.; Vittoria, V.; Galli, G.; Chiellini, E. *Journal of Polymer Science: Part B: Polymer Physics* **2002**, 40, (11), 1118–1124.
11. Gorrasi, G.; Tortora, M.; Vittoria, V.; Kaempfer, D.; Mulhaupt, R. *Polymer* **2003**, 44, (13), 3679–3685.
12. Gorrasi, G.; Tortora, M.; Vittoria, V.; Pollet, E.; Lepoittevin, B.; Alexandre, M.; Dubois, P. *Polymer* **2003**, 44, (8), 2271–2279.
13. Jacquelot, E.; Espuche, E.; Gerard, J.-F.; Duchet, J.; Mazabraud, P. *Journal of Polymer Science: Part B: Polymer Physics* **2006**, 44, 431–440.

14. Kumar, S. A.; He, Y. L.; Ding, Y. M.; Le, Y.; Kumaran, M. G.; Thomas, S. *Industrial and Engineering Chemistry Research* **2008**, 47, (14), 4898–4904.

15. Low, H. Y.; Liu, T. X.; Loh, W. W. *Polymer Interanational* **2004**, 53, 1973–1978.

16. Maksimov, R. D.; Gaidukov, S.; Zicans, J.; Jansons, J. *Mechanics of Composite Materials* **2008**, 44, (5), 505–514.

17. Muralidharan, M. N.; Kumar, S. A.; Thomas, S. *Journal Membrane Science* **2008**, 315, (1–2), 147–154.

18. Nielsen., L. E. *Journal of Macromolecular Science: Part A* **1967**, 1, (5), 929–942.

19. Bharadwaj, R. K. *Macromolecules* **2001**, 34 (26), 9189–9192.

20. Picard, E.; Vermogen, A.; Gerard, J. F.; Espuche, E. *Journal of Membrane Science* **2007**, 292, (1–2), 133–144.

21. Sorrentino, A.; Gorrasi, G.; Tortora, M., *Polymer Nanocomposites.* Woodhead Publishing Limited: Cambridge, 2006.

22. Sorrentino, A.; Tortora, M.; Vittoria, V. *Journal of Polymer Science: Part B: Polymer Physics* **2006**, 44, (2), 265–274.

23. Falla, W. R.; Mulski, M.; Cussler, E. L. *Journal of Membrane Science* **1996**, 119, (1), 129–138.

24. Xu, B.; Zheng, Q.; Song, Y. H.; Shangguan, Y. *Polymer* **2006**, 47, (8), 2904–2910.

25. Burnside, S. D.; Giannelis, E. P. *Journal of Polymer Science: Part B: Polymer Physics* **2000**, 38, 1595–1604.

26. Murase, S.; Inoue, A.; Miyashita, Y.; Kimura, N.; Nishio, Y. *Journal of Polymer Science: Part B: Polymer Physics* **2002**, 40, 479–487.

27. Lokhandwala, K. A.; Nadakatti, S. M.; Stern, S. A. *Journal of Polymer Science: Part B: Polymer Physics* **1995**, 33, 965–976.

28. Etxeberria, A.; Garcia, A.; Iriarte, M.; Iruin, J. J.; Uriarte, C. *Journal of Applied Polymer Science* **2006**, 102, (3), 2034–2042.

29. Patton, C. J.; Felder, R. M.; Koros, W. J. *Journal of Applied Polymer Science* **1984**, 29, 1095–1110.

30. Anderson, R. B. *Journal of American Chemical Society* **1946**, 68, 686.

31. Perrin, L.; Nguyen, Q. T.; Sacco, D.; Lochon, P. *Polymer Interanational* **1997**, 42, (1), 9–16.

32. Lim, L.; Britt, I. J.; M. A. Tung. *Journal of Applied Polymer Science* **1999**, 71, (2), 197–206.

33. Tsami, E.; Vagenas, G. K.; Marinos-Kouris, D. *Journal of Food Processing and Preservation* **1992**, 16, (3), 151–61.

34. Kachrimanis, K.; Noisternig, M. F.; Griesser, U. J.; Malamataris, S. *European Journal of Pharmaceuticals and Biopharmaceuticals* **2006**, 64, 307-315.

35. Schult, K. A.; Paul, D. R. *Journal of Applied Polymer Science* **1996**, 61, (11), 1865–1876.

36. Watari, T.; Wang, H.; Kuwahara, K.; Tanaka, K.; Kita, H.; Okamoto, K. *Journal of Membrane Science* **2003**, 219, (1–2), 137–147.

37. Dubey, V.; Kuthe, S.; Saxena, C.; Jaiswal, D. K. *Journal of Applied Polymer Science* **2003**, 88, (7), 1760–1767.

38. Ugrozov, V. V.; Shebershneva, N. N.; Filippov, A. N.; Sidorenko, Y. I. *Colloid Journal* **2008**, 70, (3), 366–371.

39. Mwesigwa, E.; Basit, A. W.; Buckton, G. *Journal of Pharmaceutical Sciences* **2008**, 1–13.

40. Ulutan, S.; Balkose, D. *Journal of Membrane Science* **1996**, 115, 217–224.

41. Hiden-Isochema, *IGA Systems User Manual*. Hiden Isochema: London, 2002.

42. Stephen, R.; Ranganathaiah, C.; Varghese, S.; Joseph, K.; Thomas, S. *Polymer* **2006**, 47, (3), 858–870.

43. Turnbull, D.; Cohen, M. H. *Journal of Chemistry and Physics* **1959**, 31, 1164–1169.

44. Ammala, A.; Pas, S. J.; Lawrence, K. A.; Stark, R.; Webb, R. I.; Hill, A. J. *Journal of Materials Chemistry* **2008**, 18, (8), 911–916.

CHAPTER 7

Conclusions and recommendations for future work

7.1 Conclusions

Copolymers of acrylonitrile (AN) and methyl acrylate (MA) were successfully prepared using free radical polymerization in emulsion, with copolymer content varying from 0% MA/100% AN to 100% MA/0% AN (mol/mol).

The T_g was found to be directly dependent on the composition of the copolymer; it showed a linear decrease with increasing MA content. On the other hand the cystalline peaks of these copolymers decreased significantly with increasing MA content, and no crystalline peak was detectable in copolymers with MA content > 30%. The fractional free volume and the o-Ps lifetime of the copolymers followed a sigmoidal increase with increasing MA content, with a positive deviation being observed in copolymers containing MA content < 30% and negative deviation in copolymers with MA content > 50%. However the o-Ps intensity linearly increased with increasing MA content although this relationship deviated from the theoretical linear relationship.

The T_g of poly(AN/MA) copolymers decreased linearly with increasing o-Ps intensity but showed a sigmoidal decrease with increasing o-Ps lifetime and fractional free volume. The o-Ps lifetime and relative fractional free volume of the crystalline copolymers showed positive deviation from linearity while the amorphous copolymers showed a negative deviation from linearity. However the o-Ps intensity increased linearity despite the changes in crystallinity.

Poly(AN-co-MA)/clay nanocomposites were successfully prepared using free radical polymerization emulsion using AMPS as clay modifier. The nanocomposites were of high molecular weight, but, the molecular weight decreased significantly upon incorporation of clay. Despite the different clay contents used in the preparation of poly(AN-co-MA)/clay

nanocomposites they all exhibited partially exfoliated morphology, and the incorporation of clay did not affect copolymer composition or the overall monomer to polymer conversion of the nanocomposites.

A significant improvement in storage modulus was observed despite there being no change in T_g values between the different nanocomposites. The nanocomposites showed a slight increase in thermal stability as the clay content increased.

A significant increase in storage modulus was observed from rheological tests of the poly(AN-co-MA)/clay nanocomposites. It was also found that the extent of shear thinning increased with increasing clay content, although all the nanocomposites showed high viscosities, including the neat copolymer. However, neat poly(AN-co-MA) and its nanocomposites were found to exhibit long relaxation behaviours and a solid-like viscoelastic behaviour within the angular frequency range studied.

Both the neat copolymer and the nanocomposites exhibited BET type II dual-mode sorption behaviour, with equilibrium water uptake increasing with increasing clay content. Hysteresis was observed in the neat copolymer poly(AN-co-MA) and its nanocomposites, because the amount of equilibrium water uptake was higher during the desorption process than during sorption. The diffusion and permeability coefficients decreased significantly with increasing clay content due to the tortuous path created by the clay platelets, but solubility increased with increasing clay content due to the hydrophilic nature of clay. The decrease in permeability and diffusion could only be attributed to the tortuous path since the incorporation of clay did not significantly affect the free volume properties of the nanocomposites.

The o-Ps lifetime (free volume hole size) remained constant irrespective of the clay content, but a small decrease in o-Ps intensity (free volume hole content) was observed with increasing clay content. The decrease in o-Ps intensity and fractional free volume confirmed that poly(AN-co-MA)/clay nanocomposites did not show significant agglomeration and the decrease in diffusion was attributed to the tortuous path and decrease in free volume.

7.2 Recommendations for future work

1. Study the evolutions taking place during the preparation of PCNs in emulsion polymerisations in order to obtain a better understating of the PCNs morphology. The question that still remains to be answered for PCNs prepared by emulsion polymerization is: “where is the clay at the start of the reaction, in the micelle or in the aqueous phase?”
2. Use controlled polymerisation techniques to control the molecular weight of the polymer chains, use techniques such as RAFT to prepare block copolymers with different block lengths, and investigate the effect of molecular weight or block length on the physical properties of the resultant nanocomposites e.g. rheological and sorption properties.
3. Correlate sorption coefficients, diffusion rates, and free volume properties to nanoclay filler orientation induced by shear of PCN in its rubbery state.

Appendix A

^{1}H NMR spectra of poly(AN-co-MA) copolymers of different compositions

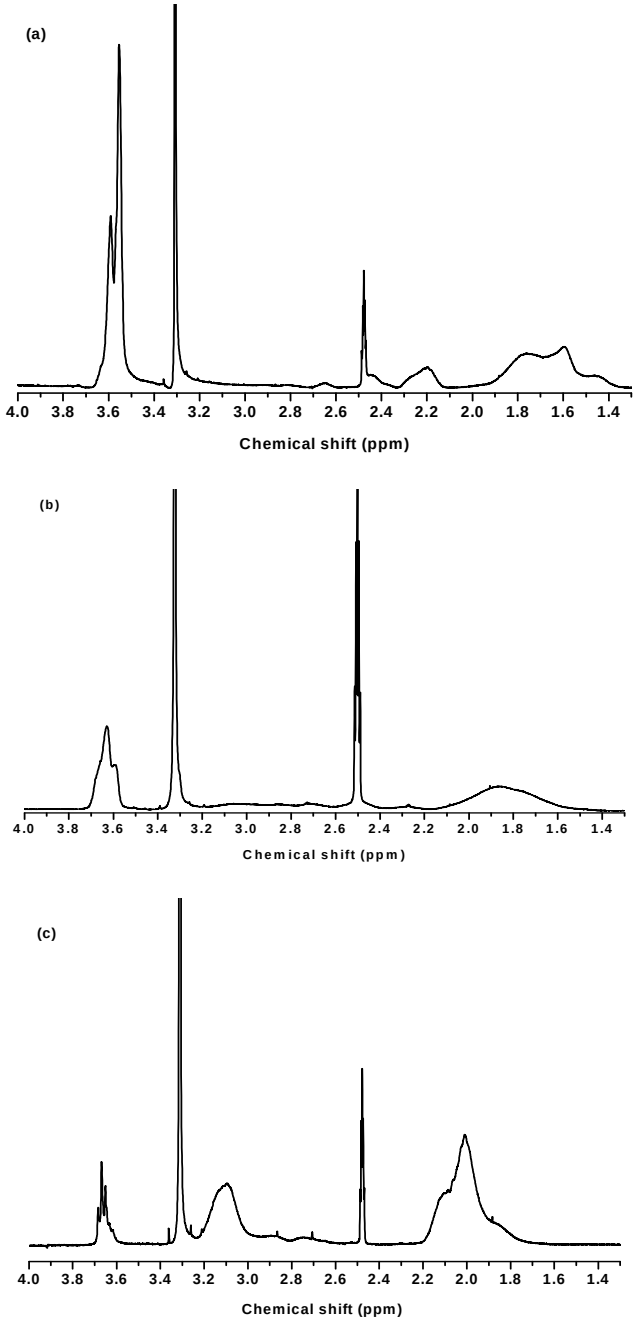

Fig. A 1: ^{1}H NMR spectra of different copolymers: (a) 20% AN:80% MA, (b) 40% AN:60% MA, (c) 80% AN:20% MA, (Solvent: *DMSO$_{-d6}$*).

Appendix B

Calculation procedure used to determine copolymer composition

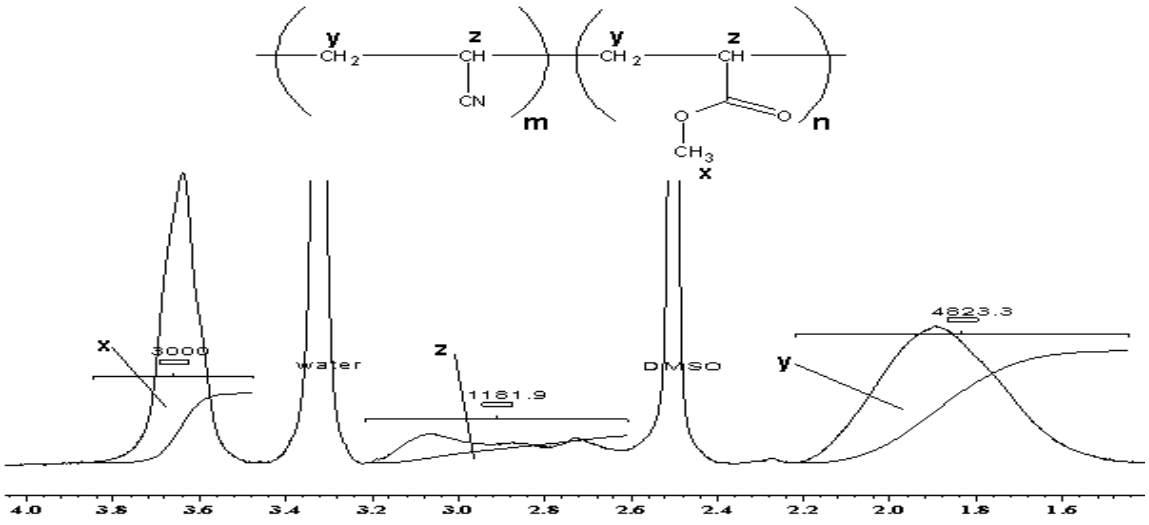

Fig. B 1: ^{1}H NMR spectra of copolymer with comonomer composition ratio of 60% AN:40% MA, (Solvent: *DMSO*$_{-d6}$).

The copolymer compositions were calculated as outlined below:

m = acrylonitrile content in the copolymer

n = methyl acrylate content in the copolymer

x = the integral due to the methyl proton from the methyl acrylate monomer only

y = the integral due to the methylene protons from both monomers

Therefore:

$$3n = x \text{ so that } n = \frac{x}{3} \qquad \textbf{(A-1)}$$

and

$$2m + 2n = y \text{ and } m = \frac{y}{2} - \frac{x}{3} \qquad \textbf{(A-2)}$$

Equation A-1 gives the amount of MA in the copolymer and A-2 gives the amount of AN in the copolymer.

Ratio of MA content = $\frac{n}{n+m}$ and ratio of AN content = 1 – MA content.

Appendix C

Determination of the onset of T_g and T_g.

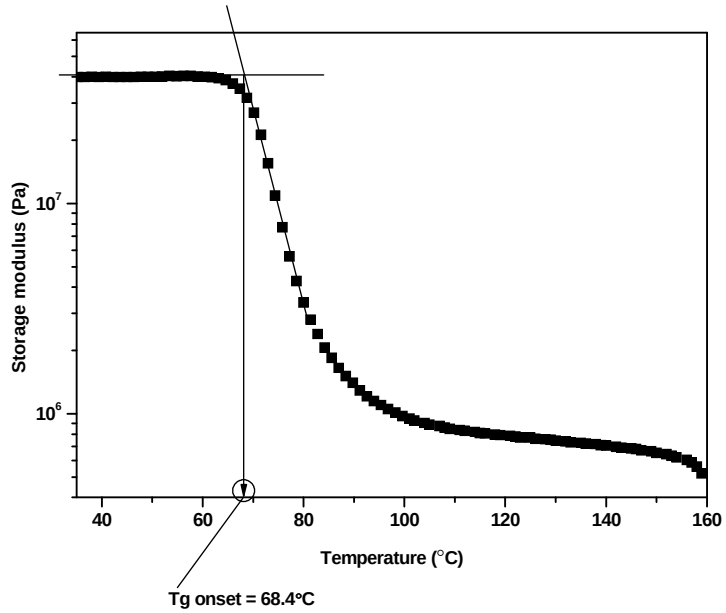

Fig. C 1: Storage modulus of poly(AN-co-MA)/1% clay nanocomposite.

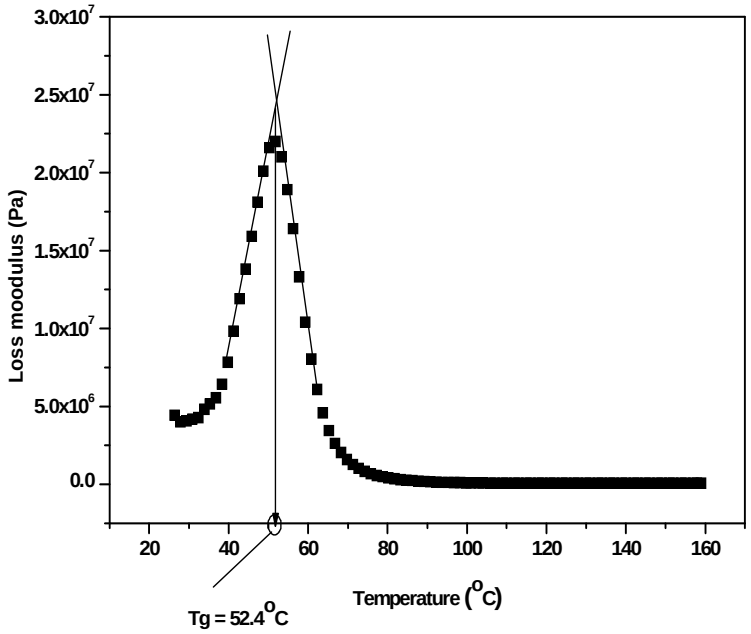

Fig. C 2: Loss modulus curve of poly(AN/MA) copolymer containing 50% AN:50% MA.

Appendix D

Effect of AMPS on particles size

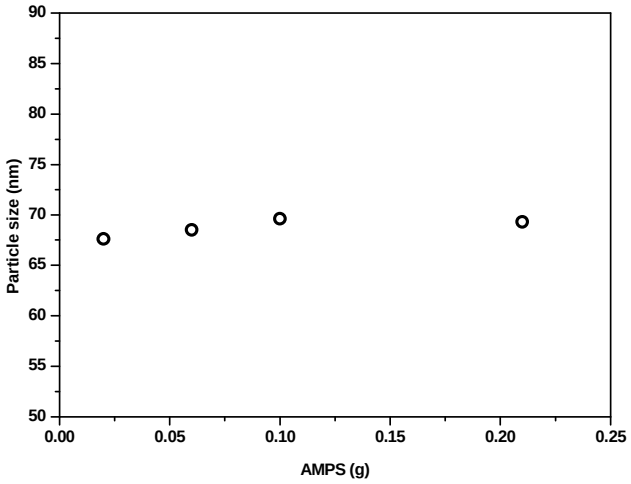

Fig. D 1: Variation of particle sizes with AMPS content corresponding to the amount used in the nanocomposites.

Appendix E

^{1}H NMR spectra of poly(AN-co-MA)/clay nanocomposites

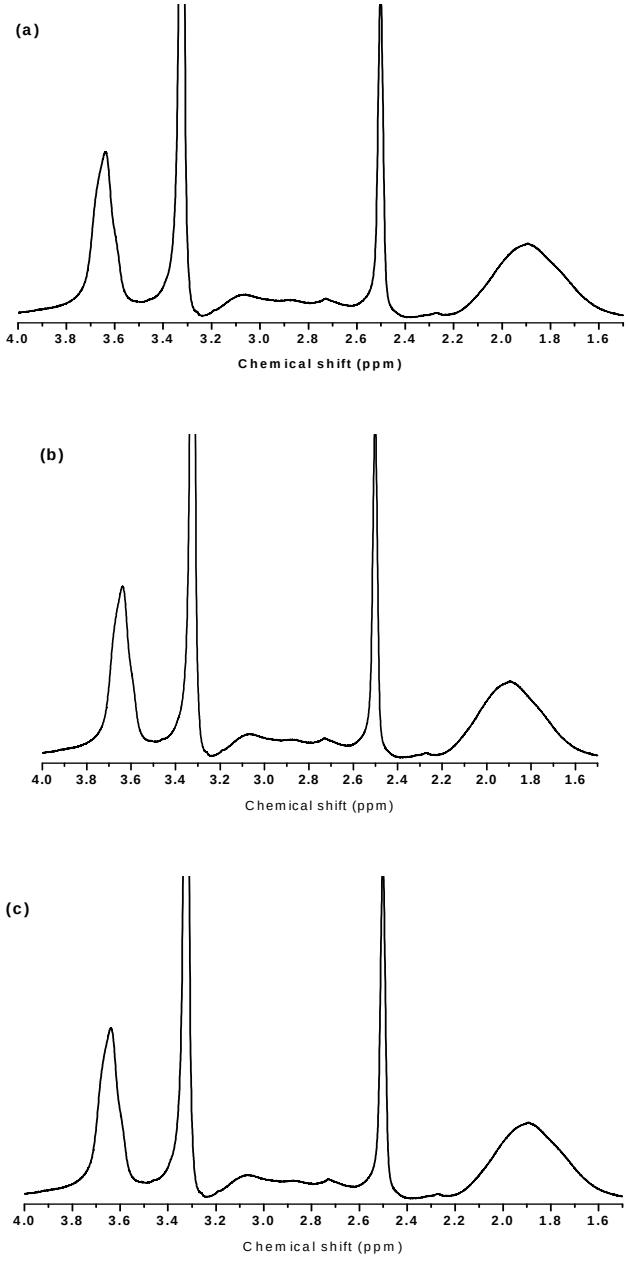

Fig. E 1: ^{1}H NMR spectra of: (a) poly(AN-co-MA)/1%clay, (b) poly(AN-co-MA)/5%clay, (c) poly(AN-co-MA)/7%clay, (Solvent: *DMSO*$_{-d6}$).

Appendix F

FTIR spectra of poly(AN-co-MA)/clay nanocomposites of different clay content

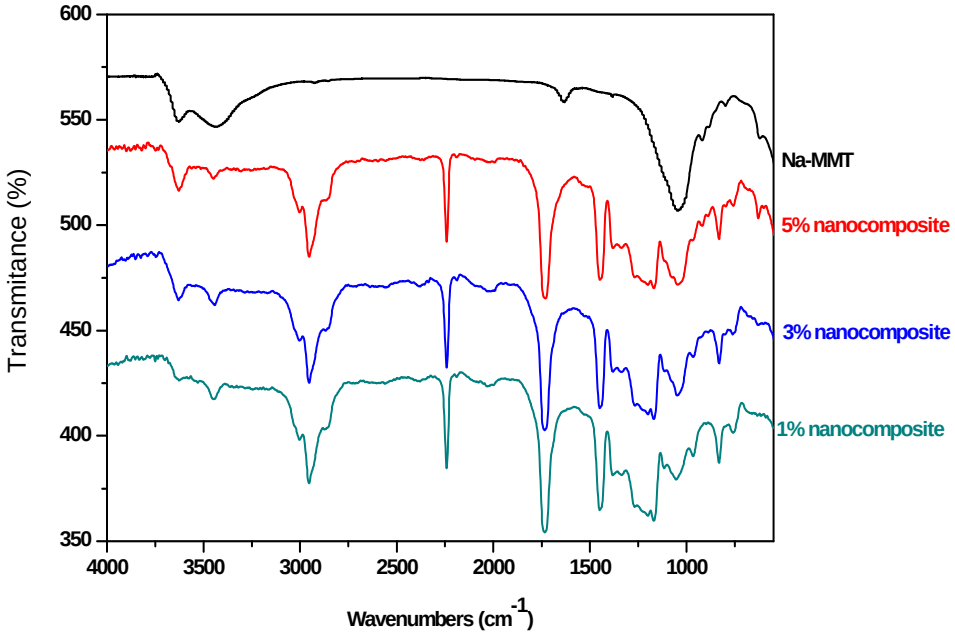

Fig. F 1: FTIR spectra of clay and poly(AN-co-MA)/clay nanocomposites with 1%, 3%, and 5% clay content.

Appendix G

TEM images of poly(AN-co-MA)/clay nanocomposites

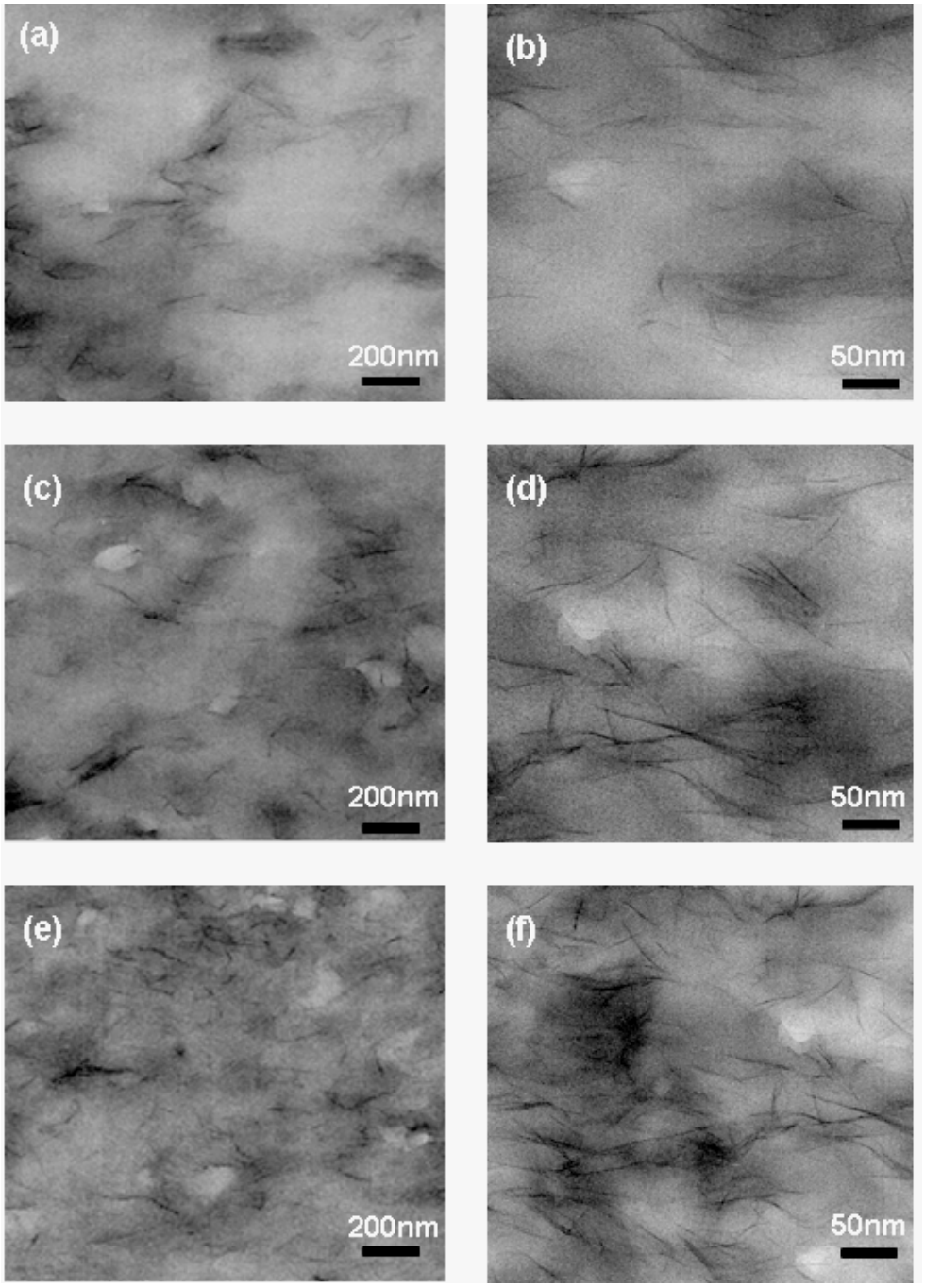

Fig. G 1: TEM images of poly(AN-co-MA)/clay nanocomposites with: (a) and (b) 1% clay content, (c) and (d) 3% clay content and, (e) and (f) 5% clay content.

Appendix H

G'/G" curves of poly(AN-co-MA)/clay nanocomposites

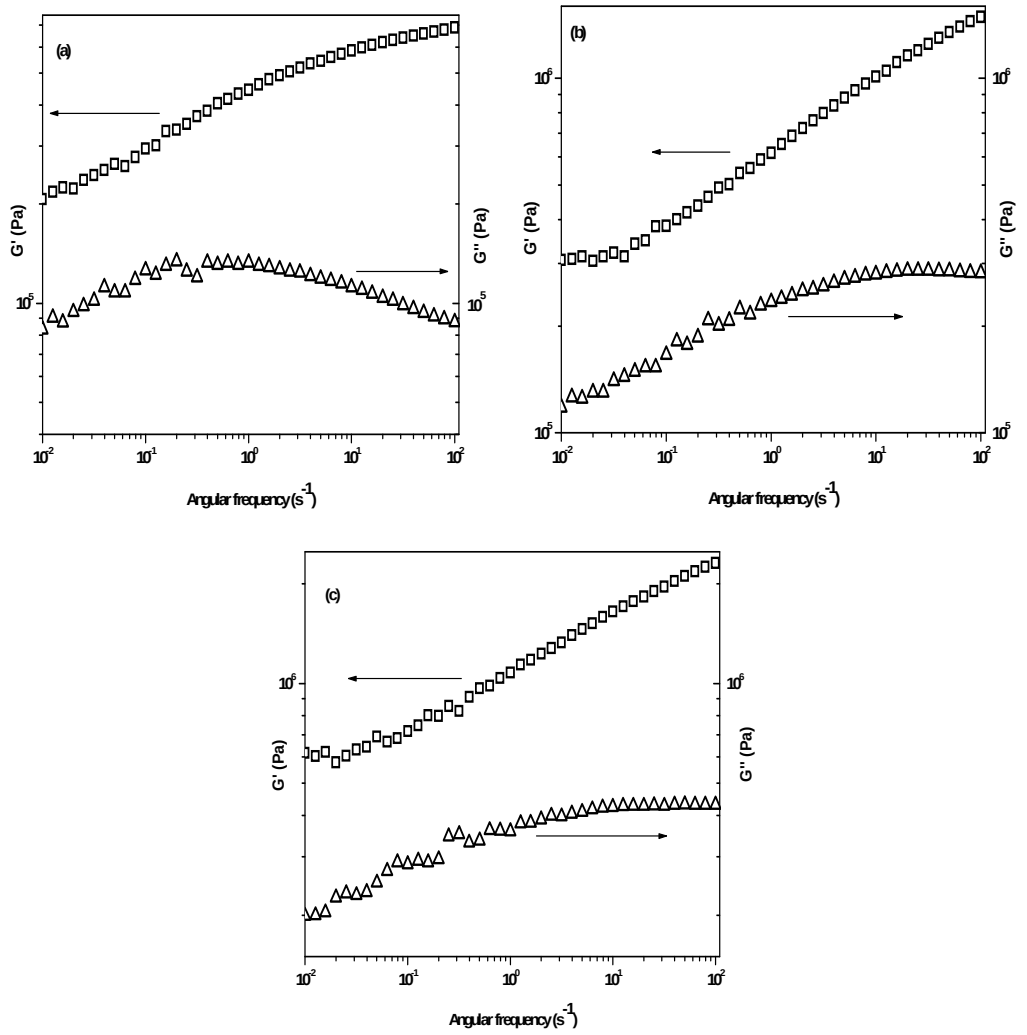

Fig. H 1: The G'/G" vs angular frequency of poly(AN-co-MA)/clay nanocompoistes with: (a)1% clay content, (b) 3% clay content and (c) 5% clay content.

Appendix I

Effect of high shear on the orientation of clay platelets during rheological tests.

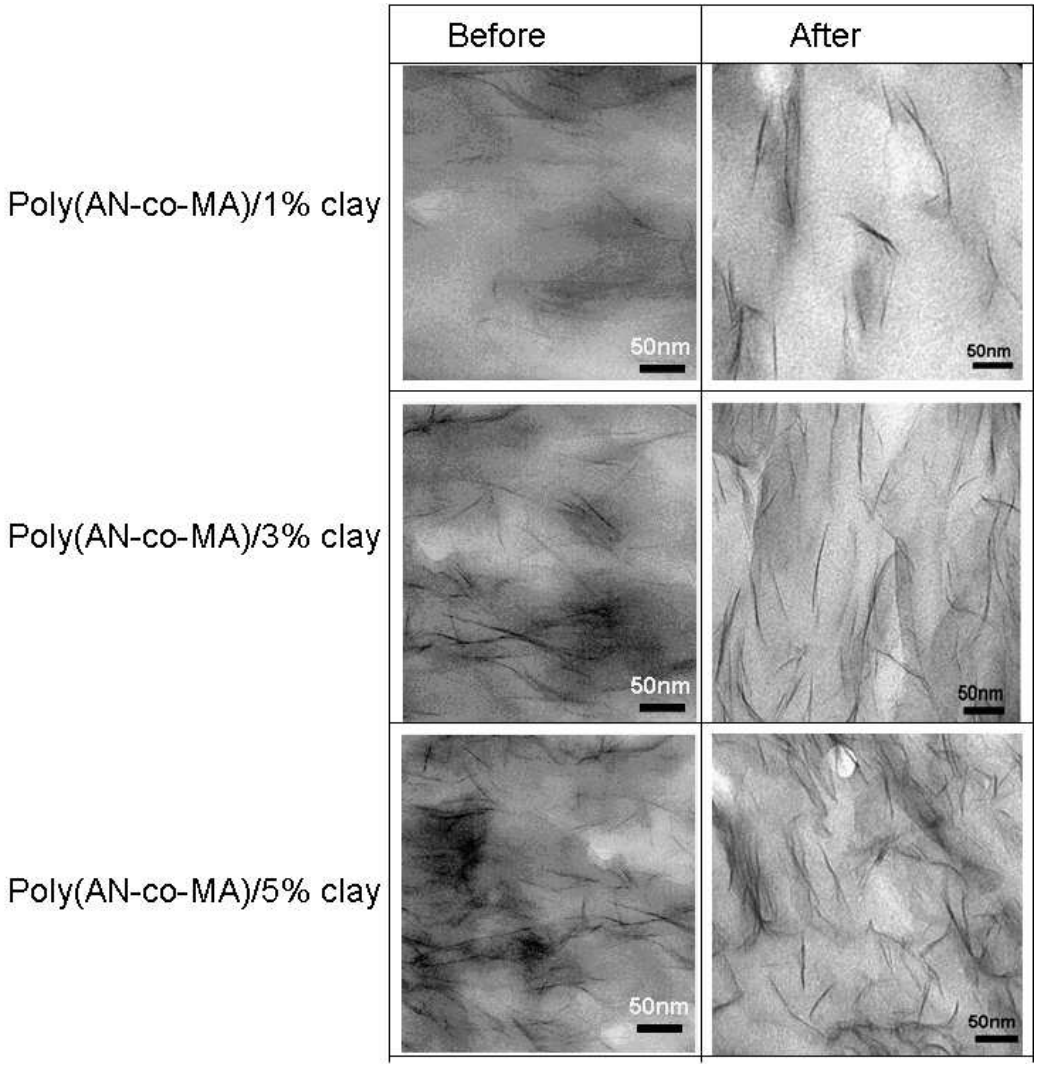

Fig I 1: TEM of poly(AN-co-MA) nanocomposites of different clay loading before and after frequency sweep measurements.

Appendix J

Articles emanating from this study and submitted for publication

	Authors	Title	Journal submitted to:
1.	Eddson Zengeni, Patrice C. Hartmann, Ron D. Sanderson	Synthesis and characterisation of poly(acrylonitrile-co-methyl acrylate)/clay nanocomposites via emulsion polymerisation.	International Journal of Nanotechnology (June 2009)
2.	Eddson Zengeni, Patrice C. Hartmann, Ron D. Sanderson, Peter E. Mallon	Poly(acrylonitrile-co-methyl acrylate) copolymers: Correlation between copolymer composition and structural properties determined by positron annihilation lifetime spectroscopy.	Journal of Applied Polymer Science (August 2009)
3.	Eddson Zengeni, Patrice C. Hartmann, Ron D. Sanderson	Rheological properties of poly(acrylonitrile-co-methyl acrylate)/clay nanocomposites prepared via emulsion polymerisation	Polymer Composites (September 2009)